SYNTHESIS, CHARACTERIZATION AND BIOLOGICAL STUDIES OF RADIOLABELLED METAL COMPLEXES

Tawfeeq Ismail

UNIVERSITY OF CAPE TOWN

2011

Synthesis, Characterization and Biological Studies of Radiolabelled Metal Complexes

Tawfeeq Ismail

A dissertation submitted in fulfilment of the requirement for the degree

Master of Science in Chemistry

University of Cape Town

Department of Chemistry

Supervisor: Dr Gregory S. Smith

Co-supervisor: Dr Daniel D. Rossouw

2011

Declaration

I declare that "**Synthesis, Characterization and Biological Studies of Radiolabelled Metal Complexes**" is my own work and, to the best of my knowledge, has never been reported or submitted for any degree or examination in any university. All sources of information used are cited, acknowledged and completely referenced at the end of each chapter.

I grant the University of Cape Town free licence to reproduce this dissertation in whole or in part for the purpose of research.

.....

Tawfeeq Ismail

...../...../.....

Dedication

This dissertation is dedicated to: my parents (whom have given me everything I needed to reach this milestone in my life), my future family (the thoughts of you and our life motivated me to no end) and the Almighty Allah (who has granted me everything in my life).

Acknowledgements

I would like to express my heartfelt gratitude and deepest appreciation to the following people, without whom this dissertation would not have been possible:

My supervisor, Dr Gregory Smith, for his guidance, encouragement and providing me with the opportunity to do this project. My supervisor at iThemba LABS, Dr Niel Rossouw, for his patience, guidance and allowing me the opportunity to learn so many new things. Ms Deidre Brooks (aka Dee) for her approachableness with regards to administrative and academic support.

The collaborators at NECSA, Dr Neil Jarvis and Dr Jan Rijn Zeevaart, for providing me with the opportunity to get involved in the NTeMBI project. Mariaana Miles for arranging everything during my stint at NECSA and Dr Zoltan Szücs (Institute of Nucha Research of H.A.S.) for making my stay at NECSA much more enjoyable. Dr Kobus Slabbert and Philip Beukes (iThemba LABS) for doing the *in vitro* biological studies.

The analytical staff at the University of Cape Town: Mr Noel Hendricks and Mr Pete Roberts for recording the NMR spectra, Mr Gianpierro Benincasa for recording the elemental analysis and EI-MS.

The University of Cape Town, KW Johnstone Foundation, NTeMBI and NRF for the financial support.

A heartfelt thank you to Dr Anwar Jardine, Banothile Makhubela, Prinessa Chellan and Preshendren Govender for proofreading my dissertation. Preshendren, Tameryn and the rest of the Synthetic Organometallic and Bioinorganic Research Group for the invaluable advice and encouragement.

My family for their unconditional support throughout my academic career. And finally, to Yumna for giving me strength when I was weak, encouragement when I needed a lift and love when I needed it the most.

Table of Contents

Chapter 2:

Synthesis and characterization of monothiosemicarbazone and dithiosemicarbazone ligands

Chapter 3:

Synthesis and characterization of cold (non-radioactive) and radiolabelled gallium(III) thiosemicarbazones. Biological evaluation of radiolabelled gallium(III) thiosemicarbazones.

Conference Contribution

January 2011 – Poster Presentation:

Tawfeeq Ismail, Daniel D. Rossouw and Gregory S. Smith, *Synthesis, Characterization and Biological Studies of Thiosemicarbazone Ligands Radiolabelled with Gallium-67*, presented at **SACI/INORG 2011** - Johannesburg, South Africa.

Abstract

A series of monothiosemicarbazone (and dithiosemicarbazone) ligands have been synthesized via a Schiff base condensation reaction. These ligands contain various aromatic groups and were isolated as solids in moderate to good yields. The ligands were characterized using various spectroscopic and analytical techniques.

Selected ligands were subsequently reacted with the highly air- and moisture-sensitive $GaCl_3$ generating gallium(III) thiosemicarbazone complexes. These complexes were fully characterized using spectroscopic and analytical techniques. The series of ligands were tested for their radiolabelling ability with ^{67}Ga (in the form of $^{67}GaCl_3$). The successfully radiolabelled complexes (with labelling efficiencies ranging from 87 % to more than 99 %) were tested for their chemical stability in saline and bovine serum. The effect of water on the radiolabelling efficiency of these ligands was also tested.

The biological cellular uptake of the chemically stable radiolabelled complexes were evaluated against the rat ovarian cancer (DMBA OC1R) cells, the human breast cancer (MCF 7) cells and the non-cancerous brain endothelial (bEND5) cells. The radiolabelled complexes show better uptake into the non-cancerous brain endothelial cells compared to the cancer cells. However, this could possibly be due to the faster cell kinetics of the brain endothelial cells compared to the cancer cells, which is contrary to what happens *in vivo*. The mononuclear complex shows better uptake into the cells compared to the binuclear complex.

A preliminary investigation into the synthesis of radiolabelled palladium poly(aryl)ether dendrimers was also undertaken. Two new dendritic poly(aryl)ether ligands were synthesized in moderate yields. These ligands were characterized using various spectroscopic and analytical techniques. These ligands were subsequently reacted with previously synthesized $PdCl_2$(cyclooctadiene) to afford dendritic (*generation 0* and generation *1*) poly(aryl)ether complexes, which were also

characterized. The ligands were tested for their radiolabelling ability with ^{109}Pd (in the form of $^{109}PdCl_2$) in different organic solvents (ethanol, acetonitrile and dichloromethane). The reaction mixtures were analyzed using a HPLC coupled to a radiodetector. There are no signs of formation of a radiolabelled complex using ethanol or acetonitrile as reaction solvents. There is, however, a currently unidentified peak in the HPLC chromatogram, found when analyzing the reaction mixture in dichloromethane as reaction solvent. This peak could not be further analyzed due to the rate of decay of ^{109}Pd. Thus, further investigations will have to be performed.

Abbreviations

°C	degrees Celsius
%	percentage
Br	broad
$^{13}C\{^{1}H\}$-NMR	carbon-13 proton-decoupled nuclear magnetic resonance
COD	cyclooctadiene
d	doublet
DCM	dichloromethane
DMSO	dimethyl sulfoxide
DNA	deoxyribonucleic acid
dNDP	deoxynucleoside diphosphate
E.A.	elemental analysis
en	ethylenediamine
EPR	enhanced permeability and retention
EI	electron impact (mass spectrometry)
ESI	electronspray ionization (mass spectrometry)
Et	ethyl
FT-IR	Fourier-transform infrared spectroscopy
g	gram(s)
hrs	hours
^{1}H-NMR	proton nuclear magnetic resonance
HPLC	High-performance Liquid Chromatography
HSQC	heteronuclear single quantum correlation

Hz	hertz
IR	infrared
J	coupling constant
keV	kilo (1000) electron volts
µCi	microcurie
µL	microlitre(s)
m	multiplet (NMR)
m	meta- (NMR);medium intensity (IR)
Me	methyl
MHz	megahertz
min.	minute(s)
mCi	millicurie
mL	millilitre(s)
mol.	mole(s)
mmol.	millimole(s)
M.P.	melting point
MS	mass spectrometry
m/z	mass to charge ratio
NMR	nuclear magnetic resonance
NECSA	South African Nuclear Energy Corporation
o	ortho-
p	para-
PAMAM	poly(amidoamine)
PET	Positron Emission Tomography
PPh_3	triphenylphosphine
ppm	parts per million

rt.	room temperature
s	singlet (NMR)
SPECT	Single photon emission computed tomography
s	strong intensity (IR)
t	triplet (NMR)
THF	tetrahydrofuran
w	weak intensity (IR)
WHO	World Health Organization

Chapter 1

Literature Review

1.1. General Introduction

Cancer is one of the leading causes of death worldwide.[1] It has been reported to account for 7.4 million deaths (around 13% of all deaths) in 2004.[2] According to later World Health Organisation (WHO) statistics, cancer causes an estimated 7.9 million deaths worldwide each year, with more than 30% of cancer deaths being preventable.[1,2] Of the 7.9 million deaths each year, it is estimated that more than 72% are now occurring in low- and middle-income countries.[1] Lung, stomach, liver, colon and breast cancer has been reported to cause the most cancer deaths each year.[2] Deaths from cancer worldwide are projected to continue rising, with an estimated 12 million deaths in 2030.[2]

Cancer is the uncontrolled growth and spread of tumour cells that can affect almost any part of the body.[3] The growths often invade surrounding tissue and can metastasize to different and distant sites in the body.[3] Metastasis is defined as a secondary cancerous growth formed by transmission of cancerous cells from a primary growth located elsewhere in the body.[4] Cancer arises from a change in one single cell, which could be started by external agents and inherited genetic factors. The transformation of a normal cell into a tumour cell is a multistage process, usually a progression from a pre-cancerous lesion to a malignant tumour. This progression is a result of the interaction between someone's genetic factors and three categories of external agents:

- Chemical carcinogens → such as asbestos, components of tobacco smoke, aflatoxin (a food contaminant) and arsenic (a drinking water contaminant).
- Biological carcinogens → such as infections from certain viruses, bacteria or parasites.
- Physical carcinogens → such as ultraviolet and ionizing radiation.[2]

Ageing is another fundamental factor with the incidence of cancer rising with age. This is most likely due to the build-up of risks for specific cancers that increase with age. The overall risk accumulation is combined with the tendancy for cellular repair mechanisms to be less effective as the person grows older.[2]

Early detection of cancer is a vital preventative measure purely based on the observation that treatment is more effective when the cancer is detected early. The aim is to detect the cancer when it is localized (i.e. before metastasis). The efforts into early detection consist of two components:

- Education → to help people recognize the early signs of cancer.
- Screening programmes → to identify early cancer or pre-cancer before signs are recognizable.

In addition, a significant proportion of cancers can be cured by surgery, chemotherapy or radiotherapy, especially if they are detected early.[3] In recent years metal complexes have gained increased attention as chemotherapeutic drugs and diagnostic tools (i.e. radiopharmaceuticals).[5]

1.2. Radiopharmaceuticals

A radiopharmaceutical (nuclear medicine) is a radioactive compound that is nothing else but the combination of a radioisotope of an element with a new molecule (complexes, perfusion agent) or with a molecule of well known biological behaviour (targeting).[6] It has also been described as the *in vivo* use of drugs labelled with radioactive atoms (radioisotopes) for the detection and therapy of diseases such as cancer.[7] Radioisotopes have primarily been associated with cancer as causal

agents, however, more recently the beneficial side has emerged as radioisotopes are now employed for tumour imaging and therapy.[7]

Radioisotopes are known to decay by emitting gamma-rays (high energy electromagnetic radiation) or particles, such as betas (electrons). These are the metal characteristics needed for use in radiopharmaceutical development. Gamma rays (especially with energies between 100-200 KeV) are usually highly penetrating in tissue and are thus useful for external imaging. Beta-particles have a much shorter penetration range in tissue and can therefore provide a localized therapeutic radiation dose.[6]

A number of radioisotopes in diverse chemical forms have been shown to accumulate in tumours relative to surrounding normal tissue such that these tumours may be detected by external imaging devices.[7] In certain cases the tumours are treated by the radiation they emit.[7] For example, radioisotopes of iodine (^{131}I, ^{123}I) as iodides are useful for the detection and, in the case of ^{131}I, the treatment of thyroid carcinomas.[7] Gallium-67 (^{67}Ga) citrate is a preferred imaging agent for soft-tissue tumours, technetium-99m (^{99m}Tc) phosphates and phosphonates have proven to be useful in the detection of bone metastasis, and radioisotopes of rhenium (^{188}Re, ^{186}Re) as the dimercaptosuccinic acid chelates are under investigation for the therapy of certain tumours.[7]

In the early 1990's, methods for the attachment of ^{99m}Tc, the radioiodines, ^{111}In and other radioisotopes to monoclonal antibodies specific for tumour-associated antigens were developed and, in this form, they were found to be useful for the detection and therapy of diverse tumour types.[7] It was also found that the radioactive isotopes ^{67}Ga and ^{68}Ga show some promise in the study of bone cancer as compounds of these isotopes are absorbed by the cancer deposits in the bone.[8] The accumulation of ^{67}Ga was first demonstrated in lymph nodes of patients with Hodgkin's disease and was subsequently found to accumulate in tumours, tissues of inflammation and bone.[8] The utility of ^{67}Ga in nuclear medicine is variable. Many types of tumours have been shown to accumulate ^{67}Ga poorly but others, such as hepatomas and lymphomas, tend to be gallium avid. However, the tumours can be inconsistent in magnitude and uniformity of uptake. Nonetheless, no other gamma-emitting

radiopharmaceutical has surpassed ^{67}Ga in cost-effectiveness, availability and use for general tumour imaging.[9]

In modern medicine, early diagnosis of diseases plays an important part in improving quality of life and reducing health care costs to society. Just as important, however, is the detection of curative progress, i.e. the progress made after therapeutic treatment of a patient's disease (eg. the regression of cancer after chemotherapy).[10,11] On the molecular level, biochemical analytical methods are well established. Since the discovery of X-rays, visualizing methods have become more important and routine X-rays are nowadays complemented with the use of magnetic resonance imaging (MRI), ultrasound and radioisotope-based scintigraphy.[6] While X-ray and MRI are structural methods, positron emission tomography (PET) or single photon emission computed tomography (SPECT) permit the visualization of organ functions and are hence functional diagnostic methods.[6] Both methods, PET and SPECT, are based on radionuclides and are included in nuclear medicine and/or radiopharmacy.[6]

PET and SPECT are nuclear medicine imaging techniques which produce three-dimensional images or pictures of functional processes in the body. These imaging techniques could allow for early detection of cancers. Both are non-invasive techniques which merely require an injection of the radionuclidic compound, which is normally attached to a biologically active molecule, into the bloodstream of the patient, followed by detection of the emitted radiation by means of a PET or SPECT camera. PET imaging makes use of radioisotopes with short half-lives (i.e. usually up to 2 hours). The system detects pairs of gamma rays, formed inside the body during the collision of a positron, generated by a positron-emitting radionuclide, with an electron (electron-positron annihilation). SPECT imaging, however, makes use of radioisotopes with longer half-lives (e.g. ^{67}Ga-citrate is used as a SPECT tracer with a half life of 78 hours). The system detects gamma rays emitted directly by a gamma-emitting isotope.

In addition, there are factors that influence the stability of the radiolabel *in vivo*, and obviously the instability, which results in the loss of the radiolabel in circulation, will contribute to low tumour accumulations.[7] Losses occurring in the tumour tissue will also result in low tumour accumulation if the free radiolabel is capable of diffusing

therefrom.[7] Most cancer therapeutics (chemo, antibody-based, radiation) are at best only partially and/or temporarily effective. In general, the causes for failure can be summarized as: (i) poor diffusion and/or nonuniform distribution of drug molecules in solid tumours; (ii) high drug concentration and retention in normal tissues (leading to side effects); (iii) requirement for plasma-membrane permeability; (iv) low uptake of drug by tumour; and (v) lack of retention of the drug within the tumour.[12] Thus, there is an increase in research into developing new metal-containing anti-cancer and imaging drugs.

1.3. Metal-containing anti-cancer/imaging compounds

Novel antitumour drugs possessing a strong inhibitory effect on ribonucleotide reductase would prove to be a useful addition to existing therapeutic regimens for the treatment of cancer.[13] Ribonucleotide reductase is known to be an essential enzyme for cellular respiration.[13] The reductive conversion of ribonucleotides to deoxyribonucleotides by the iron-dependent enzyme ribonucleotide reductase has been reported to be a crucial rate-controlling step in the pathway leading to the biosynthesis of deoxyribonucleic acids (DNA).[13-18] Thus inhibition of the iron binding site in ribonucleotide reductase could prove to be key in proliferating tumour cells. Ribonucleotide reductase is thus considered to be an excellent target for cancer chemotherapy.[16]

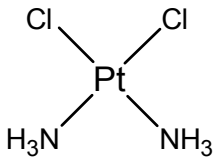

Fig. 1.1: The structure of cisplatin, one of the best selling anticancer drugs

The field of medicinal chemistry has been dominated by the synthesis of organic compounds as medicinal drugs but metal complexes have gained considerable attention in the field as pharmaceuticals[17] for use as diagnostic tools or as chemotherapeutic drugs against cancer.[5] Research in medicinal chemistry has been

stimulated by the worldwide success of cisplatin (**Fig. 1.1**), *cis*-diamminedichloroplatinum(II), which is one of the best selling anticancer drugs.[5] Cisplatin was first synthesized in 1844 by Michel Peyrone[5], but its anti-cancer properties were only discovered by chance more than a century later, in the 1960's, by Barnett Rosenberg as a result of an investigation looking at the effect of electric fields on the growth of bacteria using platinum electrodes.[5,18] The mode of action of cisplatin is now widely accepted to be through the interaction of the drug with DNA.[5] Since the discovery of the anticancer properties of cisplatin, there has been considerable effort made in the design of drugs based on platinum and other metals. Some of the most promising recent developments are in the fields of ruthenium and gallium complexes, where some of these complexes have successfully undergone Phase I and II human clinical trials.[5] An important issue is the development of drugs that could be taken orally, rather than by intravenous injection. To achieve this, the active metal would have to be bound to the right type of organic ligand in order for the resultant complex to survive the harsh stomach environment, be absorbed in the intestine and then slowly release the active component in the blood plasma or tumour.

The essential role of metal ions, especially transition metal ions, in biological systems is well known.[5] The wide range of coordination numbers and geometries, accessible redox states, thermodynamic and kinetic characteristics, and the intrinsic properties of the cationic metal ion and ligand itself offer the medicinal chemist a wide spectrum of reactivities that can be exploited.[19] Studies of metal complexes have thus drawn considerable attention, and are growing increasingly more important, as chemotherapeutic drugs in the treatment of cancer.[5,20] Metal-complexed anticancer prodrugs may be activated selectively in the hypoxic tumour tissue upon reduction by biological reducing agents.[21-23] Electron transfer can occur either to the metal center or to the binding ligand resulting in reactive species capable of attacking biologically relevant target molecules either by ligand displacement at the low valent metal center or by radicals formed at the ligand entity, respectively.[21]

1.3.1. Platinum-based complexes

Although metals have long been used in medicinal chemistry, the potential of metal-based agents has only fully been realized since the discovery of the biological properties of cisplatin, a platinum-based anticancer drug.[19,24-26] It has been reported that, in addition to its intrinsic tumour-killing ability, cisplatin has been shown to work in synergy with external radiation. Thus, the use of cisplatin in combination with external radiation provides greater levels of tumour killing than either modality alone.[27] So, in order to take advantage of the radiation-enhancing effects of cisplatin, a radioactive form of cisplatin as a cancer therapy agent was proposed in a patent by Wayne Court and Isotope Solutions, Inc. (patent number WO/2003/000298).[28]

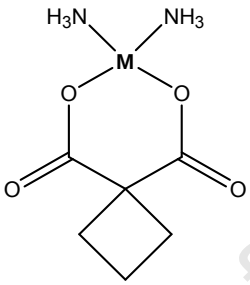

M = Pt-191, Pt-193m

Fig. 1.2: Structural representation of ^{191}Pt-labelled and ^{193m}Pt-labelled 1,1-cyclobutanedicarboxylate diammine platinum(II).

It has also been reported that other radiolabelled platinum drugs, such as ^{191}Pt-labelled 1,1-cyclobutanedicarboxylate diammine platinum(II) (**Fig. 1.2**), ^{193m}Pt-labelled 1,1-cyclobutanedicarboxylate diammine platinum(II) (**Fig. 1.2**) and ^{191}Pt-labelled *cis*-dichloro-trans-dihydroxybis-isopropylamine platinum(IV), could have therapeutic uses.[28]

However, it should be noted that platinum-based drugs show activity against a limited number of tumours.[5] In addition, there are often significant side effects, such as neurotoxicity, nephrotoxicity, myelosuppression and the problem of developing drug resistance during treatment.[5,29]

1.3.2. Ruthenium-based complexes

Various aspects of the advances in the development of tumour-inhibiting ruthenium-complexed drugs have been reviewed since the late 1990's.[5,30,31] Among the most remarkable achievements in ruthenium-based anticancer research is the entering into phase I clinical trials of the ruthenium-based complex, NAMI-A (**Fig. 1.3**) in 1999 by Allessio *et al*.[32] Another ruthenium(II) complex, Hind[*trans*-$RuCl_4(ind)_2$] (i.e. KP1019 – **Fig. 1.3**), developed by Keppler and co-workers[33] has attracted attention as a potential anticancer agent and has since entered clinical trials.

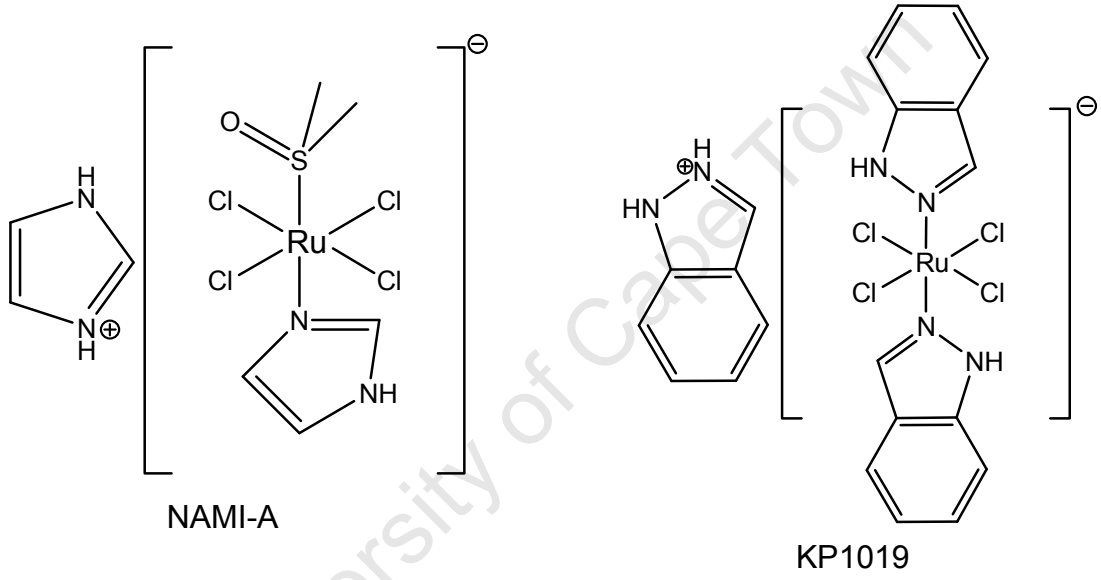

Fig. 1.3: The structural representation of NAMI-A (left) and KP1019 (right).

Research into other ruthenium complexes such as [(η^6-*p*-cymene)Ru(II)Cl(en)]PF_6 has made a serious contribution to getting an insight into the mode of action of this class of organometallic antitumour compounds.[5] The compound [(η^6-*p*-cymene)Ru(II)Cl(en)]PF_6 has been shown to undergo rapid hydrolysis in aqueous solution resulting in the substitution of the chloride ligand by a water molecule.[34] The presence of hydrophobic planar ligands in these types of ruthenium-complexes may facilitate recognition and transport of these species through cell membranes.[34] It should also be noted that hydrophobic derivatives showed higher tumour-inhibiting activity.[34] The relative conformational flexibility of the ligands makes the intercalation into DNA with simultaneous binding of ruthenium(II) to DNA compatible.[34] DNA was supposed to be the main target for these complexes. The complex [(η^6-*p*-

cymene)Ru(II)Cl(en)]PF_6 has been found to distort duplex DNA structure by forming monofunctional adducts with the guanine base.[34] These results have provided conditions for optimisation of ruthenium-arene DNA interactions to achieve higher anticancer activity.[34]

Research into ruthenium complexes as anti-cancer compounds has also led to the design of possible ruthenium imaging agents. In 2007, Sadler and co-workers[35] synthesized a ruthenium radiolabelled complex, [(η^6-fluorene)^{106}Ru(en)Cl]PF_6 (**Fig. 1.4**). This was the first reported example of a prospective ruthenium anti-tumour agent which has been radiolabelled and used in biodistribution studies. The distribution studies in the tissues of a rat 15 minutes post-injection showed that ^{106}Ru was well distributed throughout the body tissues. The highest levels were associated with the liver and kidney, with the lower levels being present in the blood, bone marrow, brown fat, cartilage, lung, preputial gland, skin/fur, submaxilliary salivary glands and testes. This report shows the potential of developing new ruthenium complexes as imaging agents.[35]

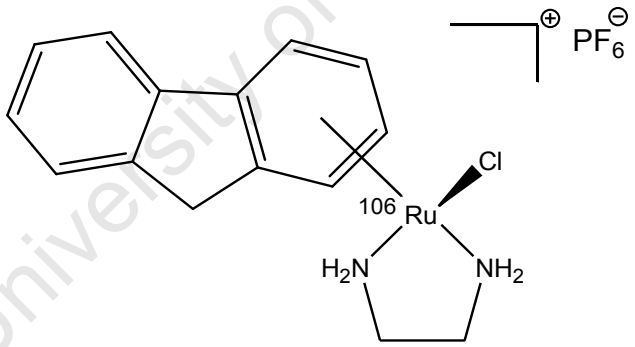

Fig.1.4: Structure of the ruthenium radiolabelled complex, [(η^6-fluorene)^{106}Ru(en)Cl]PF_6.

1.3.3. Palladium-based complexes

Until developments made by Khan and co-workers[36], there had been little or no application of palladium complexes as antitumour drugs.[29] This is due to the high lability and fast hydrolysis reactions presented by palladium complexes in biological environments when compared to platinum complexes.[29,36] To circumvent this problem, Khan and co-workers used chelating ligands in the synthesis of palladium

complexes. The results demonstrate that the palladium complex [Pd(meth)(2-merpy)Cl]Cl (where meth = methionine and merpy = mercaptopyrimidine) has a significant cytotoxicity and could act as a powerful antitumour agent.[36] Hence, other works involving palladium complexes started to have other perspectives of use, especially the class of cyclopalladated complexes.[29]

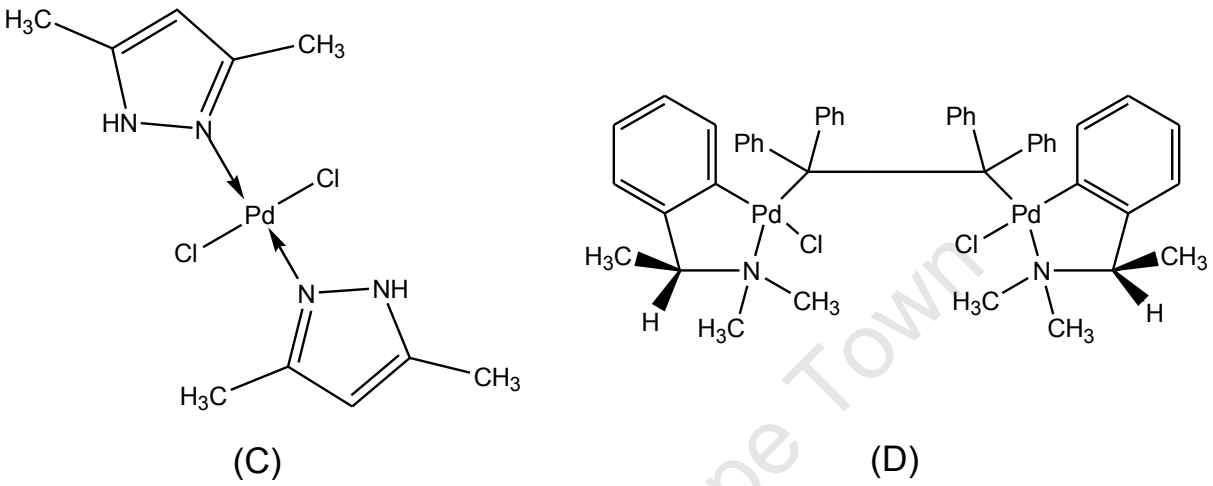

Fig. 1.5: Structures of the *trans*-palladium complex with pyrazol **(C)** and the cyclopalladated complex $[Pd_2(C^2,N\text{-}S_{(-)}dmpa)_2(\mu\text{-}dppe)Cl_2]$ **(D)**.

Many palladium compounds show high activity in cisplatin-resistant cells, which might suggest that the biochemical mechanism of action differs to that of cisplatin. It has been suggested that non-covalent interactions (such as major/minor groove binding, electrostatic interaction, intercalation and hydrogen bonding) might play a vital role in the interactions between some palladium complexes and DNA.[37] Results published by Al-Allaf and Rashan[38] indicate that most of the *trans*-palladium complexes (representative structure shown in **Fig. 1.5-C**) show better activity than the *cis*-platinum and *cis*-palladium isomers.[29] The *trans*-palladium complexes were also found to show activities equal to, or superior than, those of cisplatin, carboplatin and oxaliplatin in *in vitro* studies. The cyclopalladated complex $[Pd_2(C^2,N\text{-}S_{(-)}dmpa)_2(\mu\text{-}dppe)Cl_2]$ (**Fig. 1.5-D**) also shows inhibitory *in vitro* activity at low concentrations (<1.25 μM) and shows good *in vivo* activity, delaying tumour growth and prolonging animal survival.[29]

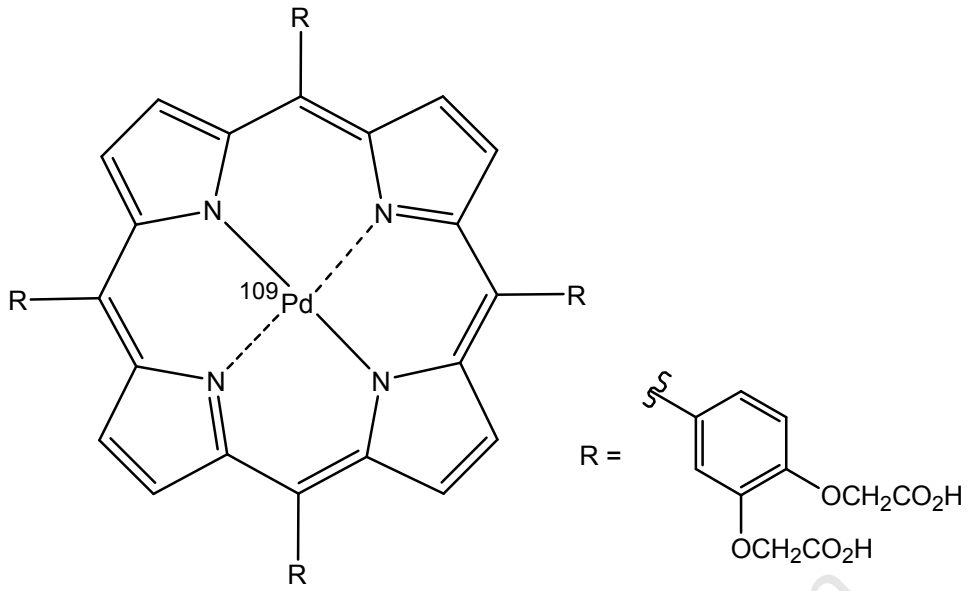

Fig. 1.6: Structure of the ^{109}Pd-porphyrin complex synthesized by Chakraborty *et al*.[39]

The promising results shown by palladium complexes have also attracted the attention of radiopharmaceutical researchers. In 2007, a ^{109}Pd-porphyrin complex (**Fig. 1.6**) was synthesized by Chakraborty *et al*.[39] for preliminary biological evaluation for possible use in targeted tumour therapy. Results of the biodistribution studies in Swiss mice bearing fibrosarcoma tumours reveal good tumour uptake within 30 minutes post-injection and it remains almost constant 24 hours post-injection. The high tumour/blood and tumour/muscle ratios exhibited by the radiolabelled palladium porphyrin complex indicate its potential for use in targeted tumour therapy.[39]

Indeed, the current focus in drug design is the development of drugs that can be transported through the cellular membrane, survive in the cell, and if possible, excrete from the body with minimal side effects. In this process, metal coordination and hydrogen bonding will be key factors and palladium complexes, especially those kinetically more stable in biological media, arise as great candidates.

1.3.4. Gallium-based complexes

Gallium has tumour-seeking and antineoplastic properties that have been recognised for over 30 years.[16] Gallium is the second metal ion, after platinum, to be used in cancer treatment. Its activities are numerous and various. Gallium has been known to modify the three-dimensional structure of deoxyribonucleic acids (DNA), and inhibits its synthesis, modulates protein synthesis and inhibits the activity of a number of enzymes, such as ATPases, DNA polymerases, ribonucleotide reductase and tyrosine-specific phosphatase. Gallium also alters plasma membrane permeability and mitochondrial functions.[15]

It is generally agreed that the critical cellular target of gallium is the enzyme ribonucleotide reductase, which catalyses the reduction of ribonucleotides to deoxyribonucleotides required for DNA synthesis and has long been recognised as a suitable target for cancer chemotherapy. The activity of this enzyme is inhibited by binding of gallium to the iron site of the R2 subunit and the resulting destabilisation of the tyrosyl radical essential for enzymatic activity. This results in the depletion of deoxynucleoside diphosphate (dNDP) pools, impairs DNA synthesis, cell cycle perturbations and apoptosis through the mitochondrial pathway involving activation of the proapoptotic factor Bax and caspase-3 (**Fig. 1.7**). Caspase-3 is a protein that is a member of the **c**ysteine-**asp**artic acid prote**ase** (caspase) family and is known as an apoptosis-related cysteine peptidase.[40]

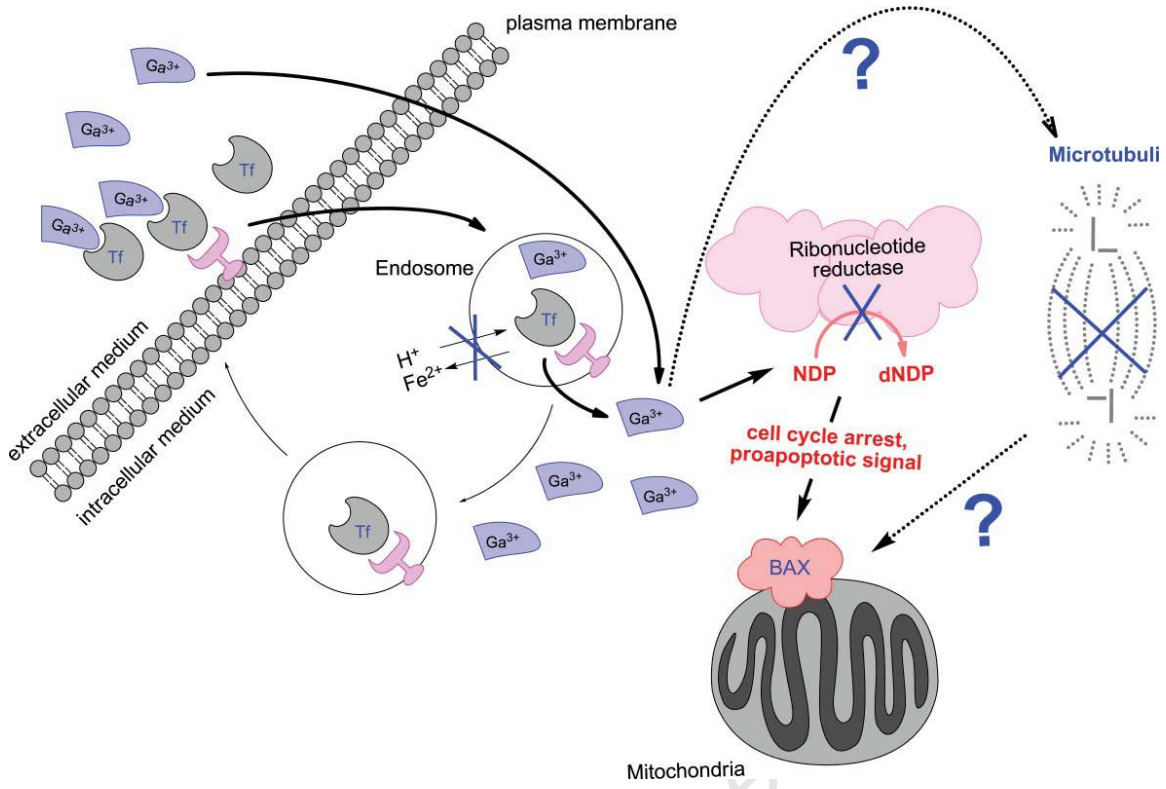

Fig.1.7: Schematic representation of the mode of action of gallium compounds.[40]

The safety and activity of gallium salts, such as gallium nitrate, have been extensively studied in clinical trials since 1975. Gallium nitrate has proved to be an effective drug for the treatment of malignancy, but its unfavourable pharmacokinetic properties prevent its use in systematic chemotherapy of cancer patients. Parenteral administration is associated with a low therapeutic index due to renal toxicity, and oral administration is inefficient due to insufficient intestinal absorption. The development of tumour-inhibiting gallium complexes have been pursued as a strategy to overcome the limitations faced with gallium salts.[16]

It has been shown that improved bioavailability compared to gallium chloride and sufficient plasma concentration can easily be reached with *tris*(8-quinolinolato)gallium(III), KP46 (**Fig. 1.8**).[5] This compound exhibits better antiproliferative properties and superior capacity for apoptosis induction *in vitro* when compared to gallium nitrate.[5] Of a series of gallium complexes studied, KP46 was selected for further development and has successfully completed phase I clinical trials.[5,41]

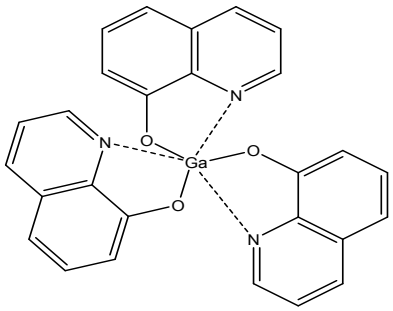

Fig. 1.8: Structure of *tris*(8-quinolinolato)gallium(III), KP46.

Gallium radioisotopes, especially ^{67}Ga and ^{68}Ga, have long been of interest in the design of radiopharmaceuticals.[42] The interesting physical properties and availability of this radioisotope makes it an interesting nuclide for research in radiopharmaceuticals.[43] It was found that the radioisotope ^{67}Ga shows some promise in the study of bone cancer as compounds of this isotope are absorbed by the cancer deposits in the bone.

Gallium-67 citrate (^{67}Ga-citrate) has been found to accumulate in certain viable primary and metastatic tumours, as well as focal sites of infection, which makes it an ideal imaging agent. The ^{67}Ga radioisotopes accumulate in the lysosomes, being bound to intracellular protein. The empirical formula of gallium-67 citrate is believed to be ^{67}Ga(citrate-(3-)) with three water molecules presumably filling the remaining coordination sites (**Fig. 1.9**). The citrate, however, is a weak chelator ligand. As soon as ^{67}Ga-citrate is injected into the bloodstream the ^{67}Ga is transchelated to transferrin. The transchelation of Ga(III) complexes *in vivo* by transferrin requires that kinetically inert complexes of Ga(III) be developed for radiopharmaceutical applications. Thus, there has been increased research into developing new gallium-based radiopharmaceuticals for tumour therapy/imaging.[44]

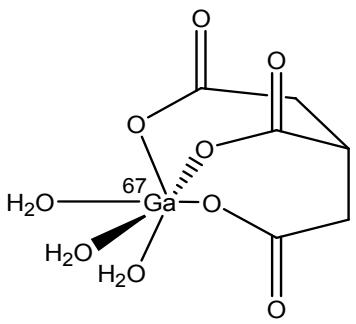

Fig. 1.9: The proposed structure of ^{67}Ga-citrate.

One of the best known chelators used for gallium (radioactive and non-radioactive) is the macrocyclic 1,4,7,10-tetraazadodecane-1,4,7,10-tetraacetic acid (DOTA) ligand (**Fig. 1.10**). $Ga(DOTA)^-$ is sufficiently stable to be used in clinical practice and several derivatives of DOTA have been reported.[45]

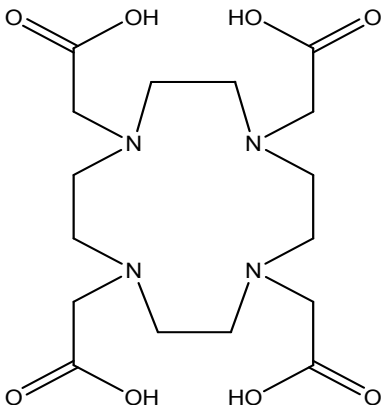

Fig. 1.10: Structural representation of the 1,4,7,10-tetraazadodecane-1,4,7,10-tetraacetic acid (DOTA) ligand.

Orvig and co-workers[46] have also reported novel bifunctional chelate alternatives to DOTA derivatives for application of radioisotopes of gallium to diagnostic nuclear medicine. In a 2 hour competition experiment against human *apo*-transferrin, $[^{67}Ga(dedpa)]^+$ (**Fig. 1.11**) showed no chemical instability. The stability of this chelate and its derivatives is higher than that of the DOTA ligands. Biodistribution studies also confirm the stability of the complexes measured *in vitro* with general clearance, rendering these frameworks a good basis for development of new gallium bioconjugates.

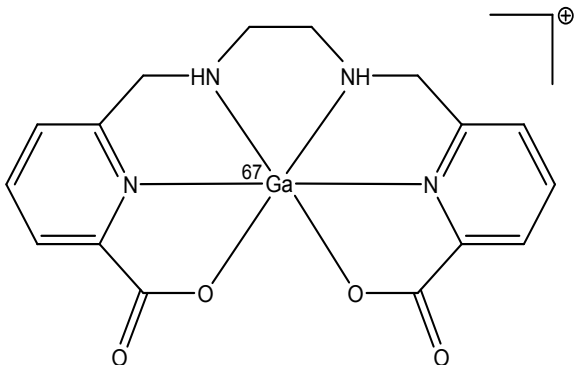

Fig. 1.11: Structure of $[^{67}Ga(dedpa)]^+$ synthesized by Orvig and co-workers.

Previous work has shown that metal salts and other metal complexes present their own problems in terms of drug resistance and other significant side effects. However, at the same time there has been an emergence of studies of new structural types of metal complexes with promising biological activity and with the ability to circumvent these issues.[29] Under this focus or drive to design new coordination compounds with anticancer/imaging properties, decreased toxicity and establishment of new biological targets is just the type of impetus to advance the bioinorganic chemistry of ruthenium, palladium and gallium complexes.[29] Literature has also shown, however, that these metals have to be bound to the right type of organic ligand, and in recent years there have been promising developments in the use of thiosemicarbazones (section 1.4.) and nanomolecules such as dendrimers (section 1.5.) as possible anti-cancer and imaging agents.

1.4. Thiosemicarbazones

Thiosemicarbazones belong to a large group of thiourea derivatives whose biological activity is a function of its parent aldehyde or ketone moiety.[38,40] Thiosemicarbazones are molecules of interest in coordination chemistry due to their pharmacological properties, which include antiparasital, antibacterial and antitumour activities.[8,16,47-49] Studies on structure-activity relationships of thiosemicarbazones have suggested that the antitumour activities of thiosemicarbazones are increased by their ability to form chelates with metal ions.[16,49] Petering and co-workers[50] first demonstrated that some heterocyclic carboxaldehyde thiosemicarbazones are activated by chelation to iron or copper.[16,51] The same effect of activation by chelation has been observed with 2-acetylpyridine thiosemicarbazones[8,52] and some other heterocyclic thiosemicarbazones[53] as well. Thiosemicarbazones (**Fig. 1.12**) usually bind to metal ions either in the neutral thione form (**i(a)**) or in the thiolate form (**ii**) as bidentate N,S-donor ligands.[54] When complexation occurs it is usually via the dissociation of the acidic proton on the sulphur atom of the thiol (**i(b)**), which results in the formation of a five-membered chelate ring (**iii**).[55]

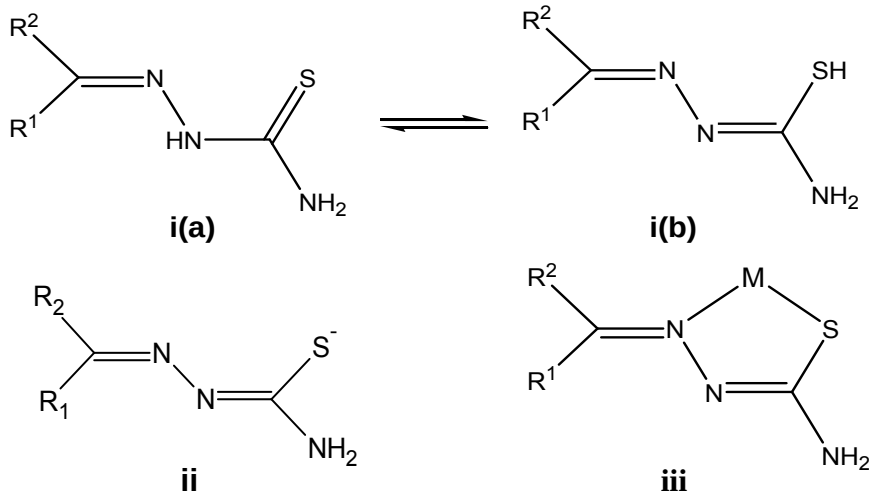

Fig.1.12: Thiosemicarbazone structures (**i(a)** – thione form, **i(b) –** thiol form, **ii** – thiolate form, **iii** – complexation of thiolate form with metal cation).

It is well known that the imine (C=N) and thiourea moieties can form stable complexes with various metal ions.[56] The introduction of a third potential donor atom to the thiosemicarbazone ligand would form a tridentate ligand that should increase its versatility and flexibility in coordination behaviour.[56]

α-*N*-Heterocyclic thiosemicarbazones are known to be amongst the most potent inhibitors of ribonucleotide reductase and it has long been generally assumed that this enzyme, in particular its iron-containing R-2 subunit, is the critical target site.[57,58] It has also been assumed that the iron chelates formed by biotransformation are the actual active species. However, there have been more recent studies that question the universal validity of these assumptions and suggest that there is an involvement of inhibition of topoisomerase II in some of these compounds and their metal complexes.[53,59] It is proposed that the thiosemicarbazones could stabilize cleavable complexes formed by topoisomerase II and DNA leading to apoptosis[47], a natural process of cell destruction in certain cells, induced either by stimulus such as irradiation or toxic drugs, that are genetically programmed to have a limited life span or that are damaged. The stabilizing effect is attributed to be mainly due to the alkylation of thiol residues on the topoisomerase II-DNA complex.[47,60] Topoisomerase is a nuclear enzyme that adjusts the topological state of DNA by breaking and resealing DNA strands resulting in alterations in the linking number.[60]

Topoisomerase II regulates the topological structure of DNA by transient breaking and rejoining of double-stranded DNA in an ATP-dependent manner.[60]

Since 1990, the chemistry of transition metal and non-transition metal complexes of thiosemicarbazones has received considerable attention, largely due to their bioinorganic relevance.[61,62] Even though the combination of a central metal ion and a ligand, which are both supposed to target the same molecular target, seems like a worthwhile task, there has been a lack of research into the biological activity of gallium thiosemicarbazone complexes.

1.4.1. Gallium (III) complexed to thiosemicarbazones

The gallium complex bis(2-acetylpyridine-4,4-dimethyl-3-thiosemicarbazonato-N,N,S)gallium(III) tetrachlorogallate(III) (KP1089, **Fig. 1.13-E**) was the first of the *α-N*-heterocyclic thiosemicarbazone complexes to be assayed for antineoplastic activity in human tumour cell lines. The *in vitro* activity of KP1089 was found to be the highest among the gallium complexes tested, which also provides some evidence implying that the combination of a metal ion and a ligand which are both pharmaceutically active and aimed at attacking the same molecular target displays optimal efficacy.[63]

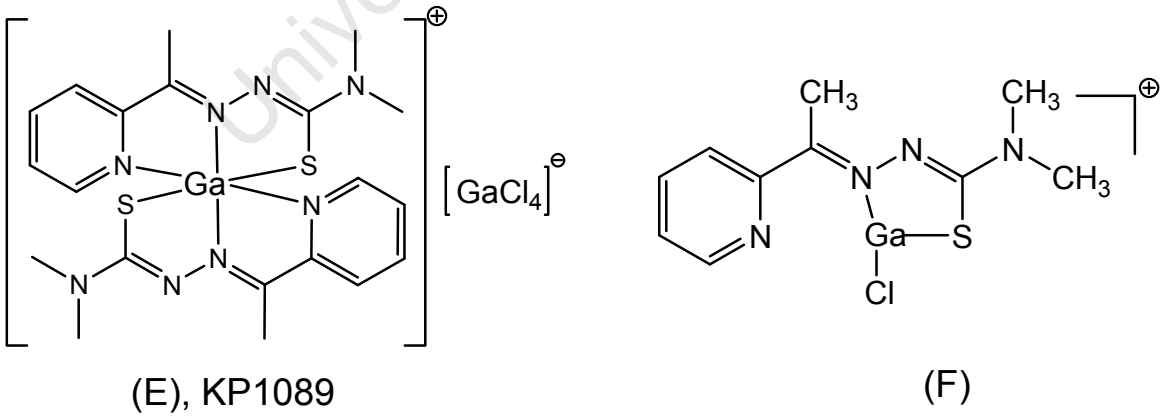

(E), KP1089 (F)

Fig. 1.13: Structures of KP1089 **(E)** and [^{67}Ga]-2-acetylpyridine-4,4-dimethylthiosemicarbazone **(F** – structure proposed by Haghighi-Moghadam *et al*.[49]**)**.

Gallium complexes of different 2-acetylpyridine thiosemicarbazone derivatives have previously been reported[42], although without biological evaluation.[16] It has also been suggested that [^{67}Ga]-2-acetylpyridine-4,4-dimethylthiosemicarbazone (**Fig. 1.13-F**, the proposed structure) could possibly act as a SPECT tracer with a long half-life for tumour imaging applications (i.e. a potential radiopharmaceutical).[64]

1.5. Dendrimers/Metallodendrimers

The basis of the dendrimer structure consists of a core encased within concentric shells formed by covalently linked branches, resulting in a nearly-perfect three-dimensional geometric pattern.[65,66] Dendrimers serve as the central platform for a new generation of nanodevices that are designed to be multifunctional diagnostic and treatment tools.[65] There are many variations of this simple structure that can be produced by following a number of proven synthetic approaches.[65] The addition of another shell corresponds to an increase in the generation (G) number, which coincides with an increase in the diameter and a multiplied increase in the number of branches (**Fig. 1.14**).[65] The average size and structure of a dendrimer within a batch can be controlled by precisely reproducing the subsequent expansion of the branching network.[65]

Generation	G0	G1	G2	G3	G4
# of Surface Groups	3	6	12	24	48
Diameter (nm)	1.4	1.9	2.6	3.6	4.4
2D Graphical Representation					
3D Chemical Structure View					

Fig. 1.14: A representation of the different generations of dendrimers.

Dendrimers can be synthesized via two major routes: (a) the divergent route and (b) the convergent route (**Fig. 1.15**), which differs in their direction of synthesis; either outward from the core or inwardly toward the core, respectively.

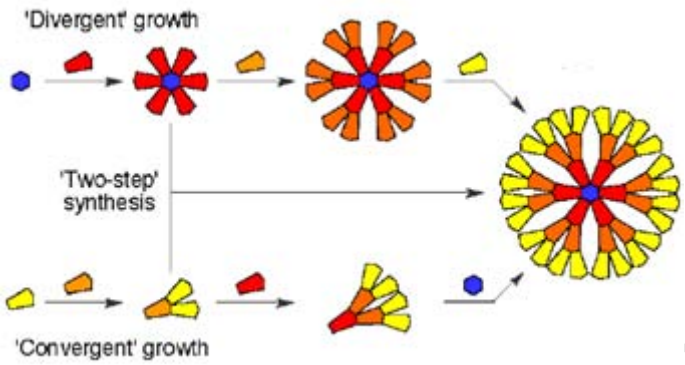

Fig. 1.15: The two major synthetic routes: Divergent (top) and convergent (bottom).

The divergent method was first introduced by Tomalia and co-workers[67] in the 1980's, where they synthesized poly(amidoamine), PAMAM, dendrimers by the growth of branches extending from the core site to the periphery.[66,67] The convergent method was first established by Hawker and Frechet[68] in 1990, whereby the dendrimer surfaces were first synthesized by gradually linking surface unit monomers together.[66] When the growing surface wedges are large enough, several are attached to a suitable core to give a complete dendrimer.[66]

Furthermore, there are many and various properties of dendrimers that include:

- nanoscale sizes that have similar dimensions to important bio-building blocks (e.g. Proteins, DNA).
- number of terminal surface groups that are suitable for bio-conjugation of drugs, signaling groups, targeting moieties or biocompatibility groups, and can be designed with functional groups to augment or resist trans-cellular, epithelial or vascular biopermeability. The surface groups can also be modified to optimize biodistribution.
- an interior void space that can be used to encapsulate small molecule drugs, metals or imaging moieties. Encapsulation in that void space reduces the drug toxicity and facilitates controlled release.[66,69]

Terminal branches of reactive dendrimers will often be capped to neutralize toxicity.[65,66,70] The size of dendrimers, which is closely associated with the generation (G) number, influences not only the cytotoxicity of the dendrimer but also its solubility in aqueous solution and its encapsulation stability.[65,71,72] The extent of the terminal surface and interior functionalities provided by the unique hyper-branched structure of the dendrimers has been researched extensively. There are several studies that have shown that a variety of molecules have retained their function while conjugated to the surface of a dendrimer.[73-76] The ability to modify the dendrimer to fit very specific needs makes dendrimers an exciting and promising subject of research.[65] Targeting agents, chemotherapeutic drugs and fluorescent markers are but a few of the functional groups that have been conjugated to the branches of a dendrimer to change the function of the nanomolecule.[65] Exploiting the multifunctional capabilities of the dendrimer allows for the approach of a problem from many perspectives while still using the same concept.[65]

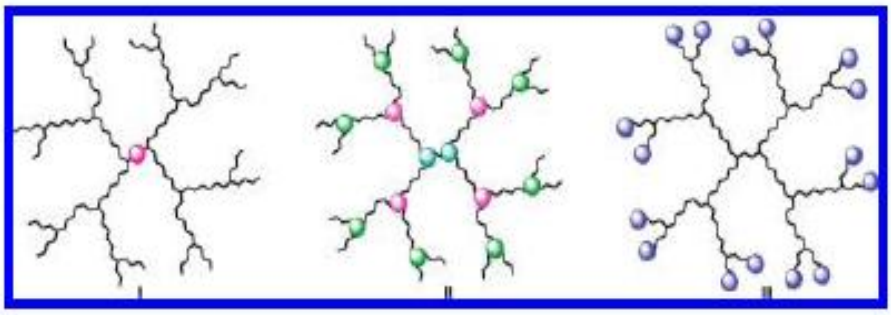

Fig. 1.16: Structural representation of metallodendrimers with emphasis on different locations of metal fragments within the dendritic frame at the center (nodal core), branching points and periphery, respectively.[77]

While the majority of dendrimers reported thus far are organic in nature, there is a rising interest in dendrimers containing transition metal ions.[77-81] Metallodendrimers are particularly interesting as the metallic moieties can easily be integrated into different parts of the dendritic structure, which includes the nodal core, branching points and periphery (**Fig. 1.16**),[79] and their specific properties (e.g. redox, electronic, optic, magnetic, etc.) can be modulated accordingly by collective effects through the hierarchization (generations) and compartmentalization (alternated or segmented constitutive lobes) of the dendritic structure and topology.[77] Enhancement of magnetic resonance imaging (MRI) diagnostic sensitivity can be

achieved through the utilization of dendrimer-based contrast agents.[65] Contrast agents are compounds used to improve the visibility of internal bodily structures in an X-ray image or a MRI. Targeted delivery of contrast agents can improve the contrast between cancerous tissue and healthy tissue.[65] Targeted methods have been proven to promote nanodevice, such as a dendrimer, internalization specifically by cancer tissue.[65] There are some reports that have shown that *in vivo* research into the incorporation of gadolinium into different types of dendrimer-based nanomolecules can produce quality contrast agents for multiple applications.[82-86] The first dendrimer-based contrast agents were developed by Wiener *et al*.[86] in the early 1990's. They created a novel contrast agent by binding Gadolinium chelates to poly(amidoamine), PAMAM, dendrimers (**Fig. 1.17**). Wiener *et al*.[86] discovered that the attachment of Gadolinium to the dendrimer actually accelerates the longitudinal relaxation more than Gadolinium on its own. It has been suggested that although the dendrimer alone has little effect on relaxation rates, the high molecular weight of the dendrimer plays an important role in altering the properties of Gadolinium.[87]

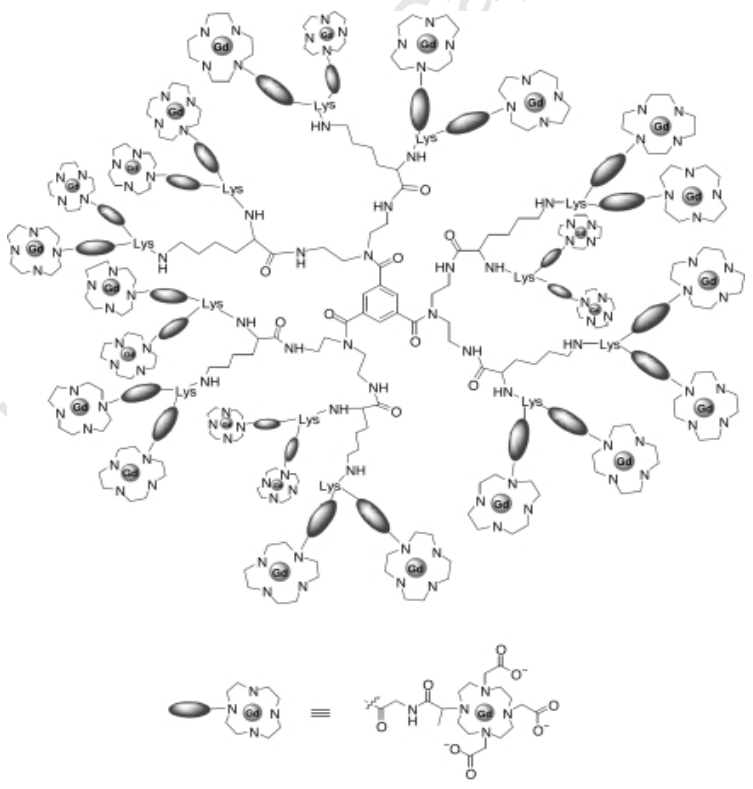

Fig. 1.17: Structure of a gadolinium(III) poly(amidoamine), PAMAM, dendrimer.

Improvements to this novel contrast agent have since been made by many researchers, most notably by Kobayashi and co-workers[82-84] from Kyoto University in Japan. An increased size and molecular weight of the nanoparticle facilitates extended presence of the contrast agent in the blood.[82] The large size of the dendrimer chelate also helps to ensure that the contrast agent does not diffuse out of the intratumoural vessels but into the tumoural tissues.[82] These properties are beneficial when monitoring changes in tumour vasculature over periods of time.[82] In this respect tumours can specifically be targeted by employing the greatest possible advantages of the 'enhanced permeability and retention' (EPR) effect displayed by dendrimers.

1.5.1. The 'enhanced permeability and retention' (EPR) effect

The 'enhanced permeability and retention' (EPR) effect (**Fig. 1.18**) can be defined as being the accumulation of macromolecules at the tumour site due to an increase in blood vessel permeability in diseased cells compared to normal cells.[88,89] The normal endothelial layer surrounding the blood vessels feeding healthy tissues restricts the size of molecules that can diffuse from the blood, whereas the endothelial layer of blood vessels in diseased tissues is more porous providing access to the surrounding tissue.[88] Furthermore, diseased tissue does not usually have a lymphatic drainage system so once macromolecules have entered the tissue they are retained.[88]

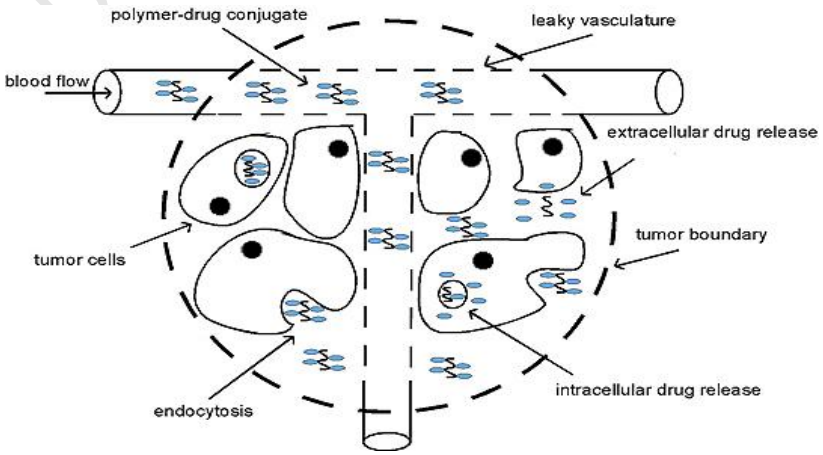

Fig. 1.18: The EPR effect of polymer-drug conjugates on a tumour.

In order to exploit the size selective uptake of drugs into tumour cells effectively, large compounds are required, and in recent years, dendrimers/metallodendrimers have found potential as molecular tools in biological applications,[88,90] especially as nano-carriers,[91] chemotherapeutics[92] and diagnostic/contrast agents[93] for use in imaging.

1.5.2. Metallodendrimers used in Imaging

There is a growing interest in dendrimers as delivery systems for small molecules and radiation contrast agents.[94] Imaging modalities can be used in oncology to diagnose, locate, stage, plan treatment and potentially to find recurrence. Computed tomography (CT) and MRI are two standard methods of imaging associated with cancer diagnoses. Gadolinium paramagnetic contrast agents for MRI have been complexed with dendrimer molecules over the last two decades for contrast enhancement, improved clearance characteristics and for potential targeting.[95] Gd-labelled PAMAM dendrimers have been used for visualizing both tumour vasculature and lymphatic involvement. Changes in tumour permeability were visualized by MRI using generation 8 Gd-PAMAM contrast agents after a single large dose of radiation treatment.[93,96] Gd-labelled generation 6 PAMAM dendrimers were also shown to accumulate in the sentinel lymph nodes (**Fig. 1.19**), which are routinely imaged before surgery for breast cancer and melanoma.[97]

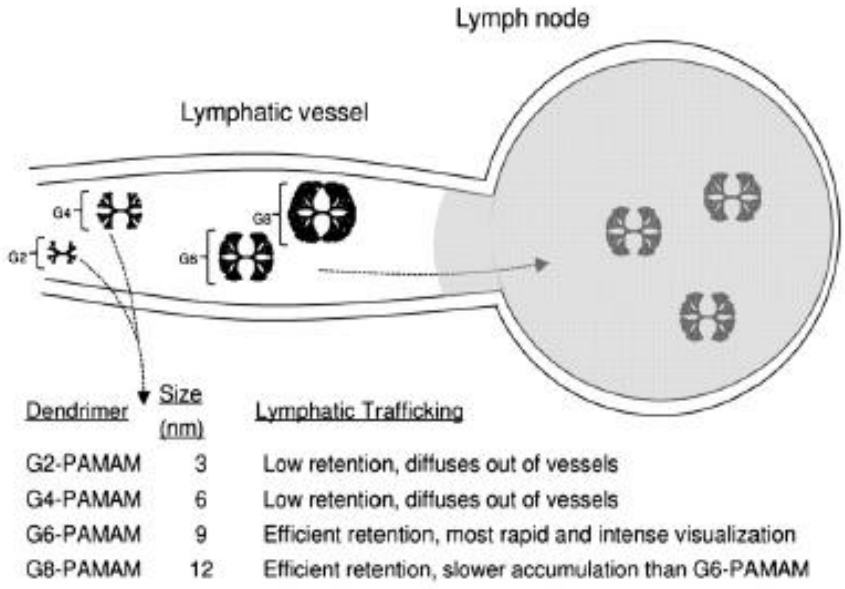

Fig. 1.19: Visualization of sentinel lymph node via gadolinium-labelled PAMAM dendrimers. Rapid and enhanced visualization of the sentinel lymph node using magnetic resonance lymphangiography is achieved by optimizing the size of gadolinium-labelled PAMAM contrast agents.[93]

Similarly to Gd-dendrimer conjugates for MRI, iodinated contrast agents used for CT could benefit from dendrimer conjugation as it provides improved retention times and the potential for targeted delivery.[93] With the growing interest in dendrimers as delivery vehicles, techniques for studying these polymers in biological systems are needed. The labelling of dendrimers with radioisotopes coupled with radiochemical detection is a very effective method for studying the uptake and fate of compounds *in vivo*.[94] There has been a few reports describing the incorporation of radioisotopes into dendrimer structures,[94,98] but overall there has been a lack of research into the synthesis and biological activity of radiolabelled dendrimers as potential radiopharmaceuticals.

1.6. General Conclusions

There has been a lot of interest shown in the chemistry of transition metal and non-transition metal complexes of thiosemicarbazones. This can mainly be attributed to the thiosemicarbazone ligand's variable donor properties, structural diversity and well established biological applications. It should be noted that, while there are quite a number of reports on the biological activities of gallium(III) thiosemicarbazones, reports on studies of radiolabelled gallium(III) thiosemicarbazones, especially as imaging agents, are still quite limited.

There has also been a large number of reports on dendrimers. However, transition metal containing dendrimers have risen as a topic of interest. In recent years metallodendrimers have shown potential in biological applications, especially as diagnostic/ contrast agents for use in imaging.

1.7. Aims and Objectives

1.7.1. Aims

The general aims of this research project are to synthesize and characterize various mononuclear, and possibly binuclear, radiolabelled gallium thiosemicarbazones, evaluate their radiolabelling properties and study their radiobiology (i.e. *in vitro* cell uptake studies).

The aims are also to synthesize α-diimine ligands containing zero (*G0*) and first generation (*G1*) dendritic wedges, and to complex these ligands with palladium. These ligands will form part of a preliminary study where they will be tested for their radiolabelling ability with ^{109}Pd.

1.7.2. Objectives

The objectives of this research project are to:

1.7.2.1. Synthesize and characterize a series of thiosemicarbazone ligands as outlined in **equation (1.1)**.

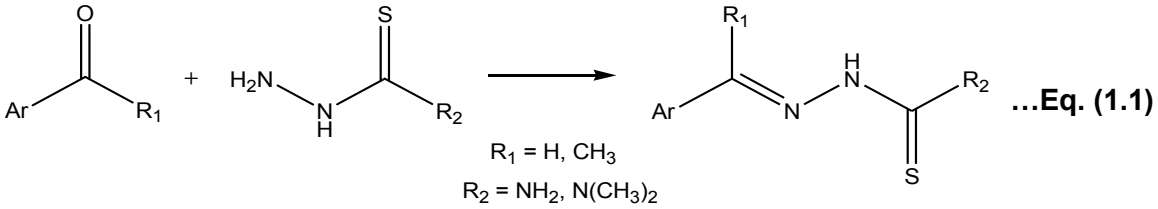

…Eq. (1.1)

1.7.2.2. Synthesize radiolabelled gallium(III) thiosemicarbazones using ligands synthesized in **equation (1.1)**.

1.7.2.3. Perform radiochemical stability studies of successfully radiolabelled gallium(III) thiosemicarbazones.

1.7.2.4. Evaluate a few of the radiolabelled gallium(III) thiosemicarbazones for their *in vitro* cell uptake abilities.

1.7.2.5. Synthesize and characterize the α-diimine core, dendritic (G0 and G1) wedges and subsequently the dendritic (G0 and G1) ligands.

1.7.2.6. Synthesize and characterize new dendritic complexes as in **equation (1.2)** using $PdCl_2$(COD).

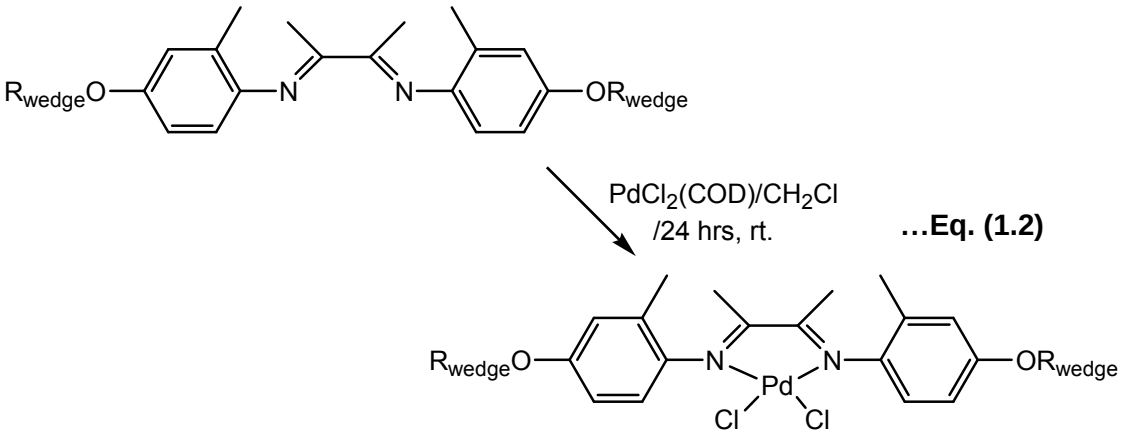

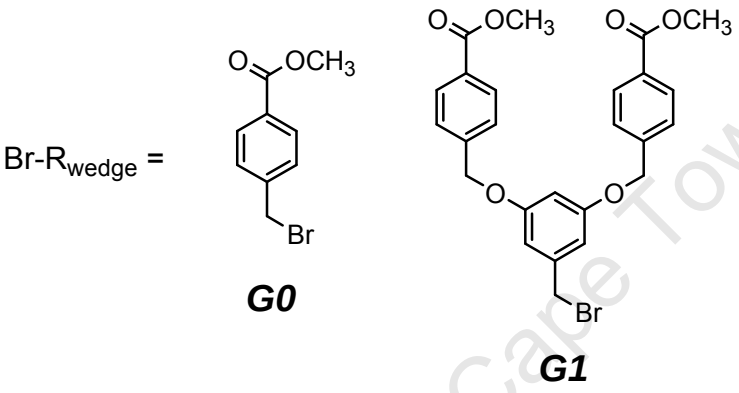

1.7.2.7. Test the radiolabelling ability of polyaryl(ether) dendrimers (*G0* and *G1*) with ^{109}Pd.

1.8. References

1. Dr Margaret Chan, http://www.who.int/dg/speeches/2008/20080827/en/index.html (accessed 21 January 2009).

2. World Health Organisation, Cancer, http://www.who.int/mediacentre/factsheets/fs297/en/index.html (accessed 19 January 2010).

3. World Health Organisation, Cancer, http://www.who.int/topics/cancer/en/ (accessed 19 January 2010).

4. The Free Dictionary, Metastasis, http://www.thefreedictionary.com/metastasis (accessed 19 January 2010).

5. M. Galanski, V. B. Arion, M. A. Jakupec and B. K. Keppler, *Curr. Pharm. Design*, 2003, **9**, 2078.

6. R. Alberto, in *Bioorganometallics: Biomolecules, Labeling, Medicine*, ed. G. Jaouen, Wiley-VCH, Weinheim, 2006, p. 97.

7. D. J. Hnatowich, in *Metal Compounds in Cancer Therapy*, ed. S. P. Fricker, Chapman & Hall, London, 1994, p. 215.

8. T. S. Lobana, R. Sharma, G. Bawa and S. Khanna, *Coord. Chem. Rev.*, 2009, **253**, 977.

9. C. A. Luttropp, J. A. Jackson, B. J. Jones, M. –H. Sohn, R. E. Lynch and K. A. Morton, *J. Nucl. Med.*, 1998, **39(8)**, 1405.

10. R. E. Weiner and M. L. Thakur, *Appl. Radiat. Isot.*, 2002, **57**, 749.

11. H. F. Kung, M. P. Kung and S. R. Choi, *Semin. Nucl. Med.*, 2003, **33**, 2.

12. A. I. Kassis, H. Korideck, K. Wang, P. Pospisil and S. J. Adelstein, *Molecules*, 2008, **13**, 391.

13. G. Krishna, J. Mao and B. Almassian, *Pharm. Dev. Technol.*, 1999, **4(1)**, 71.

14. H. L. Elford, M. Freese, E. Passamani and H. P. Morris, *J. Biol. Chem.*, 1970, **245**, 5228.

15. P. Collery, B. Keppler, C. Madoulet and B. Desoize, *Crit. Rev. Oncol. Hemat.*, 2002, **42**, 283.

16. V. B. Arion, M. A. Jakupec, M. Galanski, P. Unfried and B. K. Keppler, *J. Inorg. Biochem.*, 2002, **91**, 298.

17. Z. Guo and P. J. Sadler, *Angew. Chem. Int. Ed. Engl.*, 1999, **38**, 1512.

18. M. J. Hannon, *Pure Appl. Chem.*, 2007, **79(12)**, 2243.

19. P. C. A. Bruijnincx and P. J. Sadler, *Curr. Opin. Chem. Biol.*, 2008, **12**, 197.

20. Y. Kang, S. Kang, B. Yoo, S. O. Kang and J. Ko, *Bull. Korean Chem. Soc.*, 1998, **19(1)**, 63.

21. C. R. Kowol, E. Reisner, I. Chiorescu, V. B. Arion, M. Galanski, D. V. Deubel and B. K. Keppler, *Inorg. Chem.*, 2008, **47**, 11032.

22. E. Reisner, V. B. Arion, B. K. Keppler and A. J. L. Pombeiro, *Inorg. Chim. Acta*, 2008, **361**, 1569.

23. M. J. Clarke, F. Zhu and D. R, Frasca, *Chem. Rev.*, 1999, **99**, 2511.

24. K. H. Thompson and C. Orvig, *Dalton Trans.*, 2006, 761.

25. Y. Jung and S. J. Lippard, *Chem. Rev.*, 2007, **107**, 1387.

26. E. Froehlich, A. Gupta, J. Provencher-Mandeville, E. Asselin, J. Bariyanga, G. Berube and H. –A. Jajmir-Riahi, *DNA Cell Biol.*, 2009, **28(1)**, 31.

27. H. A. Barot, M. Laverick and A. H. Nias, *Br. J. Radiol.*, 1985, **58(685)**, 51.

28. Int. Patent Application No. PCT/US2002/019859, Publication No. WO/2003/000298 (published Jan. 3, 2003)(Isotope Solutions, Inc. and Wayne Court, applicants).

29. A. C. F. Caires, *Anti-Cancer Agents Med. Chem.*, 2007, **7**, 484.

30. Z. Guo and P. J. Sadler, *Adv. Inorg. Chem.*, 1999, **49**, 183.

31. M. J. Clarke, *Coord. Chem. Rev.*, 2003, **236**, 209.

32. G. Sava, R. Gagliardi, A. Bergamo, E. Allessio and G. Mestroni, *Anticancer Res.*, 1999, **19**, 969.

33. B. K. Keppler, M. Henn, U. M. Juhl, M. R. Berger, R. Niebl and F. E. Wagner, *Prog. Clin. Biochem. Med.*, 1989, **10**, 41.

34. R. E. Morris, R. E. Aird, P. Del S Murdoch, H. Chen, J. Cummings and N. D. Hughes, *J. Med. Chem.*, 2001, **44**, 3616.

35. J. D. Hoeschele, A. Habtemariam, J. Muir and P. J. Sadler, *Dalton Trans.*, 2007, **43**, 4974.

36. B. T. Khan, J. Bhatt, K. Najmuddin, S. Shamsuddin and K. Annapoorna, *J. Inorg. Biochem.*, 1991, **44**, 55.

37. G. Enjun, L. Cong, Z. Mingchang, L. Huakuan, W. Qiong and L. Lei, *Anti-cancer agents in Med. Chem.*, 2009, **9(3)**, 356.

38. Al-Allaf and Rashan, *Boll. Chem. Farmac.*, 2001, **140**, 205.

39. S. Chakraborty, T. Das, S. Banerjee, H. D. Sarma and M. Venkatesh, *J. Nucl. Med. Mol. Imaging*, 2007, **51(1)**, 16.

40. M. A. Jakupec, M. Galanski, V. B. Arion, C. G. Hartinger and B. K. Keppler, *Dalton Trans.*, 2008, **2**, 183.

41. M. Frezza, C. N. Verani, D. Chen and Q. P. Dou, *Lett. Drug Des. Discov.*, 2007, **4**, 311.

42. C. L. Ferreira, E. Lamsa, M. Woods, Y. Duan, P. Fernando, C. Bensimon, M. Kordos, K. Guenther, P. Jurek and G. E. Kiefer, *Bioconjugate Chem.*, 2010, **21**, 531.

43. A. R. Jalilian, P. Mehdipour, M. Akhlaghi, H. Yousefnia and K. Shafaii, *Sci. Pharm.*, 2009, **77**, 343.

44. S. Jurisson, D. Berning, W. Jia and D. Ma, *Chem. Rev.*, 1993, **93**, 1137.

45. M. Fani, J. P. Andre and H. R. Maecke, *Contrast Media Mol. I.*, 2008, **3**, 67.

46. E. Boros, C. L. Ferreira, J. F. Cawthray, E. W. Price, B. O. Patrick, D. W. Wester, M. J. Adam and C. Orvig, *J. Am. Chem. Soc.*, 2010, **132**, 15726.

47. I. Dilovic, M. Rubcic, V. Vrdoljak, S. K. Pavelic, M. Kralj, I. Piantanida and M. Cindric, *Bioorgan. Med. Chem.*, 2008, **16**, 5189.

48. X. Du, C. Guo, E. Hansall, P. S. Doyle, C. R. Caffrey, T. P. Holler, J. H. Mokerrov and F. E. Cohen, *J. Med. Chem.*,2002, **45**, 2695.

49. J. P. Scovill, D. L. Klayman and D. G. Franchino, *J. Med. Chem.*, 1982, **25**, 1261.

50. L. A. Saryan, E. Ankel, C. Krishnamurti, D. H. Petering and H. Elford, *J. Med. Chem.*, 1979, **22**, 1218.

51. A. G. Quiroga and C. N. Ranninger, *Coord. Chem. Rev.*, 2004, **248**, 119.

52. L. A. Saryan, E. Ankel, C. Krishnamurti, D. H. Petering and H. Elford, *J. Med. Chem.*, 1979, **22**, 1218.

53. D. X. West, S. B. Padhye and P. B. Sonawane, *Struct. Bonding (Berl.)*, 1991, **76**, 1.

54. J. Easmon, G. P. Pürstinger, G. Heinisch, T. Roth, H. H. Fiebig, W. Holzer, W. Jäger, M. Jenny and J. Hofmann, *J. Med. Chem.*, 2001, **44**, 2164.

55. R. Prabhakaran, R. Huang, S. V. Renukadevi, R. Karvembu, M. Keller and K. Natarajan, *Inorg. Chim. Acta*, 2008, **361**, 2547.

56. I. Pal, F. Basuli and S. Bhattacharya, *Proc. Indian Acad. Sci.(Chem. Sci.)*, 2002, **114**, 255.

57. W. Liu, X. Li, Z. Li, M. Zhang and M. Song, *Inorg. Chem. Commun.*, 2007, **10**, 1485.

58. L. Thelander and A. Gräslund, *J. Biol. Chem.*, 1983, **258**, 4063.

59. E. C. Moore and A. C. Sartorelli, *Pharmcol. Ther.*, 1984, **24**, 439.

60. M. C. Miller III, C. N. Stineman, J. R. Vance, D. X. West and I. H. Hall, *Appl. Organomet. Chem.*, 1999, **18**, 4131.

61. J. Chen, Y. –W. Huang, G. Liu, Z. Afrasiabi, E. Sinn, S. Padhye and Y. Ma, *Toxicol. Appl. Pharmacol.*, 2004, **197**, 40.

62. S. Halder, S. –M. Peng, G. –H. Lee, T. Chatterjee, A. Mukherjee, S. Dutta, U. Sanyal and S. Bhattacharya, *New J. Chem.*, 2008, **32(1)**, 105.

63. A. V. Rudnev, L. S. Foteeva, C. Kowol, R. Berger, M. A. Jakupec, V. B. Arion, A. R. Timerbaev and B. K. Keppler, *J. Inoorg. Biochem.*, 2006, **100**, 1819.

64. F. Haghighi Moghadam, A. R. Jalilian, A. Nemati and M. Abedini, *J. Radioanal. Nucl. Ch.*, 2007, **272(1)**, 115.

65. I. J. Majoros, C. R. Williams and J. R. Baker Jr., *Curr. Top. Med. Chem.*, 2008, **8**, 1165.

66. D. J. Bharali, M. Khalil, M. Gurbuz, T. M. Simone and S. A. Mousa, *Int. J. Nanomed.*, 2009, **4**, 1.

67. D. A. Tomalia, H. Baker, J. Dewald, M. Hall, G. Kallos, S. Martin, J. Roeck, J. Ryder and P. Smith, *Polym. J.*, 1985, **17(1)**, 117.

68. C. J. Hawker and J. M. J. Frechet, *J. Am. Chem. Soc.*, 1990, **112**, 7638.

69. D. A. Tomalia, L. A. Reyna and S. Svenson, *Biochem. Soc. Trans.*, 2007, **35(1)**, 61.

70. R. Duncan and L. Izzo, *Adv. Drug Deliv. Rev.*, 2005, **57**, 2215.

71. U. Gupta, H. B. Agashe, A. Asthana and N. K. Jain, *Biomacromolecules*, 2006, **7**, 649.

72. I. Lee, B. D. Athey, A. W. Wetzel, W. Meixner and J. R. Baker Jr., *Macromolecules*, 2002, **35**, 4510.

73. J. F. Kukowska-Latallo, K. A. Candido, Z. Cao, S. S. Nigavekar, I. J. Majoros, T. P. Thomas, L. P. Balogh, M. K. Khan and J. R. Baker Jr., *Cancer Res.*, 2005, **65**, 5317.

74. C. C. Lee, E. R. Gillies, M. E. Fox, S. J. Guillauden, J. M. J. Frechet, E. E. Dy and F. C. Szoka, *Proc. Natl. Acad. Sci. U.S.A.*, 2006, **103**, 16649.

75. S. Gurdag, J. Khandare, S. Stapels, L. H. Matherly and R. M. Kannan, *Bioconjug. Chem.*, 2006, **17**, 275.

76. E. R. Gillies and J. M. J. Frechet, *Drug Discov. Today*, 2005, **10**, 35.

77. C. Cordovilla, S. Coco, P. Espinet and B. Donnio, *J. Am. Chem. Soc.*, 2010, **132(4)**, 1424.

78. G. R. Newkome, C. N. Moorefield and F. Vogtle, In *Dendrimers and Dendron: Concepts, Synthesis and Applications*, Wiley & Sons., Weinheim, 2001.

79. E. C. Constable, *Chem. Commun.*, 1997, 1073.

80. M. A. Hearshaw and J. R. Moss, *Chem. Commun.*, 1999, 1.

81. D. Méry and D. Astruc, *Coord. Chem. Rev.*, 2006, **250**, 1965.

82. H. Kobayashi, N. Sato, S. Kawamoto, T. Saga, A. Hiraga, T. Ishimori, J. Konishi, K. Togashi and M. W. Brechbiel, *Magn. Reson. Med.*, 2001, **46**, 579.

83. H. Kobayashi, S. Kawamoto, T. Saga, N. Sato, T. Ishimori, J. Konishi, K. Ono, K. Togashi and M. W. Brechbiel, *Bioconjug. Chem.*, 2001, **12**, 587.

84. H. Kobayashi, T. Saga, S. Kawamoto, N. Sato, A. Hiraga, T. Ishimori, J. Konishi, K. Togashi and M. W. Brechbiel, *Cancer Res.*, 2001, **61**, 4966.

85. S. D. Konda, M. Aref, M. W. Brechbiel and E. C. Wiener, *Investig. Radiol.*, 2000, **35**, 50.

86. E. C. Wiener, M. W. Brechbiel, H. Brothers, R. L. Magin, O. A. Gansow, D. A. Tomalia and P. C. Lauterbur, *Magn. Reson. Med.*, 1994, **31**, 1.

87. S. D. Swanson and C. R. Williams, In *Dendrimer based nanomedicine*, eds. I. J. Majoros and J. R. Baker Jr., Pan Stanford Publishing, 2008.

88. P. Govender, N. C. Antonels, J. Mattson, A. K. Renfrew, P.J. Dyson, J. R. Moss, B. Therrien and G. S. Smith, *J. Organomet. Chem.*, 2009, **694**, 3470.

89. D. F. Baban and L.W. Seymour, *Adv. Drug Delivery Rev.*, 1998, **34**, 109.

90. D. A. Tomalia, L.A. Reyna and S. Svenson, *Biochem. Soc. Trans.*, 2007, **35**, 61.

91. F. Aulenta, W. Hayes and S. Rannard, *Eur. Polym. J.*, 2003, **39**, 1741.

92. A. Agarwal, S. Saraf, A. Asthana, U. Gupta, V. Gaibhive and N. K. Jain, *Int. J. Pharm.*, 2008, **350**, 3.

93. J. B. Wolinsky, and M. W. Grinstaff, *Adv. Drug Deliv. Rev.*, 2008, **60**, 1037.

94. B. D. Maxwell, H. Fujiwara, S. Habibi-Goudarzi, J. P. Ortiz and S. J. Logusch, *J. Labelled Cpd. Radiopharm.*, 1998, **XLI**, 935.

95. E. C. Wiener, S. Konda, A. Shadron, M. Brechbiel and O. Gansow, *Invest. Radiol.*, 1997, **32**, 748.

96. H. Kobayashi, K. Reijnders, S. English, A. T. Yordanov, D. E. Milenic, A. L. Sowers, D. Citrin, M. C. Krishna, T. A. Waldmann, J. B. Mitchell and M. W. Brechbiel, *Clin. Cancer Res.*, 2004, **10**, 7712.

97. H. Kobayashi, S. Kawamoto, M. Bernardo, M. W. Brechbiel, M. V. Knopp and P. L. Choyke, *J. Control. Release*, 2006, **111**, 343.

98. M. C. Parrott, S. R. Benhabbour, C. Saab, J. A. Lemon, S. Parker, J. F. Valliant and A. Adranov, *J. Am. Chem. Soc.*, 2009, **131**, 2906.

Chapter 2:

Synthesis and characterization of monothiosemicarbazone and dithiosemicarbazone ligands

2.1. Introduction

Thiosemicarbazones have been known to exhibit various biological activities and have thus attracted considerable attention.[1-4] Thiosemicarbazones belong to a large group of thiourea derivatives and they have been known for their donor ligand ability.[1,5-8] Thiosemicarbazone ligands can be synthesized via the condensation of an aldehyde or ketone with thiosemicarbazide.[9] A thiosemicarbazone ligand has different R (R^1-R^4), alkyl or aryl, substituents (**Fig. 2.1**), thus various derivatives of the ligand can be formed.[9]

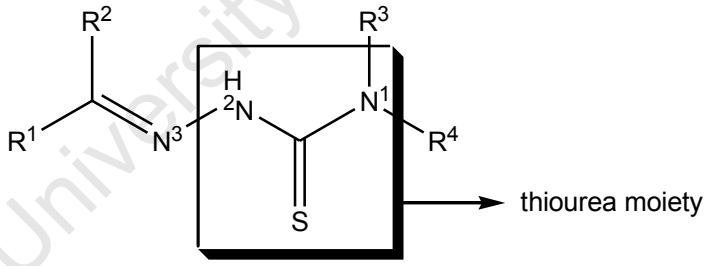

Fig. 2.1: A structural representation of a thiosemicarbazone ligand.

A thiosemicarbazone ligand based on an aldehyde has a hydrogen atom as the R^2 substituent, whereas the ligand based on a ketone may have different alkyl or aryl groups as the R^2 substituent. A thiosemicarbazone based on a ketone may at times have R^1 and R^2 substituents that are the same. The R^1 substituent may be alkyl, aryl or heteroaromatic. The heteroaromatic group provides the nitrogen, oxygen or sulphur that acts as the third donor atom in coordination of a metal to the ligand.

The substituents on the N^1 nitrogen (i.e. R^3 and R^4) may be hydrogens, alkyls, aryls or part of a cyclic group.[9]

Dithiosemicarbazone ligands are dimeric structures that consist of two thiosemicarbazone moieties. These thiosemicarbazone moieties are connected via their thioamide nitrogen atoms to an aliphatic or aromatic spacer (**Fig. 2.2**).[10]

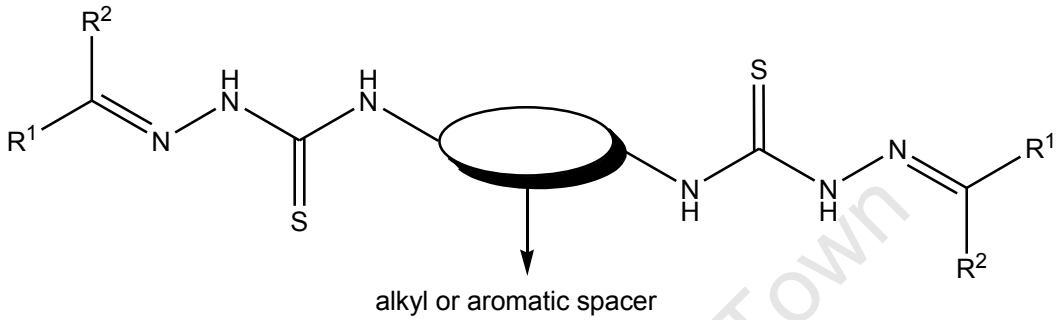

Fig. 2.2: A structural representation of a dithiosemicarbazone ligand.

Thiosemicarbazones are interesting molecules as biologically active compounds, as have been shown in literature studies.[1-9] It would thus also be interesting to study the radiolabelling ability of a series of these ligands as their respective radiolabelled complexes could possibly act as imaging agents. This study should prove interesting as similar studies on the radiolabelling abilities of thiosemicarbazones as a function of their chemical structures have, to this author's knowledge, not previously been reported in literature.

2.2. Monothiosemicarbazone ligands

2.2.1. Synthesis of monothiosemicarbazones

The monothiosemicarbazones (**Table 2.1**, **1**-**18** and **20**-**21**) were prepared by either dissolving the respective thiosemicarbazide in distilled water or by having the respective thiosemicarbazide suspended in ethanol and adding an ethanolic solution of the aldehyde/ketone to the thiosemicarbazide solution/suspension. The reaction

is represented by **equation (2.1)**. The mixture was reacted at room temperature or using temperatures ranging between 60-100°C.

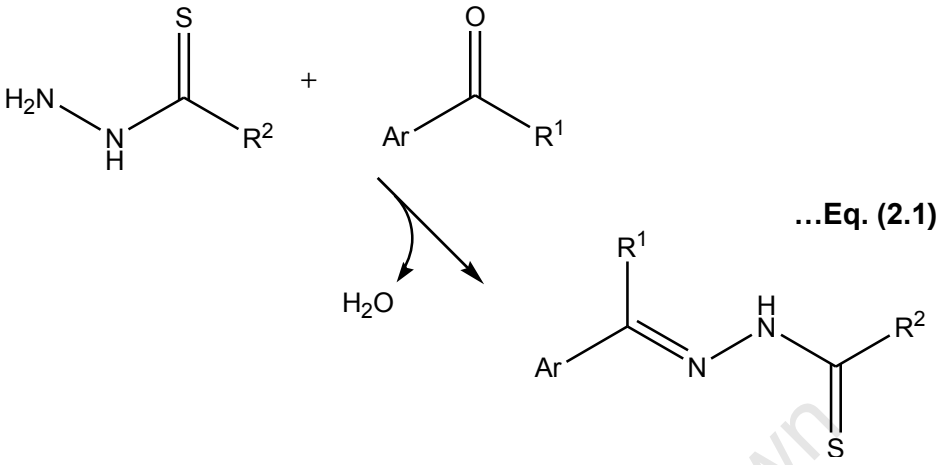

…Eq. (2.1)

Table 2.1: The series of monothiosemicarbazone ligands (**1**-**18**, **20** and **21**) that were synthesized.

Ar	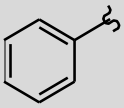 (R^1; R^2)	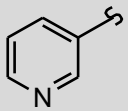 (R^1; R^2)	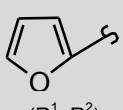 (R^1; R^2)	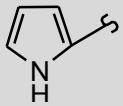 (R^1; R^2)	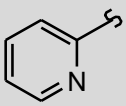 (R^1; R^2)
Ligands	**1** (H; NH_2)	**4** (H; NH_2)	**2** (H; NH_2)	**9** (CH_3; NH_2)	**5** (H; NH_2)
	3 (H; $N(CH_3)_2$)	**17** (H; $N(CH_3)_2$)	**7** (CH_3; NH_2)	**12** (CH_3; $N(CH_3)_2$)	**6** (CH_3; NH_2)
	8 (CH_3; NH_2)	**18** (CH_3; $N(CH_3)_2$)	**15** (H; $N(CH_3)_2$)	**13** (H; $N(CH_3)_2$)	**10** (CH_3; $N(CH_3)_2$)
			16 (CH_3; $N(CH_3)_2$)	**14** (H; NH_2)	**11** (H; $N(CH_3)_2$)
					20 (H; NHPh)
					21 (CH_3; NHPh)

The synthesis of the *N,N*-dimethylthiosemicarbazone ligands produced four new ligands (**12**, **16**, **17** and **18**) as part of this study. Acetic acid was used in the synthesis of the ligands where a methyl (R^1 = CH_3) was attached to the imine bond due to the fact that the ketones are generally less reactive than their respective

aldehydes. This is due to the alkyl chain of a ketone having an inductive effect that causes the carbon (in the carbonyl group) to be less electrophilic, thus being less reactive when compared to the aldehyde. The synthesis of the monothiosemicarbazone ligands proceeds via a Schiff-base condensation reaction mechanism (**Scheme 2.1**) whereby an imine bond is formed and water is produced as a by-product. The synthesis of the thiosemicarbazones produced white or orange-yellow powders in low to good yields (33% – 87%). The monothiosemicarbazone ligands are soluble in ethanol, methanol and DMSO. The *N,N*-dimethylthiosemicarbazone ligands are also soluble in dichloromethane and chloroform. The ligands were characterized using ^{1}H-NMR and IR spectroscopy, as well as elemental analysis.

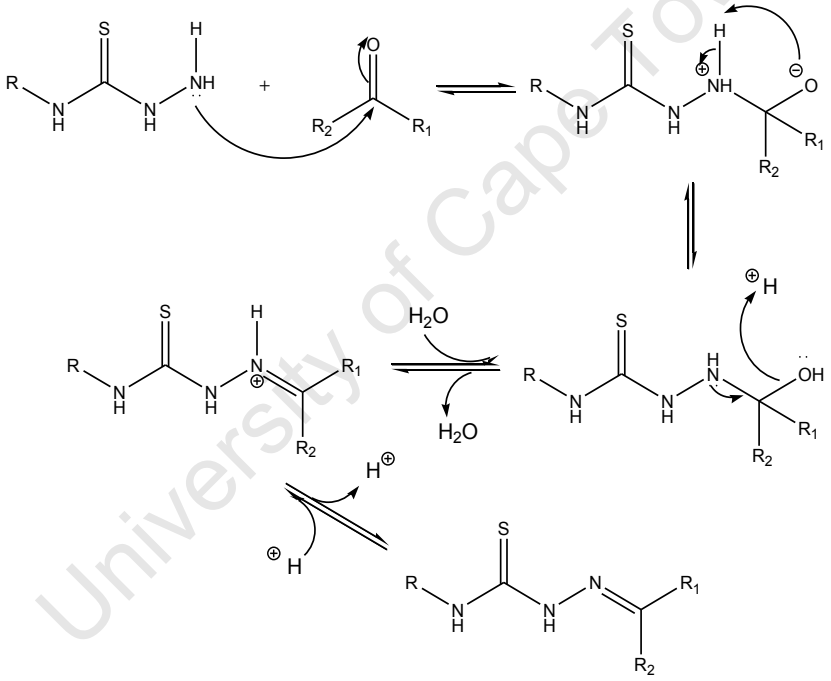

Scheme 2.1: Mechanism of a Schiff-base condensation reaction.

2.2.2. NMR spectra of monothiosemicarbazones

2.2.2.1. ^{1}H-NMR spectra

The ^{1}H-NMR spectra of the thiosemicarbazone ligands (non-substituted terminal amines **1**, **2**, **4**-**9** and **14**) show two peaks between 7.61-8.38 ppm accounting for the

protons on the primary/terminal amine (-NH_2). A peak is seen at 7.61-8.13 ppm whereas the other peak occurs slightly further downfield at 8.19-8.38 ppm. This type of splitting was also observed by Dilovic *et al.*[1] in the synthesis of a salicylaldehyde thiosemicarbazone and reported by Lobana *et al*.[9] in a review on thiosemicarbazone derivatives of metals. The reason for this splitting could be due to the lone pair of electrons on the amine nitrogen donating back to form a double bond with the electrophilic carbon, which would cause the C=S bond to push electrons onto the sulphur to give it a negative charge (**Fig. 2.3**).[9] There would thus be no free rotation about the carbon-nitrogen bond, which means the amine protons are in different environments. This would thus give two separate peaks in the ^{1}H-NMR spectrum.

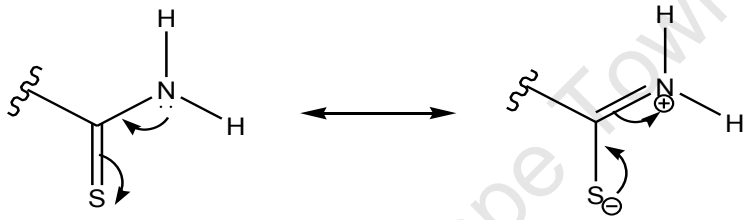

Fig. 2.3: Resonance occurring at the amine terminal of a thiosemicarbazone.

The thiosemicarbazone ligands (non-substituted terminal amines) where R^1 = H (**1**, **2**, **4**, **5** and **14**) shows a singlet peak occurring just above 8.00 ppm accounting for the proton on the imine carbon (as can be seen in **Fig. 2.4**). There is, however, a singlet peak appearing at 2.33-2.41 ppm in the spectrum of the thiosemicarbazone (where R^1 = CH_3, **6**-**9**) that accounts for the methyl group on the imine bond. The aromatic/heteroaromatic protons are found to occur between 6.04-8.95 ppm for all ligands.

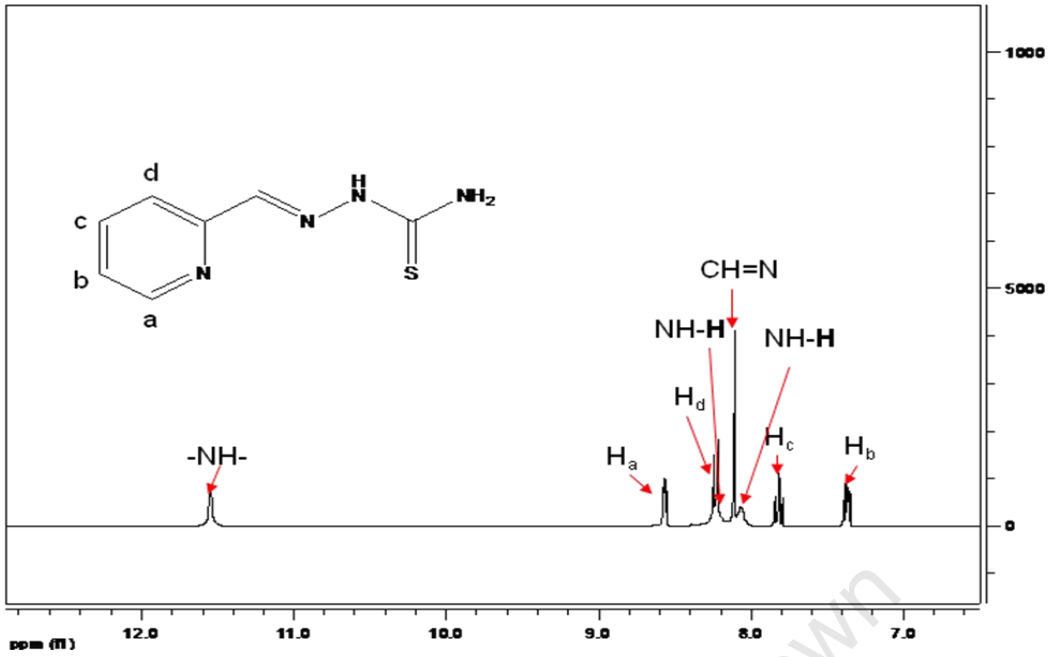

Fig. 2.4: ^{1}H-NMR (in DMSO-d_6) spectrum of 2-formylpyridine thiosemicarbazone, **5** (representative spectrum).

The hydrazinic protons (-NH-) of the thiosemicarbazone ligands are found to be the furthest downfield of all the proton peaks (**Table 2.2**, on the next page). This is partially due to the fact that the proton is directly bonded to a nitrogen that is situated between an imine bond (C=N) and a C=S group, all of which are significant electron-withdrawing groups. Another reason for the downfield shift of the hydrazinic proton was reported by Mendes *et al.*[11] and Rebolledo *et al.*[12] Both reported that the downfield shift of the hydrazinic proton in a thiosemicarbazone could be due to hydrogen bonding that occurs between the proton and an oxygen of the deuterated dimethyl sulfoxide solvent. However, the hydrazinic proton still appears downfield when the sample is submitted in deuterated chloroform. The hydrazinic proton of the ligands where $R^1 = CH_3$ appears more upfield (10.21-10.24 ppm) when compared to the hydrazinic proton of the ligands where $R^1 = H$ (11.41-11.56 ppm). This could possibly be due to the inductive effect exerted on the ligand by the methyl group bonded to the imine. This inductive effect provides some shielding of the hydrazinic proton when compared to the ligands where a proton is bonded to the imine moiety (i.e. $R^1 = H$). There is also no evidence of both E and Z isomers being present.

Table 2.2: Summary of ^{1}H-NMR shifts (ppm) of thiosemicarbazone ligands (non-substituted terminal amines) in DMSO-d_6.

Compound	Ar	R	-CH=N-	-CH_3	-NH_2	-NH-
1	Benzene	H	8.09	—	7.98/8.19	11.42
2	2-furan	H	8.00	—	7.61/8.19	11.41
4	3-pyridine	H	8.10	—	8.26	11.56
5	2-pyridine	H	8.11	—	8.07/8.22	11.55
6	2-pyridine	CH_3	—	2.41	8.13/8.38	10.29
7	2-furan	CH_3	—	2.26	7.69/8.24	10.24
8	Benzene	CH_3	—	2.33	7.95/8.26	10.21
9	2-pyrrole	CH_3	—	2.15	8.08/8.21	11.35
14	2-pyrrole	H	7.80	—	7.85/7.95	11.28

The ^{1}H-NMR spectrum (in $CDCl_3$) of the 2-acetylpyridine-4,4-dimethylthiosemicarbazone ligand, **10**, shows that the product contains a mixture of isomers (possibly a *Z*, *E* and thiol form), as was reported by J. Chan *et al*.[13] The ^{1}H-NMR spectrum of ligand **10** displays broad peaks when submitted in DMSO-d_6. There are peaks occurring between 2.37-2.61 ppm that account for the protons on the methyl group of each of the isomers. The methyls attached to the terminal (tertiary) nitrogen of the isomers occur as a multiplet at 3.48 ppm. The protons on the pyridine ring of the isomers appear between 7.25-8.73 ppm, occurring mostly as multiplets. Interestingly, the hydrazinic proton of one of the isomers occurs at 8.46 ppm as a broad singlet, whereas the hydrazinic proton of the other isomers occurred further downfield at 14.82 and 15.51 ppm. The reason for this is still not quite understood.

The other *N,N*-dimethylthiosemicarbazones (**3**, **10**-**13** and **15**-**18**) show the presence of just one set of peaks, i.e. one isomer. The aromatic protons are found to appear between 6.39-8.63 ppm for the ligands. The dimethyl protons appear more upfield at

3.36-3.37 ppm for the pyrrole derivatives (**12** and **13**), 3.43-3.48 ppm for the pyridine derivatives (**10**, **11, 17** and **18**), 3.29 ppm for the benzyl derivative (**3**) and 3.27-3.39 ppm for the furan derivatives (**15** and **16**). The peak accounting for the proton on the imine bond of ligands **11** (**Fig. 2.5**) and **13** appears between the aromatic peaks at 7.50 and 7.20 ppm, respectively. The peak for the proton on the imine bond of **15** occurs slightly more downfield at 8.08 ppm, however, the ligand was run in deuterated-DMSO. The spectrum of **15** in $CDCl_3$ displays very broad peaks. The peak accounting for the imine proton of the *N,N*-dimethylthiosemicarbazones appears more upfield when compared to the imine proton peak of the thiosemicarbazones with a free terminal amine. The corresponding protons on the methyl bonded to the imine moiety of **12**, **16** and **18** appear further upfield at 2.27-2.53 ppm, which corresponds to similar peaks found for **10**.

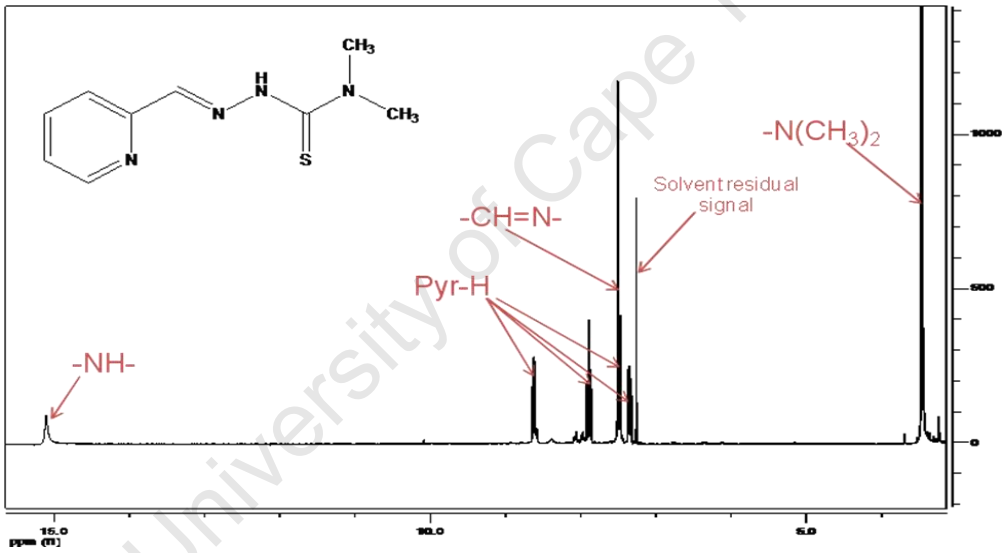

Fig. 2.5: ^{1}H-NMR (in $CDCl_3$) spectrum of 2-formylpyridine-4,4-dimethylthiosemicarbazone, **11** (representative spectrum).

The aromatic/heteroaromatic protons of the *N,N*-dimethylthiosemicarbazone ligands are found to occur in similar regions as is seen for the thiosemicarbazone ligands with the non-substituted terminal amines. The hydrazinic protons of the *N,N*-dimethylthiosemicarbazone ligands are not as consistent in their peak shifts as is seen for the thiosemicarbazone ligands with the non-substituted terminal amines (**Table 2.3**). The hydrazinic protons are found to appear between 7.03-15.51 ppm. Unlike the non-substituted terminal amine thiosemicarbazone ligands, the *N,N*-

dimethylthiosemicarbazones do not always have the hydrazinic proton of the ligands where R^1 = H slightly more downfield when compared to the hydrazinic protons of the ligands where $R^1 = CH_3$.

Table 2.3: Summary of ^{1}H-NMR shifts (ppm) of *N,N*-dimethylthiosemicarbazone ligands in $CDCl_3$ (unless otherwise stated).

Compound	Ar	R^1	-CH=N-	$-CH_3$	$-N(CH_3)_2$	-NH-
3[a]	Benzene	H	8.17	—	3.29	10.81
10	2-pyridine	CH_3	—	2.65/2.41 /2.55	3.48	8.46/14.82 /15.51
11	2-pyridine	H	7.50	—	3.48	15.10
12	2-pyrrole	CH_3	—	2.53	3.36	12.97
13	2-pyrrole	H	7.15	—	3.37	12.90
15[a]	2-furan	H	8.08	—	3.27	10.78
16	2-furan	CH_3	—	2.46	3.39	7.03
17	3-pyridine	H	7.70	—	3.45	8.94
18	3-pyridine	CH_3	—	2.27	3.43	8.39

[a] Compound was analyzed in DMSO-d_6.

The aromatic (pyridyl and phenyl) protons of the 2-pyridine-4-phenylthiosemicarbazones (formyl, **20**, and acetyl, **21**) appear in similar regions to each other, i.e. 7.22-8.60 ppm, and to the thiosemicarbazones previously mentioned in this chapter. The hydrazinic proton of the R^1 = H derivative is more downfield compared to the $R^1 = CH_3$ derivative, which is also seen in the previously mentioned 2-pyridinethiosemicarbazones. The proton on the terminal amine (-N**H**-Ph) occurs just above 10 ppm for both 4-phenylthiosemicarbazone derivatives (**Table 2.4**). The proton on the imine bond of **20** appears at 8.22 ppm, which is in a similar region to what has previously been seen with other 2-formylpyridinethiosemicarbazone derivatives (**5** and **11**). The peak accounting for the protons of the methyl group bonded to the imine moiety of **21** appears at 3.21 ppm. This is slightly more

downfield when compared to ligands **6** and **10** (2-acetylpyridinethiosemicarabzone derivatives).

Table 2.4: Summary of ^{1}H-NMR shifts (ppm) of 4-phenylthiosemicarbazone ligands in DMSO-d_6.

Compound	Ar	R	-CH=N-	-CH_3	-N*H*-Ph	-NH-
20	2-pyridine	H	8.22	—	10.17	11.91
21	2-pyridine	CH_3	—	3.21	10.12	10.55

2.2.2.2. $^{13}C\{^{1}H\}$-NMR spectra

$^{13}C\{^{1}H\}$-NMR spectroscopy was also used in the characterization of newly synthesized ligands (**12**, **16**-**18**). The imine carbon of the ligands appears at 135.5-152.2 ppm (**Table 2.5**), which is slightly downfield when compared to the heteroaromatic carbon peaks (111.4-150.1 ppm). The individual heteroaromatic carbon peaks are assigned using Heteronuclear Single Quantum Correlation (HSQC). The thione carbon, at the center of the thiourea moiety, is found to be the most downfield at just above 180 ppm (with the exception of **16,** which showed a peak accounting for the thione carbon at 146.0 ppm). This is most likely due to the fact that carbon is surrounded by electron withdrawing groups (nitrogen and sulfur, with electronegativity of 3.04 and 2.58, respectively).

Table 2.5: Summary of ^{13}C-NMR shifts (ppm) of newly synthesized 4,4-dimethylthiosemicarbazone ligands in DMSO-d_6.

Compound	Ar	C(***R*^{1}**)=N	Aromatic *C*	***C***(R^{1})=N	***C***=S	-(***C***H$_3$)$_2$	***C***H$_3$
12	2-pyrrole	CH_3	111.4-125.4	135.5	182.5	40.2	17.8
16	2-furan	CH_3	111.8-121.3	144.0	146.0	43.1	17.1
17	3-pyridine	H	123.7-149.0	151.0	181.6	43.8	—
18	3-pyridine	CH_3	123.3-150.1	152.2	183.1	44.1	12.5

The methyl carbons bonded to the terminal amine are found to be more upfield at 40.2-44.1 ppm for all ligands. However, the methyl carbons bonded to the imine moiety are the most upfield of all the carbons, with a peak at 12.5-17.8 ppm for all 3 of the ligands where $R^1 = CH_3$.

2.2.3. Infrared (IR) spectra of monothiosemicarbazones

The IR spectra of the ligands are in accordance to the literature data for similar types of compounds.[14] The characteristic medium-strong intense absorption bands in the range of 1583-1638 cm^{-1} for the thiosemicarbazone ligands are attributed to the imine functionality. This is also confirmation of the ligands forming via a Schiff base condensation mechanism. It is noted that the thiosemicarbazone ligands where $R^1 = CH_3$ (**6**-**10**, **12**, **16**, **18** and **21**) have frequencies attributed to imine functionalities occurring slightly higher (1588-1638 cm^{-1}) compared to their respective thiosemicarbazone ligands (**1**-**5**, **11**, **13**-**15**, **17** and **20**) where $R^1 = H$ (1583-1628 cm^{-1}). This could possibly be due to the inductive effect (electron-donating) of the methyl group bonded to the imine. The *N,N*-dimethylthiosemicarbazone ligands (except for **10**, the 2-acetylpyridine derivative) are also found to occur at a higher frequency when compared to their non-substituted terminal amine thiosemicarbazone ligand derivatives. The reason for this might be due to the electron donating property of the methyl groups on the *N,N*-dimethylthiosemicarbazones, which increases the electron density on the ligands and thus the frequency at which the functional groups vibrate will increase. The IR spectra for the 4-phenylthiosemicarbazone derivatives also showed a peak at 1597 (medium intensity) and 1588 cm^{-1} (weak intensity) for the 2-formylpyridine and 2-acetylpyridine derivatives, respectively. The ν(NH) frequencies of the thiosemicarbazone ligands occur above 3000 cm^{-1}.

2.2.4. Melting points, elemental analyses and mass spectrometry of monothiosemicarbazones

The melting point ranges (between 114°C and 213°C) of the monothiosemicarbazone ligands are found to be relatively high, with the exception of the 2-formylpyrrole-4,4-dimethylthiosemicarbazone which has a relatively low melting

point of 76-79°C. The melting points of the different known monothiosemicarbazone ligands are in close agreement with the literature melting points[11,12,14-19] for the respective thiosemicarbazones. The 2- and 3-formylpyridine thiosemicarbazone ligands have high melting points over 200°C, whereas the other thiosemicarbazone ligands have melting points just above 150°C. This excludes **7** and **8**, which have their melting points at 74-77°C and 114-115°C respectively. It was noted that the *N,N*-dimethylthiosemicarbazones have lower melting points than their respective thiosemicarbazones with non-substituted terminal amines, with the exception of the 2-acetylfuran derivative. The 4-phenylthiosemicarbazone derivatives (**20** and **21**) are also found to have relatively high melting points (204-206°C and 173-177°C, respectively) when compared to the other 2-pyridine derivatives (with the exception of **5**).

The purity of the thiosemicarbazone ligands was confirmed by elemental analysis, which found the percentage composition of the elements to be in close agreement with the calculated values for their respective thiosemicarbazone ligands. Mass spectrometry (EI+) was also used for all new ligands (**12**, **16-18**) where the four ligands show a peak accounting for the protonated molecular ion, i.e. $[M + H]^+$.

2.3. Dithiosemicarbazone ligands

2.3.1. Synthesis of ethane-1,2-dithiosemicarbazide, 22.

Dithiosemicarbazones have previously been reported in literature and have shown biological (i.e. antifungal and anticancer) activity.[10,20,21] Literature has also shown that in some cases a multimeric system displays more biological activity than its monomeric counterpart[22-25], thus dithiosemicarbazones were also ligands of interest to this study. The method described by M. Christlieb *et al*.[26] was used to prepare ethane-1,2-dithiosemicarbazide, **22**, from ethane-1,2-diamine via the di-acid (**Scheme 2.2**). The product, **22**, was isolated as a white solid in a low yield of 40%.

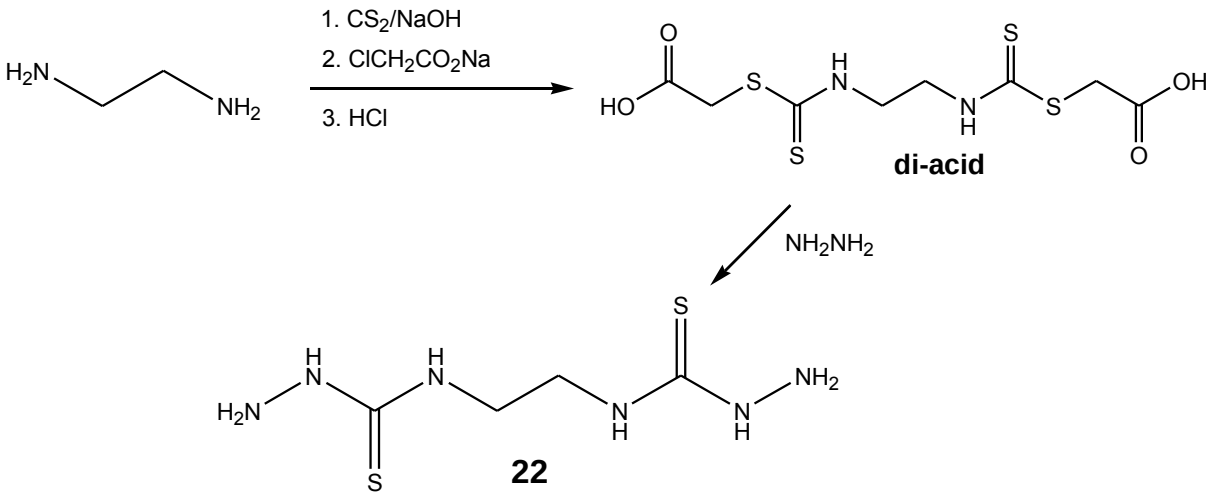

Scheme 2.2: Outline to the synthesis of ethane-1,2-dithiosemicarbazide, 22.

2.3.2. ^{1}H-NMR spectrum of 22

The ^{1}H-NMR spectrum shows the same peaks (with similar shifts) as was reported by M. Christlieb *et al*.[26] The ethane bridge protons appear as a singlet at 3.61 ppm. The singlet is due to the symmetrical nature of the compound. The terminal (primary) amine proton peaks are slightly further downfield at 4.39 ppm as singlets, whereas the hydrazinic protons and the secondary amine protons (next to the ethane bridge) appear, as singlets, further downfield at 7.91 and 8.52 ppm, respectively.

2.3.3. Melting point of 22

The melting point of **22** is 213-214°C, which is in agreement with the literature melting point range of 212-214°C reported by T. Yabuuchi *et al*.[27]

2.3.4. Synthesis of dithiosemicarbazones (23 and 24)

Both ethylenedithiosemicarbazones, **23** (the newly synthesized 2-formylpyridine derivative) and **24**, were prepared using the procedure described by Stringer *et al.*[10] and these reactions, as represented by **equation (2.2)**, also proceeded via Schiff-base condensation. Acetic acid was used in the synthesis (as described by Al-Hazmi *et al.*[28]) of the ligands where a methyl group (i.e. R = CH_3) was bonded to the imine. This is due to the fact that the ketones are less reactive than their respective

aldehydes. The 2-formylpyridine ethane-1,2-dithiosemicarbazone was also prepared in an ethanolic reaction mixture, which required a longer reaction time (24 hours). The dithiosemicarbazones were isolated as light-yellow solids in moderate to good yields (43% - 89%).

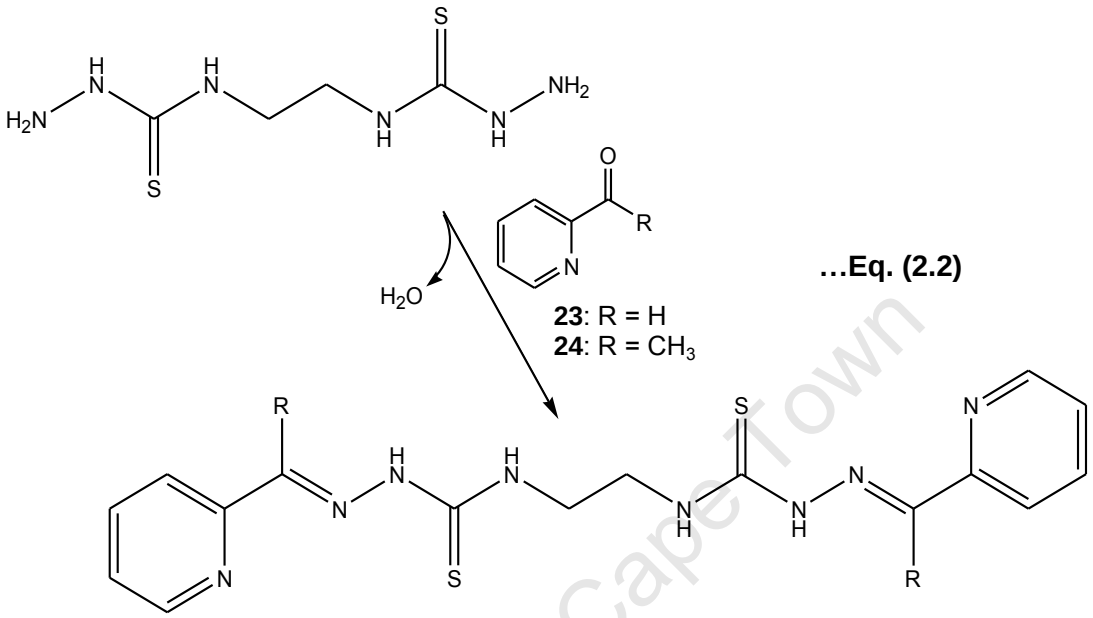

2.3.5. ^{1}H-NMR spectra of dithiosemicarbazones (23 and 24)

The ^{1}H-NMR spectra of the dithiosemicarbazone ligands show a peak between 8.79-8.80 ppm accounting for the protons on the secondary amines occurring next to the ethylene bridge (**Fig. 2.6**). The hydrazinic protons occur at 11.79 ppm for the 2-formylpyridinedithiosemicarbazone ligand, whereas the 2-acetylpyridinedithiosemicarbazone ligand's hydrazinic protons occur more upfield at 10.46 ppm. This is due to the inductive effect of the methyl group that shields the hydrazinic protons when compared to the formyl ligand. The protons attached to the imine bonds of **23** appear at 8.11 ppm, whereas the protons of the methyl groups attached to the imine bonds of **24** occur more upfield at 2.42 ppm. The 2-pyridine ligands' aromatic protons occur between 7-9 ppm. The ^{1}H-NMR spectra of both dithiosemicarbazone ligands show the ethylene bridge protons occurring between 3.88-3.93 ppm as singlets, due to the symmetrical nature of the ligands.

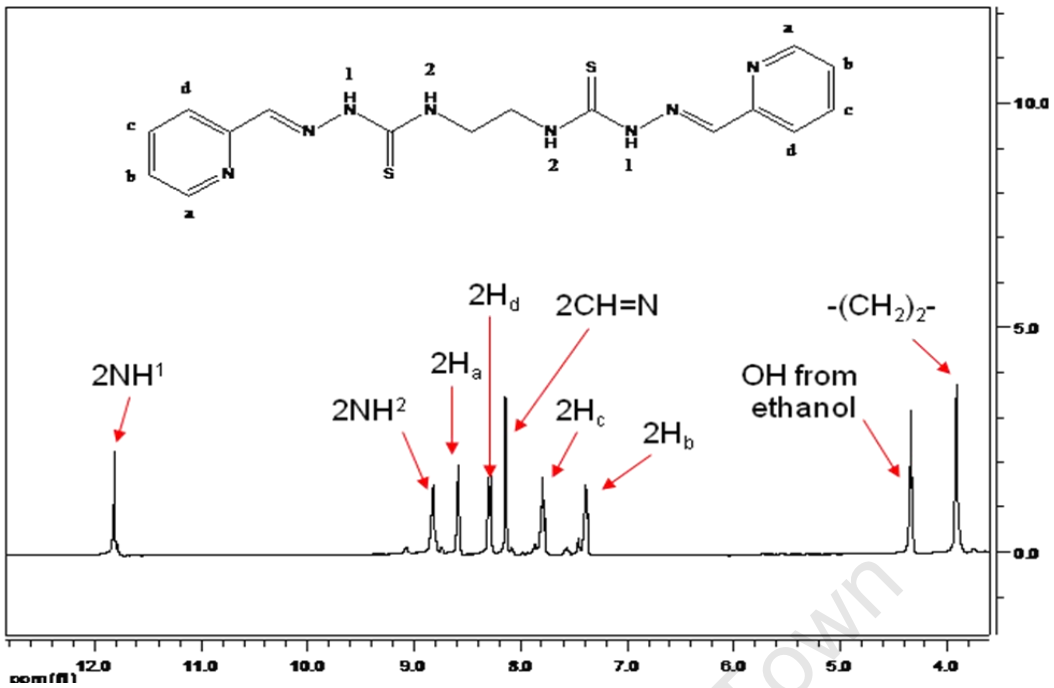

Fig. 2.6: ^{1}H-NMR (in DMSO-d_6) spectrum of 2-formylpyridinedithiosemicarbazone, **23** (representative spectrum).

The pyridyl protons of the dithiosemicarbazones have similar chemical shifts between 7.38-8.60 ppm for both ligands (**23** and **24**), which compares favourably with the mononuclear 4,4-dimethylthiosemicarbazone derivatives **10** and **11** (**Table 2.6**). The pyridyl protons of the mononuclear derivatives (**10** and **11**) have peaks appearing between 7.37-8.73 ppm. The proton on the imine bond of **23**, however, has its proton peak appearing at 8.12 ppm, further downfield compared to the mononuclear formyl derivative (7.50 ppm). This was opposite to what was observed for the hydrazinic protons of the ligands where R = H. The mononuclear ligand has its hydrazinic proton further downfield compared to the dithiosemicarbazone derivative. The same is observed with the derivatives where R = CH_3 (i.e. the mono ligand has its hydrazinic proton more deshielded compared to the dithiosemicarbazone derivative). The protons on the methyl bonded to the imine for both derivatives where R = CH_3 has similar shifts around 2.4 ppm.

Table 2.6: Summary of ^{1}H-NMR shifts (ppm) of 2-pyridine-dithiosemicarbazones (**23** and **24**) vs. 2-pyridine-4,4-dimethylthiosemicarbazones (**10** and **11**), i.e. mono- vs. binuclear ligands.

Ligand	pyr-H	CH=N	C(CH_3)=N	N^1H	N^2H	$(CH_2)_2$
23: ***R=H***	7.38-8.56	8.12	—	11.80	8.80	3.88
24: ***R=CH$_3$***	7.39-8.60	—	2.42	10.43	8.80	3.93
11: ***R=H***	7.37-8.63	7.50	—	15.10	—	—
10: ***R=CH$_3$***	7.25-8.73	—	2.41/2.55 /2.65	8.46/14.82 /15.51	—	—

2.3.6. Infrared (IR) spectra and melting points of dithiosemicarbazones (23 and 24)

The characteristic medium-intense absorption band occurring between 1582-1587 cm^{-1} for the dithiosemicarbazone ligands is attributed to the imine functionality. This is also confirmation of the Schiff-base condensation reaction having taken place in the synthesis of the respective dithiosemicarbazone ligand. The ν(imine) frequencies of the dithiosemicarbazones are found in similar regions to their mononuclear pyridyl counterparts (1582-1600 cm^{-1}). The ν(NH) frequencies of the dithiosemicarbazone ligands occur above 2900 cm^{-1}.

The melting point of the dithiosemicarbazone ligands are found to be relatively high when compared to their respective monothiosemicarbazone derivatives. The dithiosemicarbazone ligand where R = H (227-229°C) has a higher melting point range than its dithiosemicarbazone ligand counterpart where R = CH_3 (196-199°C). Ligand **24** is found to have a lower melting point when compared to the literature value of 214-216°C reported by Scovill.[29]

The purity of the dithiosemicarbazone ligands was confirmed by elemental analysis, which found the percentage composition of the elements to be in close agreement with the calculated values for their respective dithiosemicarbazone ligands.

2.4. Conclusion/Summary

A series of aromatic thiosemicarbazone ligands were synthesized. This series included four newly synthesized monomeric ligands and one newly synthesized dimeric ligand. The ligands were characterized using ^{1}H-NMR, ^{13}C{^{1}H}-NMR and IR spectroscopy, elemental analysis and mass spectrometry. Such characterizations confirmed the integrity of the ligands and showed that all of the compounds were sufficiently pure to be used in the synthesis of the respective ^{67}Ga complexes.

2.5. References

1. I. Dilovic, M. Rubcic, V. Vrdoljak, S. K. Pavelic, M. Kralj, I. Piantanida and M. Cindric, *Bioorgan. Med. Chem.*, 2008, **16(9)**, 5189.

2. W. X. Hu, W. Zhou, C. N. Xia and X. Wen, *Bioorg. Med. Chem. Lett.*, 2006, **16(8)**, 2213.

3. J. A. Lessa, I. C. Mendes, P. R. Da Silva, M. A. Soares, R. G. dos Santos, N. L. Speziali, N. C. Romeiro, E. J. Barreiro and H. Beraldo, *Eur. J. Med. Chem.*, 2010, **45(12)**, 5671.

4. R. A. Finch, M. Liu, S. P. Grill, W. C. Rose, R. Loomis, K. M. Vasquez, Y. Cheng and A. C. Sartorelli, *Biochem. Pharmacol.*, 2000, **59**, 983.

5. A. E. Liberta and D. X. West, *Biometals*, 1992, **5**, 121.

6. Z. Y. Yang and Y. Wang, *Bioorg. Med. Chem. Lett.*, 2007, **17**, 2096.

7. A. Husain, S. A. A. Nami and K. S. Siddiqi, *J. Mol. Struct.*, 2010, **970**, 117.

8. M. C. Rodriguez-Arguelles, S. Mosquera-Vasquez, J. Sanmartin-Matalobos, A. M. Garcia-Deibe, C. Pelizzi and F. Zani, *Polyhedron*, 2010, **29**, 864.

9. T. S. Lobana, R. Sharma, G. Bawa and S. Khanna, *Coord. Chem. Rev.*, 2009, **253**, 977.

10. T. Stringer, P. Chellan, B. Therrien, N. Shunmoogam-Gounden, D. T. Hendricks and G. S. Smith, *Polyhedron*, 2009, **28**, 2839.

11. I. C. Mendes, M. A. Soares, R. G. dos Santos, C. Pinheiro and H. Beraldo, *Eur. J. Med. Chem.*, 2009, **44(5)**, 1870.

12. A. P. Rebolledo, M. Vieites, D. Gambino, O. E. Piro, E. E. Castellano, C. L. Zani, E. M. Souza-Fagundes, L. R. Teixeira, A. A. Batista and H. Beraldo, *J. Inorg. Biochem.*, 2005, **99(3)**, 698.

13. J. Chan, A. L. Thompson, M. W. Jones and J. M. Peach, *Inorg. Chim. Acta*, 2010, **363(6)**, 1140.

14. S. Chandra and A. Kumar, *Spectrochim. Acta Part A*, 2007, **68**, 1410.

15. S. S. Meher, S. Naik, R. K. Behera and A. Nayak, *J. Indian Chem. Soc.*, 1981, **58(3)**, 274.

16. N. Youssef and K. Hegab, *Synth. React. Inorg. Met. –Org. Nano. –Met. Chem.*, 2005, **35(5)**, 391.

17. C. Yamakazi, *Can. J. Chem.*, 1975, **53(4)**, 610.

18. F. Haghighi Moghadam, A. R. Jalilian, A. Nemati and M. Abedini, *J. Radioanal. Nucl. Chem.*, 2007, **272**, 115.

19. A. Wengel, N. Jacobsen, H. Kolind-Andersen and P. Bjerregaard, *Pesticide Science*, 1990, **30(2),** 223.

20. D. M. Wiles, B. A. Gingras and T. Suprunchuk, *Can. J. Chem.*, 1967, **45**, 1735.

21. P. A. Barrett, E. Beveridge, P. L. Bradley, C. G. D. Brown, S. R. M. Bushby, M. L. Clarke, R. A. Neal, R. Smith and J. K. H. Wilde, *Nature*, 1965, **206(991)**, 1340.

22. P. Govender, N. C. Antonels, J. Mattson, A. K. Renfrew, P.J. Dyson, J. R. Moss, B. Therrien and G. S. Smith, *J. Organomet. Chem.*, 2009, **694**, 3470.

23. G. T. Dolphin, S. Chierici, M. Ouberia, P. Dumy and J. Garcia, *ChemBioChem*, 2008, **9**, 952.

24. N. Raman, A. Sakthivel and R. Jeyamurugan, *Cent. Eur. J. Chem.*, 2010, **8(1)**, 96.

25. J. Zhang, Y. Gong, X. Zheng, M. Yang and J. Cui, *Chinese Sci. Bull.*, 2006, **51(8)**, 911.

26. M. Christlieb, H. S. R. Struthers, P. D. Bonnitcha, A. R. Cowley and J. R. Dilworth, *Dalton Trans.*, 2007, 5043.

27. T. Yabuuchi, M. Hisaki and R. Kimura, *Chem. Pharm. Bull.*, 1975, **23**, 663.

28. G. A. Al-Hazmi, N. M. El-Metwally, O. A. El-Gammal and A. A. El-Asmy, *Spectrochim. Acta Part A*, 2008, **69**, 56.

29. J. P. Scovill, *Phosphorus Sulfur*, 1991, **60(1-2)**, 15.

Chapter 3:

Synthesis and characterization of cold (non-radioactive) and radiolabelled gallium(III) thiosemicarbazones. Biological evaluation of radiolabelled gallium(III) thiosemicarbazones.

3.1. Introduction

Gallium is a grayish semi-metallic element with an atomic number of 31, atomic weight of 69.72 amu and a melting point of 29.78°C.[1,2] In most of its compounds gallium has an oxidation state of +3.[2] The chemical behavior of gallium is closely associated to that of Fe^{3+}, in terms of its electric charge, ion diameter, coordination number and its electron configuration.[2] It has an electron configuration of $[Ar]3d^{10}4s^24p^1$, with the loss of two 4s electrons and one 4p electron yielding the stable trivalent cation Ga^{3+}. The trivalent form of gallium is reported to be redox-inactive, because gallium(II) would exhibit an energetically unfavourable $[Ar]3d^{10}4s^1$ electron configuration and because the process $Ga^{3+} \rightarrow Ga^{4+} + e^-$ would require considerable energy (6200 $kJ.mol^{-1}$).[1] Gallium is of particular interest as the metal is diamagnetic and does not suffer from the excited state relaxation through internal conversion.[3]

Gallium(III) complexes have shown two biomedical properties worth exploiting for the development of antitumour gallium(III) compounds. Firstly, the anti-tumour activity of gallium(III) nitrate has been evaluated in phase I and phase II clinical trials[4,5] after gallium nitrate had shown high antitumour activity in experimental animal tumours.[6] Secondly, ^{67}Ga, a low energy gamma emitting radionuclide with a half-life of 78 hours, is a very useful tumour diagnostic agent and has been used extensively (mostly as ^{67}Ga-citrate) in the detection of a number of human malignancies.[7,8]

The careful choice of radionuclide allows gallium to be used as a PET (Photon Emitting Tomography) or SPECT (Single photon Emitting Computerised Tomography) imaging agent, depending on the radioisotope used.[3]

In the earliest studies of gallium, it was found that the radioactive isotope ^{72}Ga, a β-emitter with a half-life of 14 hours that yields ^{72}Ge, could accumulate in animal tissues and some bone cancers.[1,9,10] However, until recently, ^{67}Ga bidimensional scintigraphy was the most widely used diagnostic modality for imaging patients with lymphoma.[1,11] The interesting physical properties and availability of ^{67}Ga has made it an interesting nuclide for radiopharmaceutical research.[12,13] The interesting trend in the production and use of PET radionuclides in nuclear medicine has presented new opportunities for focused research on the production of new gallium-radiopharmaceuticals for feasibility studies for future PET gallium homologs.[12]

Gallium(III) thiosemicarbazones have shown promising anti-proliferative activity *in vitro* and *in vivo*.[14] Due to the importance of thiosemicarbazones in antineoplastic activity and the necessity of gallium complexation to enhance their activity,[12,15] the idea of developing possible tumour imaging agents incorporating ^{67}Ga into suitable chelates, such as thiosemicarbazones, was investigated.

3.2. Synthesis of cold (non-radioactive) gallium(III) thiosemicarbazone complexes

A 'cold' complex can be defined as a non-radioactive complex. The main function of the cold complexes (in this study) was to confirm the structures of the radiolabelled complexes by comparing their respective HPLC profiles. The reactions (**equation (3.1)**) were performed under inert atmosphere. The gallium(III) thiosemicarbazone complexes (**25**-**27**) were synthesized by dissolving the respective ligand (**6**, **10** and **11**) in dry ethanol and adding dropwise a solution of $GaCl_3$ (approximately 5 equivalents) in dry ethanol. Care was taken in the handling of the air- and moisture-sensitive $GaCl_3$ which was weighed out in a glove-box. For the synthesis of **26** the reaction mixture was stirred at room temperature for 2 hours, whereas for the synthesis of **25** and **27** the reaction mixture was refluxed for 2 hours. The synthesis for all complexes produced bright-yellow solids in moderate to good yields (54% - 75%). The gallium(III) complexes were also found to be soluble in ethanol, methanol, acetone and DMSO.

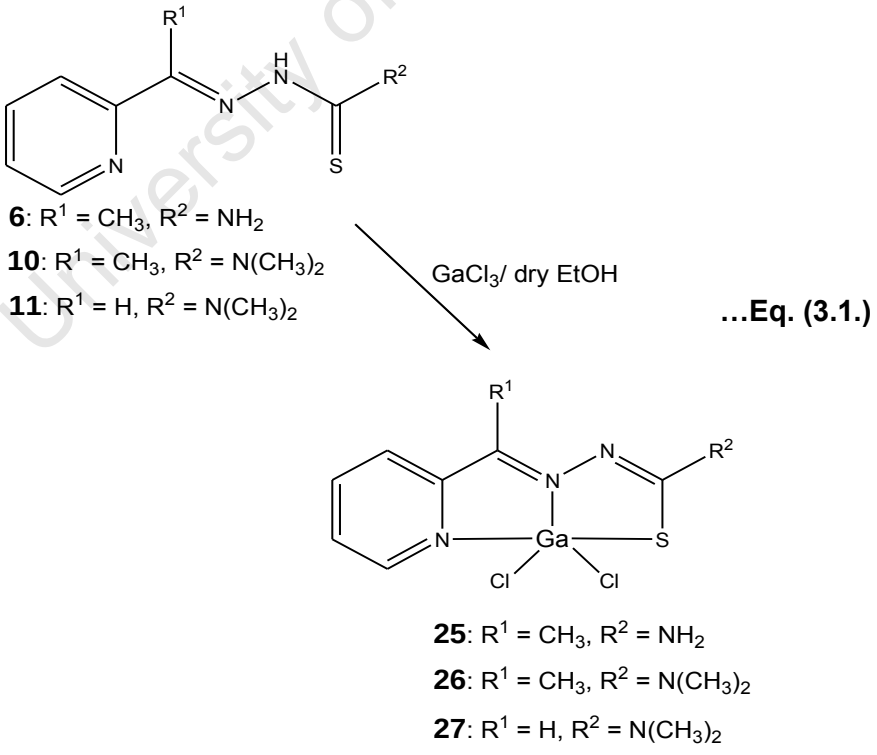

In the synthesis of the complexes, the gallium serves as the Lewis acid (soft) whereby it accepts electrons from the tridentate (thiolate sulfur, imine nitrogen and pyridyl nitrogen) thiosemicarbazone ligand. It should be noted that in order to obtain a 1:1 ligand to metal ratio complex, $GaCl_3$ was added in excess (more than 5 equivalents) during the synthesis. This was employed to prevent the possibility of different ratios of gallium(III) to thiosemicarbazone complexes forming.[7] Of the complexes formed, **25** and **26** had previously been reported by Kratz *et al*.[7], whereas **27** was newly synthesized. The complexes were characterized using ^{1}H-NMR and IR spectroscopy, as well as by melting point determination and elemental analysis.

3.2.1. ^{1}H-NMR spectra of cold complexes (25-27)

The ^{1}H-NMR spectrum of **26** shows the pyridyl proton peaks appearing between 7.57-8.25 ppm. The protons on the methyl group attached to the imine bond are found to appear at 2.77 ppm, whereas the protons on the methyl groups attached to the tertiary amine appear slightly more downfield at 3.31 ppm.

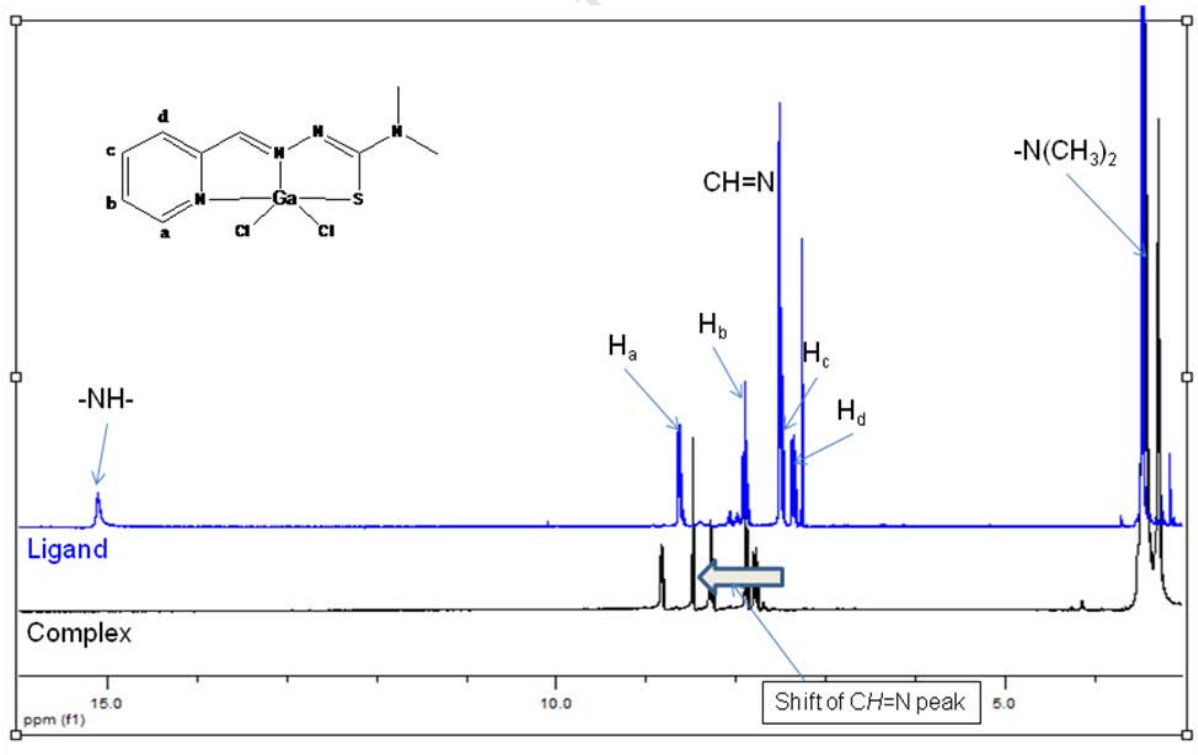

Fig. 3.1: ^{1}H-NMR spectra of 2-formylpyridine-4,4-dimethylthiosemicarbazone, **11**, (ligand) and gallium(III)-2-formylpyridine-4,4-dimethylthiosemicarbazone, **27** (complex).

The ^{1}H-NMR spectrum of **27** (**Fig. 3.1**) shows the pyridyl proton peaks appearing between 7.57-8.80 ppm, slightly shifted downfield when compared to **26** due to the shielding effect of the electron-donating methyl group attached to the imine of **26**. The spectrum of **25**, however, shows the pyridyl protons slightly further downfield when compared to **26** and **27**. The reason for this might be due to the electron-donating methyl groups on the terminal amine of **26** and **27** that provide some shielding when compared to **25**, which has a free terminal amine (i.e. no electron donating group). The spectrum of **25** also shows a downfield shift of the pyridyl protons when compared to ligand **6** (**Table 3.1**). A downfield shift is also seen in the spectrum of **25** for the protons on the methyl group attached to the imine bond when compared to the respective ligand. The protons on the methyl groups attached to the terminal/tertiary amine of **27** appear at 3.27 ppm, similar to **26** (3.31 ppm). The peak for the proton bonded to the imine moiety of **27** appears at 8.47 ppm. There are downfield shifts of the pyridyl and imine protons of **27** when compared to its respective ligand **(Fig. 3.1)**. Most notably, there is no peak seen for the hydrazinic proton which suggests that the complexation occurs via the thiolate form of the ligand. The complexation via the thiolate form of the ligand is also reported by Kratz *et al*.[7]

Table 3.1: Summary of the ^{1}H-NMR shifts (ppm) of the complexes (**25**-**27**) vs. their respective ligands (**6**, **10** and **11**).

Compound	pyr-H	CH=N	C(CH_3)=N	NH
25	7.90-9.02	—	2.72	—
6	7.40-8.60	—	2.41	10.29
26	7.57-8.25	—	2.77	—
10	7.25-8.73	—	2.41/2.55/2.65	8.46/14.82/15.51
27	7.76-8.80	8.47	—	—
11	7.37-8.63	7.50	—	15.10

3.2.2. Infrared (IR) spectroscopy of cold complexes (25-27)

The characteristic strong and medium intense absorption bands occurring at 1603 (*s*) and 1558 cm^{-1} (*m*) for **25**, 1601 (*s*) and 1553 cm^{-1} (*m*) for **26** and 1606 (*s*) and 1566 cm^{-1} (*m*) for **27** are attributed to the imine functionalities. The second imine band is also confirmation that the sulphur bonds to the metal in the thiolate form. The IR spectra show a shift of the imine band from 1599, 1582 and 1592 cm^{-1} (ligands) to 1603, 1601 and 1606 cm^{-1} for **25**, **26** and **27**, respectively (**Table 3.2**).

Table 3.2: Summary of the imine (C=N) band frequencies in the infrared spectra (using KBr pellets) of the complexes (**25**, **26** and **27**) vs. their respective ligands.

	ν(C=N), cm^{-1}	
Compound	**Ligand**	**Complex**
6/25	1599	1603, 1558
10/26	1582	1601, 1553
11/27	1592	1606, 1566

3.2.3. Melting point determination, elemental analysis and mass spectrometry of cold complexes (25-27)

The melting point of **26** was determined to be 251-254°C. The melting point of **27** is relatively low between 116-120°C when compared to **26**. Elemental analysis of the complexes (**25**-**27**) is in close agreement with the calculated values for the 1:1 ligand to metal ratio complexes, supporting the integrity of the cold complexes. Mass spectrometry (EI+) was also used to further characterize the complexes (**25**-**27**) where the complexes show a peak accounting for the molecular ion, i.e. $[M]^+$.

3.3. Synthesis and characterisation of ^{67}Ga complexes

3.3.1. Synthesis of radiolabelled complexes (28-34)

The synthesis of the ^{67}Ga complexes (**28**-**34**) was performed by adding an ethanolic solution of the relative ligand to $^{67}GaCl_3$ pre-dried from an aqueous or acetonic solution. The reaction mixture was heated at ~80°C for 20-60 minutes to give the radiolabelled complex (**28**-**34**) in a high (quantitative) radiochemical yield. The radiochemical yield can be expressed as a percentage of the activity originally present. The synthesis of the radiolabelled gallium(III) thiosemicarbazones differed slightly from that of the cold (non-radioactive) gallium(III) thiosemicarbazones with respect to the reaction conditions (i.e. time and temperature).

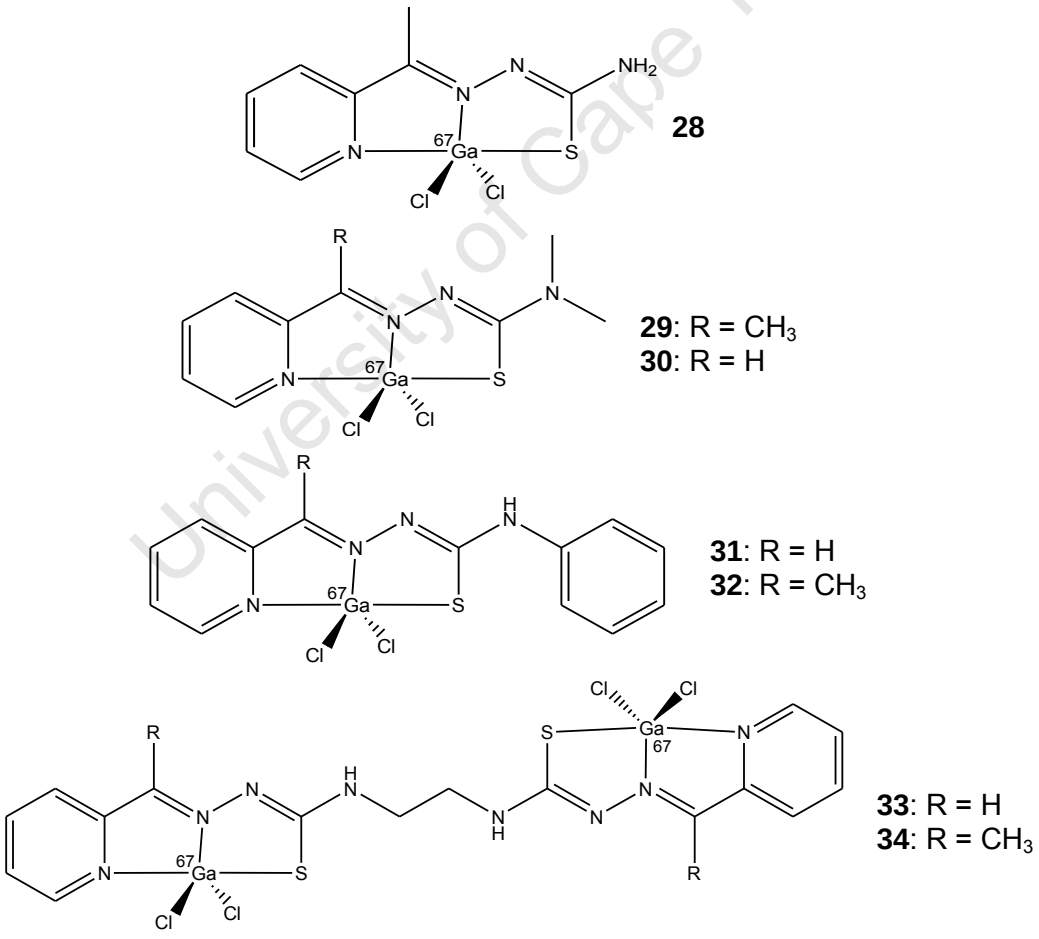

Fig. 3.2: Proposed structures of ^{67}Ga thiosemicarbazone complexes (**28**-**34**).

3.3.2. High Performance Liquid Chromatography (HPLC) analysis of radiolabelled complexes (28-34)

The radiolabelling of ligands with a gallium cation affects their chromatographic properties and the final complexes (**Fig. 3.2**) are found to be less polar than their respective ligands.[16] HPLC radiochromatograms are generated by detecting the separated radioactive components in the column effluent with a radioactivity detector. Radiochromatograms of the successfully radiolabelled complexes show the presence of a new peak, with free $^{67}GaCl_3$ eluting early at 2.9-3.0 minutes (**Fig. 3.3(i)**). The successfully radiolabelled complexes (**28**-**34**) are found to exhibit high radiochemical yields of at least 87%. All successful radiolabelling experiments were performed in duplicate.

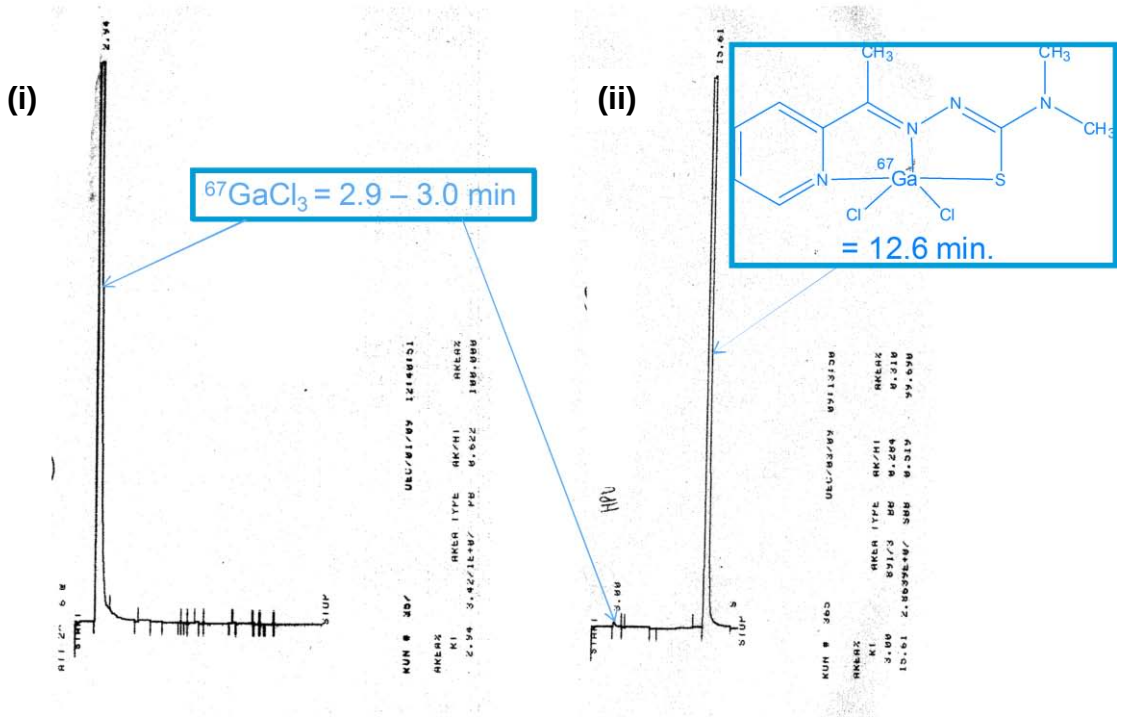

Fig. 3.3: HPLC chromatograms of **(i)** free $^{67}GaCl_3$ (2.9-3.0 min.) and **(ii)** [^{67}Ga]-2-acetylpyridine-4,4-dimethylthiosemicarbazone (12.6 min.).

The chromatograms of **28**, **29** and **30** show the presence of a new peak at 5.5, 12.6 and 11.8 minutes, respectively, as well as labelling efficiencies (**Table 3.3**, **Fig. 3.4**) of 87% (for **28**) and more than 99% (for **29** and **30**). The chromatograms of **31** (13.0 minutes) and **32** (13.7 minutes) also show high yields of 90% and more than 99%,

respectively. The chromatograms of **33** and **34** each show a broad radiolabelled complex peak with a smaller peak on the shoulder (i.e. at the start of the broad peak). Compound **34** shows more than 99% labelling efficiency when accounting for the total sum of the major and minor peaks, while **33** shows approximately 95% labelling efficiency when accounting for both peaks. The major peaks appear at 11.5 (85%) and 12.5 (91%) minutes for **33** and **34**, respectively. The minor peaks, appearing at 10.7 (11%) and 11.3 minutes (~ 9%) for **33** and **34**, respectively, could possibly arise from the ^{67}Ga cation binding only to 1 site in the ligand or as a result of possible isomerization of the ligand in the ethanolic solution before complexation. The latter is more likely as the HPLC chromatogram of the ligands show 2 significant peaks for both ligands (i.e. **23** and **24**). The chemical/molecular identities of **28**-**30** were ascertained by comparison of their HPLC profiles with those of the corresponding cold complexes (**25**-**27**). The structures of **31**-**34** were obtained by the apparent binding nature of gallium-67 to a 2-pyridinethiosemicarbazone ligand (i.e. in a N,N,S-tridentate manner).

Table 3.3: Summary of the successfully radiolabelled complexes, their retention times using HPLC, their radiolabelling efficiency and the comparison with the cold complexes.

Radio-labelled complex	Ar	R^2	R^1	Labelling(%)	Radio-labelled complex, t_r(min.)	Cold complex, t_r(min.)
28	2-pyridine	CH_3	NH_2	87	5.5	5.5
29	2-pyridine	CH_3	$N(CH_3)_2$	>99	12.6	12.6
30	2-pyridine	H	$N(CH_3)_2$	>99	11.8	11.5
31	2-pyridine	H	$NH(C_6H_5)$	90	13.0	—[b]
32	2-pyridine	CH_3	$NH(C_6H_5)$	>99	13.7	—[b]
33	2-pyridine	H	$NH(CH_2)_2$-TSC	95	10.7-11.5[a]	—[b]
34	2-pyridine	CH_3	$NH(CH_2)_2$-TSC	>99	11.3-12.5[a]	—[b]

[a]A broad peak is observed for the [^{67}Ga]-dithiosemicarbazone complexes, with a relatively small peak at the shoulder. [b]Cold complex was not synthesized.

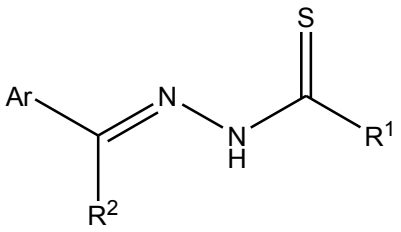

Fig. 3.4: Structure of thiosemicarbazone ligands used in the radiolabelling studies.

Table 3.4: Summary of the ligands that were unsuccessfully radiolabelled.

Ligand	Ar	R^2	R^1	Ligand	Ar	R^2	R^1
1	Benzene	H	NH_2	**12**	2-pyrrole	CH_3	$N(CH_3)_2$
2	2-furan	H	NH_2	**13**	2-pyrrole	H	$N(CH_3)_2$
3	Benzene	H	$N(CH_3)_2$	**14**	2-pyrrole	H	NH_2
4	3-pyridine	H	NH_2	**15**	2-furan	H	$N(CH_3)_2$
5	2-pyridine	H	NH_2	**16**	2-furan	CH_3	$N(CH_3)_2$
7	2-furan	CH_3	NH_2	**17**	3-pyridine	H	$N(CH_3)_2$
8	Benzene	CH_3	NH_2	**18**	3-pyridine	CH_3	$N(CH_3)_2$
9	2-pyrrole	CH_3	NH_2				

There are some thiosemicarbazone ligands (**Table 3.4**) that cannot be labelled with ^{67}Ga. When comparing their structures with those of the ligands that were successfully labelled, there appears to be a few structural conditions for successful labelling. It was found that the presence of 2-pyridine (or perhaps any 6 membered heteroaromatic group, with the heteroatom at the 2-position) in conjunction with an electron donating group (methyl) on the imine carbon atom and/or the presence of lipophilic non-polar groups (such as methyls or phenyls) on the terminal amine provide the best structural features for thiosemicarbazone ligands to ensure successful labelling with ^{67}Ga. There are two possible reasons that the ligands in **Table 3.4** could not be labelled with ^{67}Ga: (i) the orientation of the lone pair(s) on the heteroatom are not suitable for complexation as they would face away from the

gallium already coordinated to the thiolate sulphur (the negatively charged sulphur would act as a more powerful nucleophile relative to heteroatoms with a lone pair), and (ii) the proximity of the lone pair(s) relative to the already bound gallium.[17] The solubility of the ligand in ethanol (as influenced by, amongst others, the lipophilic groups on the terminal amine) could also be an important characteristic. However, if the ligand is soluble in ethanol it does not necessarily mean that it would be successfully labelled with ^{67}Ga.

3.3.3. Comparison between mono- and bi-nuclear ligands in labelling with ^{67}Ga

When looking comparatively at the mono- and bi-nuclear ligands with regards to their labelling efficiencies with ^{67}Ga, it can be seen that there are no significant differences in the incorporation of the ^{67}Ga into the ligands. The amount of ^{67}Ga used in the reactions ranged between 1.26 and 1.46 mCi. The mono-nuclear ligands (**29** and **30**) show >99% labelling efficiencies, whereas the bi-nuclear ligands (**33** and **34**) show 95% and >99% incorporation of ^{67}Ga, respectively. This is, however, not a conclusive study of the effects of using a bi-nuclear versus a mono-nuclear ligand in labelling with ^{67}Ga. More conclusive evidence might be obtained by using a range of smaller amounts of the ligands.

3.3.4. Effect of $^{67}GaCl_3$ quality

When a $^{67}GaCl_3$ batch was between 2-3 days old, the radiochemical yield is found to remain approximately the same. This is contradictory to what has been reported by Haghighi Moghadam *et al*.[16], who claim that when a $^{67}GaCl_3$ batch was older than 2 days, the radiochemical yield drastically drops. This could be explained by the formation of non-radioactive zinc atoms during the decay process, resulting in the latter competing with radiogallium for complexation with the ligands. Zn-thiosemicarbazone complexes are reported to be very stable[18]. It is obvious that, in the current study, the number of atoms of the decay product Zn was not sufficiently high enough to compete with the radioactive ^{67}Ga atoms for complexation. It is, however, noted that, as a result of the decay process, a $^{67}GaCl_3$ batch loses some of its activity after 2 days. This was compensated for by using a bit more of the $^{67}GaCl_3$ solution in order to maintain a similar starting activity for each reaction.

3.4. Stability Studies of ^{67}Ga complexes (28-34)

The radiochemical stabilities (i.e. ability to retain the ^{67}Ga radionuclide under specified conditions) of the successfully radiolabelled complexes (**28**-**34**) were also tested in saline solution (0.9% NaCl in water) and bovine serum. The stability of the radiolabelled complexes (**Fig. 3.5**) was tested by incubating the respective radiolabelled complex in 50 µL of saline/serum solution at 37°C for 30, 60 and 120 minutes, respectively. Each test (saline/serum) for a specific time period (30, 60 and 120 minutes) was performed individually (i.e. no removal of aliquots). After incubation, the proteins (from the serum test) were precipitated with 50 µL acetonitrile, as is described by Kumar *et al*.[19] The samples were centrifuged for approximately 1 minute and the cleared lysate was analyzed by HPLC to assess the integrity of the radiolabelled complex.

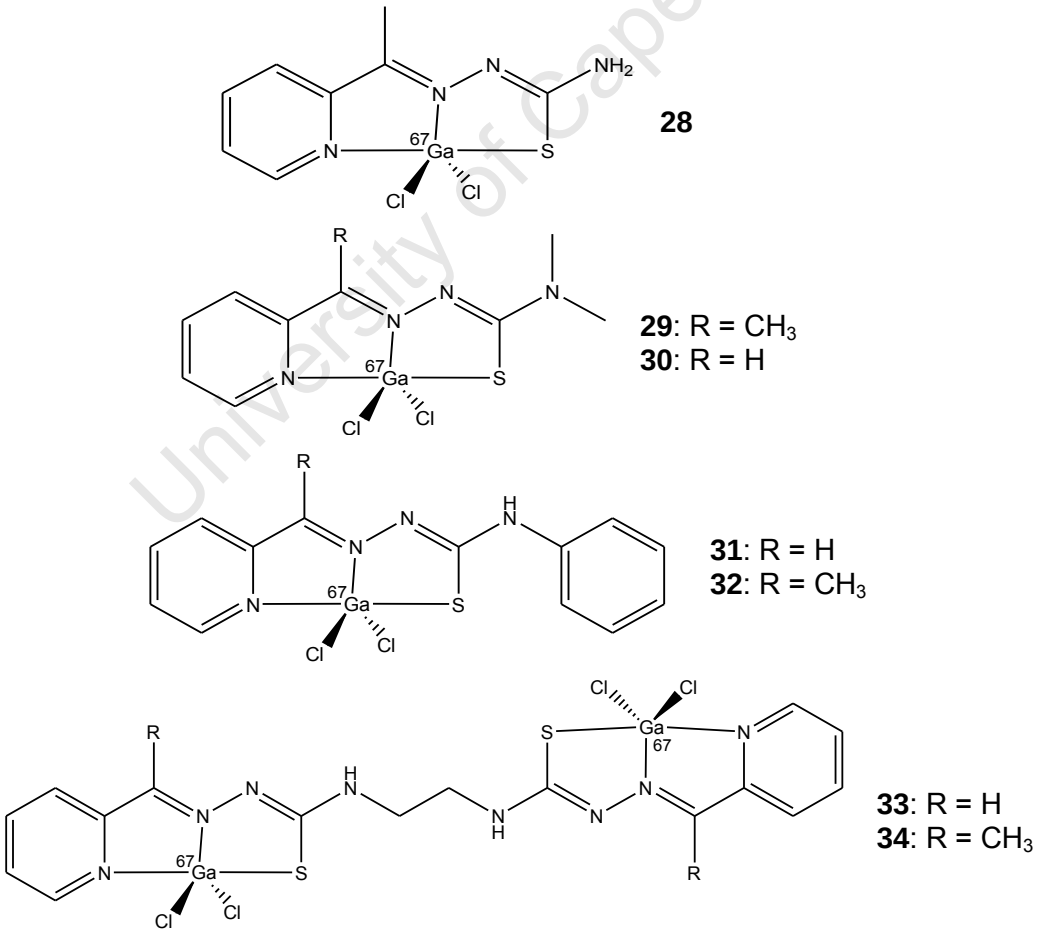

Fig. 3.5: Radiolabelled complexes (**28**-**34**) that were tested for their stability.

It was found that the radiolabelled complexes are all stable in saline solution. This implies that they are all stable against radiolysis. However, only **29** and **34** are relatively stable in the bovine serum (**Fig. 3.6**). The stability test of **29** in bovine serum shows that there is little decrease in stability of **29** after 2 hours of incubation at 37°C. The graph (**Fig. 3.6A**) shows 95%, 97% and 90% radiolabelled complex (**29**) present after 30, 60 and 120 minutes, respectively. The serum (or protein within the serum), however, has a more profound effect on **34**. The graph shows 91%, 67% and 66% radiolabelled complex (**34**) present after 30, 60 and 120 minutes, respectively. The graph (**Fig. 3.6B**) also shows that there is a levelling off of the percentage of **34** remaining after 1 hour. Stability tests with all other successfully radiolabelled complexes show less than 3% of the radiolabelled complex remaining after 30 minutes. This implies that only **29** and **34** are suitable candidates for further biological studies. The serum instability of the other radiolabelled complexes could be ascribed to possible interaction with the protein molecules in the serum, which results in the expulsion of the radiometal from the ligand. This interaction comprises an exchange of the gallium between the radiolabelled complex and the apotransferrin in the serum.[20] This means that *in vivo* testing of these radiolabelled complexes would most likely show that the complexes would not survive the body's physiological conditions.

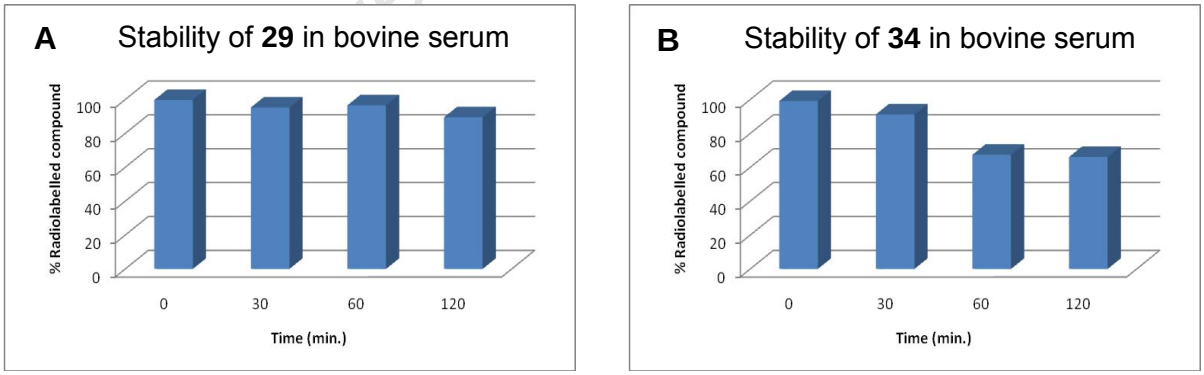

Fig. 3.6: Stability study of (**A**) **29** and (**B**) **34** in bovine serum (at 37°C).

3.5. Effect of water on radiolabelling efficiency

Two of the successfully radiolabelled complexes (**28** and **29)** representing the relatively least and most efficiently radiolabelled complexes, respectively, were selected for the study of the effect of water on the radiolabelling efficiency of gallium(III) thiosemicarbazones. This study was performed to test a claim made by Jalilian *et al*.[12] who stated that the labelling of a thiosemicarbazone with gallium-67 is not satisfactory when water is present in the reaction solvent. The radiolabelling reactions were performed with varying percentages (0% - 40%) of water present in the reaction mixtures. Both results show that water has no significant effect on the radiolabelling efficiency (**Fig. 3.7**). These results, thus, contradict the statement made by Jalilian *et al.*[12]

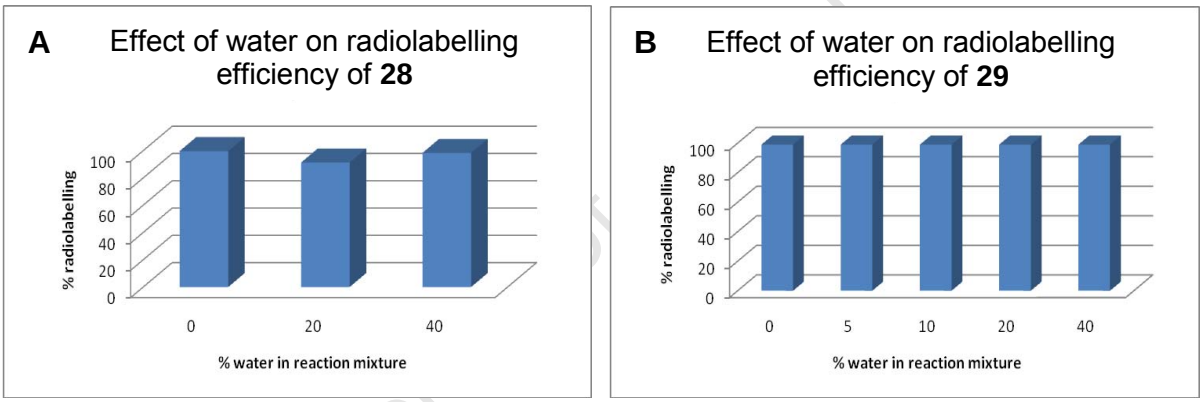

Fig. 3.7: Effect of water on radiolabelling efficiency of (**A**) **28** and (**B**) **29**.

3.6. Biological evaluation of the ^{67}Ga complexes: *in vitro* cellular uptake studies

The *in vitro* cellular uptake experiments were performed to test the ability of the radiolabelled complexes (**29** and **34**) to bind to various cell lines, such as a rat ovarian cancer cell line (DMBA OC1R), human breast cancer cell line (MCF 7) and non-cancerous brain endothelial cell line (bEND5) as the control. The cells, grown in culture flasks, were trypsinized, released and re-suspended in cell growth medium. The cells were allowed to attach and grow in the medium for four hours. Cells were seeded in quantities of 50 000, 100 000, 150 000, 200 000 and 250 000 cells per

well in 24-well plates. It was noted that the non-cancerous brain endothelial cell line had the fastest cell kinetics compared to the cancer cell lines, which is opposite to what happens *in vivo* (i.e. the cancer cells grow faster). The cell kinetics is determined by how fast the cells undergo cell division (**Fig. 3.8**).

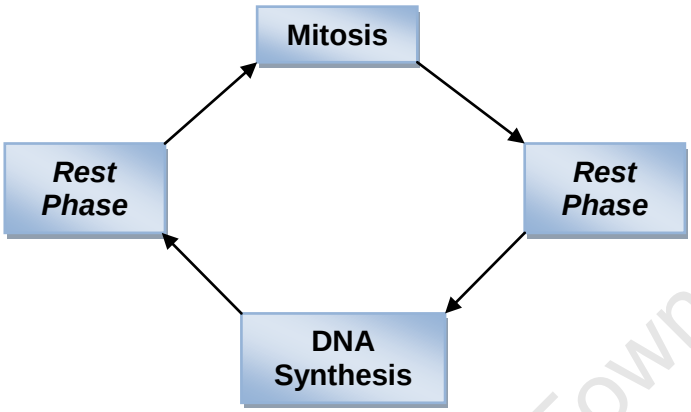

Fig. 3.8: A cycle summizing the cell division of the cells.

The radiolabelled compound was added to each well in a final concentration of 1.36 µCi/well to three sets of 24 well plates, containing the bEND5, DMBA OC1R and MCF 7 cells, respectively. The cultures were incubated for 2 hours (at 37°C) to allow uptake of the radiolabelled compounds. After incubation the cultures were terminated, and the medium and extracellular activity were removed by repeatedly washing the cells with phosphate buffered saline solution. The cell monolayer was lysed using 1M NaOH and transferred to test tubes to quantify radioactivity. Radioactivity bound to the cells was quantified in a gamma (γ) counter and is reported (in **Table 3.5**) as a factor of the counts from the γ counter measured in one minute to the total cell count multiplied by 100 (i.e. [counts from the γ counter in one minute / total cell count] x 100).

The results (**Fig. 3.9**) show that there are clearly more uptake of the radiolabelled complexes (**29** and **34**) into the non-cancerous brain endothelial cells compared to the cancer cell lines. This correlated to the cell kinetics of the cell lines, and since cancer cells grow much faster *in vivo*, SPECT imaging studies of carcinoma-bearing mice would give a better understanding of the cellular uptake of these radiolabelled complexes. The results do show that **29** has better cellular uptake into both cancer

cells compared to **34**. This could be attributed to the increased solubility of **29** compared to **34**.

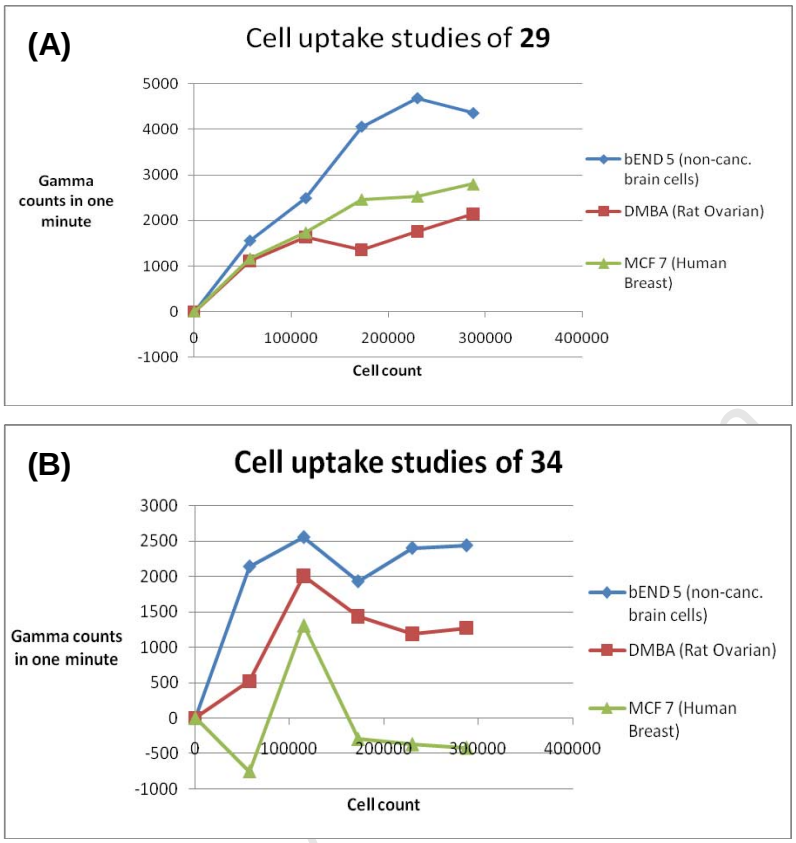

Fig. 3.9: The results of *in vitro* cellular uptake studies of (**A**) **29** and (**B**) **34**.

Table 3.5: The average comparative cellular uptake ([counts from the γ counter in one minute / total cell count] x 100) of **29** and **34** into the various cell lines.

Compound	bEND5	MCF 7	DMBA OC1R
29	2.15	1.30	1.16
34	1.79	N/A[a]	0.91

[a]The background γ count was found to be higher than the total γ count after cellular uptake studies.

3.7. Conclusions/Summary

The total labelling of the thiosemicarbazone ligands with ^{67}Ga took 20-60 minutes, with a radiochemical purity of at least 87% achieved. All the radiolabelled complexes

(**28**-**34**) are stable in an aqueous solution. However, only **29** and **34** relatively are stable in bovine serum, for 2 hours at 37°C. Studies show that the presence of water (up to 40%) in the reaction mixture has no significant effect on the radiolabelling efficiency. Cellular uptake studies (*in vitro*) of **29** and **34** show that there is more uptake into the non-cancerous brain endothelial cells compared to the cancerous cells. The results also show that **29** (mononuclear ligand) has better cellular uptake in the rat ovarian cancer and human breast cancer cells compared to **34** (binuclear ligand). *In vivo* studies would give a better indication as to the promise these compounds possess as imaging agents and it would also show how they compare against existing imaging agents.

3.8. References

1. M. Frezza, C. N. Verani, D. Chen and Q. Ping Dou, *Lett. Drug Des. Discov.*, 2007, **4**, 311.

2. P. Collery, B. Keppler, C. Madoulet and B. Desoize, *Crit. Rev. Oncol. Hemat.*, 2002, **42**, 283.

3. J. Chan, A. L. Thompson, M. W. Jones and J. M. Peach, *Inorg. Chim. Acta*, 2010, **363(6)**, 1140.

4. M. K. Samson, *Cancer Clin. Trials*, 1980, **3**, 131.

5. B. J. Foster and B. Leyland-Jones, *Cancer Treat. Rep.*, 1986, **70**, 1311.

6. R. H. Adamson, G. P. Canellos and S. M. Sieber, *Cancer Chemother. Rep.*, 1975, **59**, 599.

7. F. Kratz, B. Nuber, J. Weiss and B. K. Keppler, *Synth. React. Inorg. Met-. Org. Chem.*, 1991, **21(10)**, 1601.

8. M. F. Gielen, In *Metal-based Antitumor Drugs*, Freund Publishing House Ltd., 1988.

9. H. C. Dudley, G. W. Imirie Jr. and J. T. Istock, *Radiology*, 1950, **55**, 571.

10. H. C. Dudley, H. A. Markowitz and T. G. Mitchell, *J. Bone Joint Surg. Am.*, 1956, **38-A**, 627.

11. K. A. Morton, J. Jarboe and E. M. Burke, *J. Nucl. Med. Technol.*, 2000, **28**, 221.

12. A. R. Jalilian, P. Mehdipour, M. Akhlaghi, H. Yousefnia and K. Shafaii, *Sci. Pharm.*, 2009, **77**, 343.

13. R. B. Firestone, V. S. Shirley, C. M. Baglin and J. Zipkin, In *Table of Isotopes*, 8th Ed., John Wiley and Sons, New York, 1996.

14. V. B. Arion, M. A. Jakupec, M. Galanski, P. Unfried and B. K. Keppler, *J. Inorg. Biochem.*, 2002, **91**, 298.

15. C. R. Kowol, R. Trondl, P. Heffeter, V. B. Arion, M. A. Jakupec, A. Roller, M. Galanski, W. Berger and B. K. Keppler, *J. Med. Chem.*, 2009, **52**, 5032.

16. F. Haghighi Moghadam, A. R. Jalilian, A. Nemati and M. Abedini, *J. Radioanal. Nucl. Chem.*, 2007, **272**, 115-121.

17. M. S. Silberberg,In *Chemistry: The Molecular Nature of Matter and Change*, 2nd Ed., McGraw-Hill, 2000.

18. M. Kubota, Y. Iida, Y. Magata, Y. Kitamura, H. Kawashima and H. Saji, *Jpn J. Pharmacol.*, 2000, **84**, 334.

19. S. R. Kumar, F. A. Gallazzi, R. Ferdani, C. J. Anderson, T. P. Quinn and S. L. Deutscher, *Cancer Biother. Radio.*, 2010, **25(6)**, 693.

20. Z. Chikh, N. –T. Ha-Duong, G. Miguel and J. –M. El Hage Chahine, *J. Biol. Inorg. Chem.*, 2007, **12(1)**, 90.

Chapter 4:

Preliminary investigation into the synthesis of radiolabelled palladium(II) poly(aryl)ether dendrimers.

4.1. Introduction

In recent years, medicinal chemists have begun to realize the key role that dendrimers may play in the future of medicine.[1] Dendrimers consist of a core encased within concentric shells formed by covalently linked branches, as is described in chapter 1.5.[1-3] It has been reported that the field of oncology will soon be revolutionized with the use of dendrimer-based nanodevices in novel strategies for diagnoses and therapy.[1] Cancer diagnoses via magnetic resonance imaging (MRI) could also be improved by incorporation of dendrimers as advanced contrast agents.[1] Dendrimers have also been reported to serve as a central platform for a new generation of nanodevices designed to be multifunctional diagnostic and therapeutic agents.[1] The average size and structure of a dendrimer within a batch can be controlled by precisely reproducing the expansion of the branching network.[1]

Dendrimers have two routes of being synthesized, which is described in chapter 1.5. Dendrimers used for *in vitro* and *in vivo* testing have been synthesized from a number of dendritic structures.[1] Terminal branches of reactive dendrimers can be capped off to neutralize toxicity,[4-6] increase biopermeability[4] and to prevent non-specific targeting during delivery.[1,2] Furthermore, terminal groups can be modified to obtain both a charged and hydrophilic or hydrophobic function for the desired biological and drug delivery application.[3,7] They are also ideal drug delivery systems due to their topology, functionality and dimensions; and their size is also very close to various important biological polymers and assembles.[3,8]

There is a degree of control over the nature and functionality of both the internal building blocks[9] and the chain ends[10,11] in the convergent synthesis of the dendritic

structures.[12] The possibility thus exists for the synthesis of unimolecular dendritic micelles capable of specific non-bonding interactions through specifically-made molecular inclusion sites.[12] It has been shown that this can be achieved through the synthesis of poly(aryl)ether dendritic macromolecules via the convergent growth approach.[12]

While dendrimers reported so far are organic in nature, there is a rising interest in metallodendrimers.[13-17] These metallodendrimers are particularly interesting as the metals can be combined into different parts of the dendritic structure.[13] It has been reported[18] that an increased number of interstrand crosslinks is a key reason for the high activity of di-nuclear compounds against cisplatin-resistant cell lines.[19] This has increased the efforts in developing molecules that will give rise to an increased number of interstrand adducts, and synthesizing multinuclear metallic compounds such as metallodendrimers is said to be a viable approach in developing new drugs.[19]

Enhancement of magnetic resonance imaging (MRI) diagnostic sensitivity can be achieved through the utilization of dendrimer-based contrast agents.[1] It has been reported that targeted delivery of contrast agents have the ability to improve the contrast between cancerous tissue and healthy tissue.[1] Targeted methods have proven to promote nanodevice internalization specifically by cancer tissue.[1]

Interesting biological results using metallodendrimers as potential anticancer agents from Smith and co-workers have also been published.[20,21] Thus, a dendrimer labelled with a radioisotope should provide an interesting look into possible new radioimaging and radiotherapeutic drugs. As there are little to no reports of palladium radioisotopes being used for medicinal purposes, dendrimers radiolabelled with palladium-109 should prove to be an interesting venture into developing new radiopharmaceuticals.

4.2. Synthesis of dendritic core and wedges (*G0* and *G1*)

4.2.1. Synthesis of 2,3-bis(2-methyl-4-hydroxylphenylimino) butane, 35.

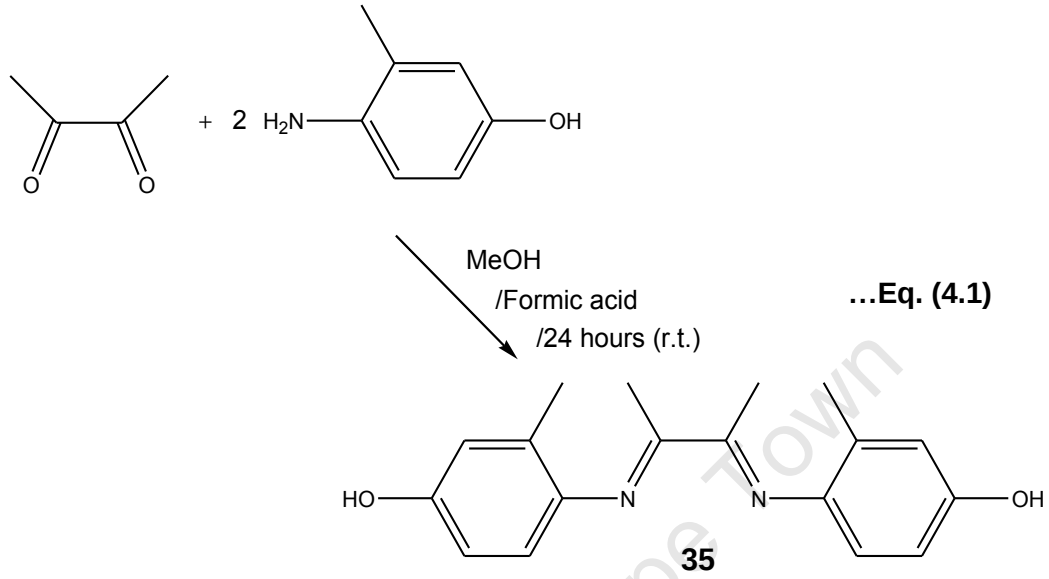

…Eq. (4.1)

35

The procedure for the synthesis (**equation (4.1)**) of this dendritic core, **35**, was described by Blom *et al*.[22] The product was isolated as a yellow/brown solid in a low yield (40%). The para-hydroxyl group allows attachments of various dendritic wedges containing an alkylbromide functionality at the focal point. Using the Williamson ether synthesis, a quantitative yield of dendritically functionalized α-diimine ligands can be expected. Frechet and co-workers[12] reported the quantitative build-up of poly(aryl)ether dendrimers when applying mild reaction conditions.

4.2.2. ^{1}H-NMR spectrum of 35.

The ^{1}H-NMR spectrum (**Fig. 4.1**) showed the same peaks (with similar shifts) as was reported by Blom *et al*.[22] The spectrum shows a broad singlet peak at 7.99 ppm which accounts for the proton on the hydroxyl groups. The spectrum also displays two doublets and one singlet between 6.45-6.75 ppm accounting for the aromatic protons. The protons on the methyl groups attached to the imine bonds and aromatic groups appear further upfield at 2.09 ppm and 2.03 ppm, respectively.

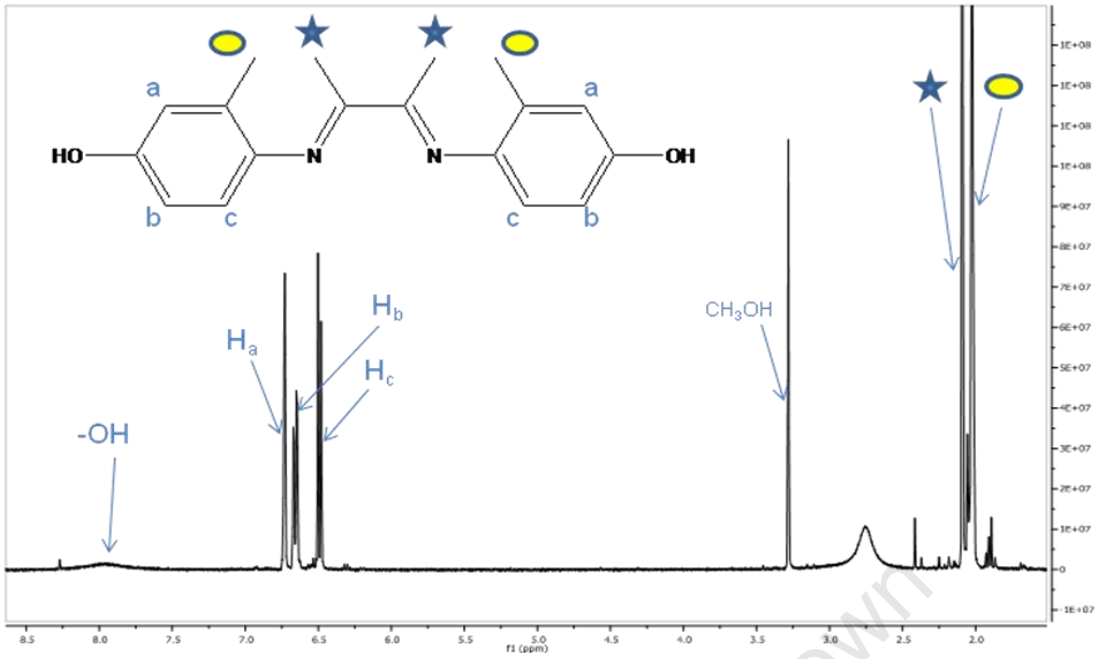

Fig. 4.1: The ^{1}H-NMR spectrum of the dendritic core, **35**.

4.2.3. Infrared spectrum and melting point of 35.

The infrared spectrum shows the presence of a strong intensity absorption band at 1629 cm^{-1} attributed to the imine functionality. This further confirms the formation of **35** via the presence of imine bonds (i.e. Schiff-base condensation reaction). The melting point of **35** occurs between 122-125°C. This is similar to what was reported by Blom *et al*.[22]

4.2.4. Synthesis of Methyl p-bromomethylbenzoate (*G0* wedge), 36.

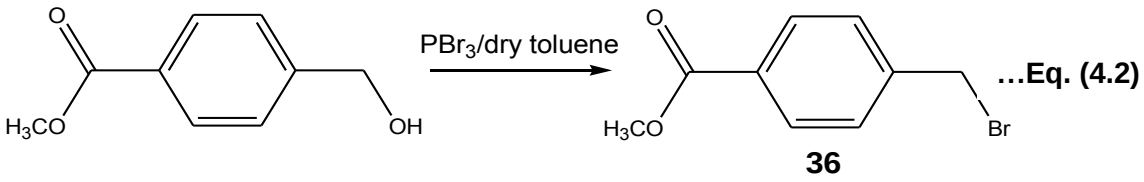

36 …Eq. (4.2)

The procedure for the synthesis of **36** (**equation (4.2)**) was carried out in accordance with that described by Hawker *et al*.[4], with the exception that dry toluene was used instead of dry benzene. A mixture of methyl *p*-hydroxymethylbenzoate and phosphorus tribromide was allowed to react for 2 hours at room temperature. After the necessary washings and extractions, the product was isolated as a white solid in a good yield (87%).

4.2.5. ^{1}H-NMR spectrum and melting point of 36.

The ^{1}H-NMR spectrum (**Fig. 3.1**) shows similar peaks as is reported by Hawker *et al*.[4] The spectrum shows a singlet appearing upfield at 3.90 ppm accounting for the protons on the methyl group. The peak for the protons on the alkylbromide (-CH_2-) appears as a singlet slightly more downfield at 4.48 ppm, whereas the peaks for the aromatic protons appear the most downfield at 7.44 ppm and 7.98 ppm as two doublets. The melting point range of **36** was recorded to be 51-53 °C, which is similar to the literature melting point range of 53-55 °C reported by Aizpurua *et al*.[23]

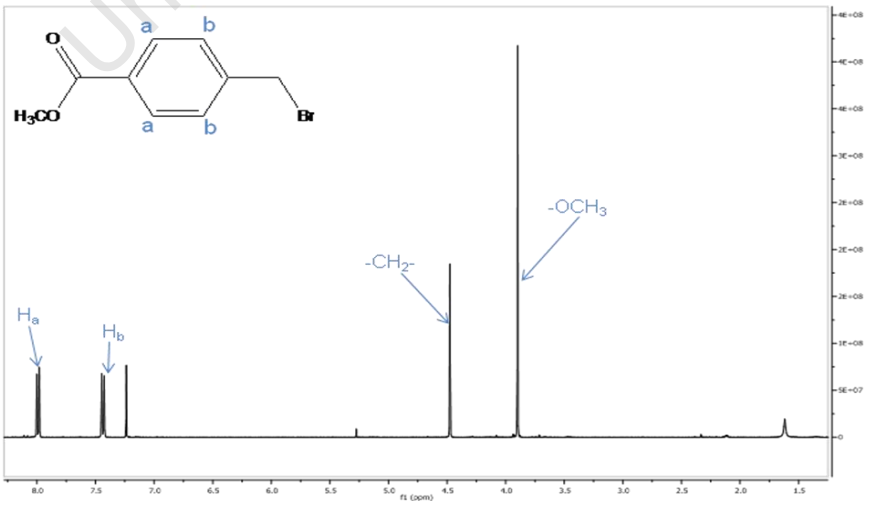

Fig. 4.2: The ^{1}H-NMR spectrum of the *G0* wedge, **36**.

4.2.6. Synthesis of dendritic benzyl alcohol (*G1*), 37.

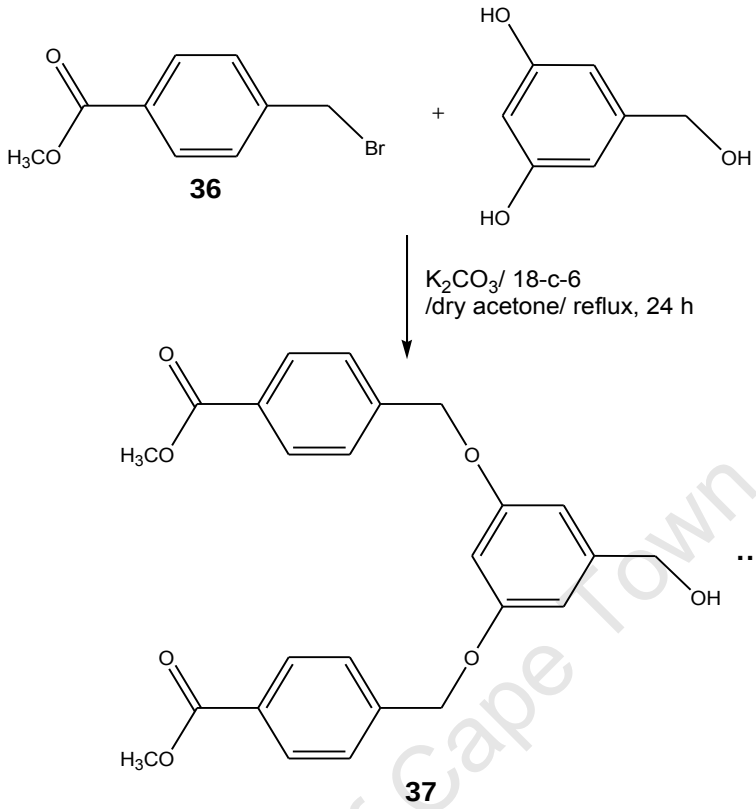

…Eq. (4.3)

The reaction for the synthesis of **37** was performed under an inert atmosphere. In the synthesis of **37** the reaction of two molar equivalents of methyl *p*-bromomethylbenzoate (**36**) to one molar equivalent 3,5-dihydroxybenzyl alcohol (**equation (4.3)**) occurred readily in the presence of potassium carbonate and 18-crown-6 in acetone heated at reflux. The potassium carbonate serves as a base that deprotonates the hydroxyl groups directly bonded to the benzene in 3,5-dihydroxybenzyl alcohol. The reaction gave the product, **37**, as a white solid in a moderate yield (63%).

4.2.7. ^{1}H-NMR spectrum of dendritic benzyl alcohol (*G1*), 37.

The ^{1}H-NMR spectrum of **37** corresponded to the literature report by Hawker *et al*.[12] The proton from the hydroxyl group is found to be most upfield at 3.66 ppm. The protons from the methoxy group, as well as the alkyl protons are also found to be upfield between 3.92-5.10 ppm as singlets. The aromatic protons on the benzyl alcohol moiety appear at 6.51 ppm and 6.61 ppm as a doublet and a triplet,

respectively, due to long range coupling. The aromatic protons on the benzoate moiety are found to be the most downfield at 7.47 ppm and 8.03 ppm as doublets.

4.2.8. Infrared (IR) spectrum and melting point of dendritic benzyl alcohol (*G1*), 37.

The infrared spectrum of **37** shows similar bands to that reported by Hawker *et al*.[12] The spectrum shows the presence of a medium intensity absorption band at 1715 cm^{-1} attributed to the C=O functionality. The melting point of **37** was duplicated and recorded to be 56-59 °C.

4.2.9. Synthesis of dendritic benzyl bromide (*G1* wedge), 38.

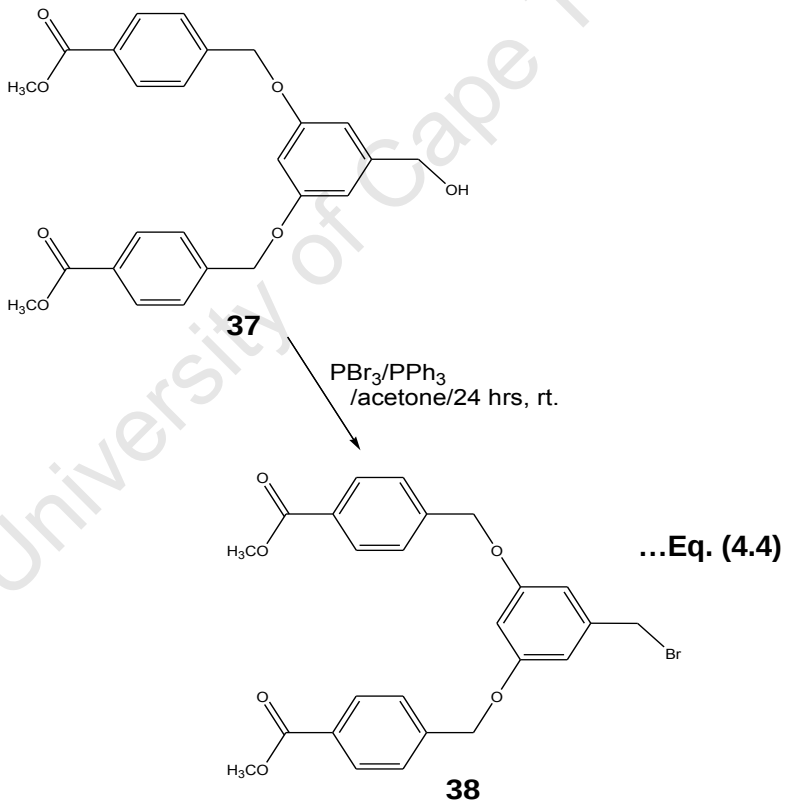

…Eq. (4.4)

The procedure for the synthesis of **38** (**equation (4.4)**) is a modification to the method described by Hawker *et al*.[12] A mixture of dendritic benzyl alcohol (**37**), phosphorus tribromide and triphenylphosphine in acetone was stirred vigorously for 24 hours. After the necessary washings and extractions, the product (**38**) was isolated as a white solid in a moderate yield (54%).

4.2.10. ^{1}H-NMR spectrum of dendritic benzyl bromide (*G1* wedge), 38.

The ^{1}H-NMR spectrum (**Fig. 4.3**) displays all the expected peaks and correlates to the literature spectrum reported by Hawker *et al*.[12] When compared to the ^{1}H-NMR spectrum of the dendritic benzyl alcohol, the absence of the hydroxyl peak in the spectrum of the product, **38**, is the most notable feature. The spectrum shows a singlet peak upfield at 3.92 ppm accounting for the protons on the methyl groups and two singlet peaks at 4.24 ppm and 5.10 ppm accounting for the alkyl protons (i.e. –CH_2Br and –OCH_2–). The aromatic proton peaks appear in the same region, with the same multiplicities, as is seen in the spectrum of **37** (i.e. between 6.51-8.03 ppm).

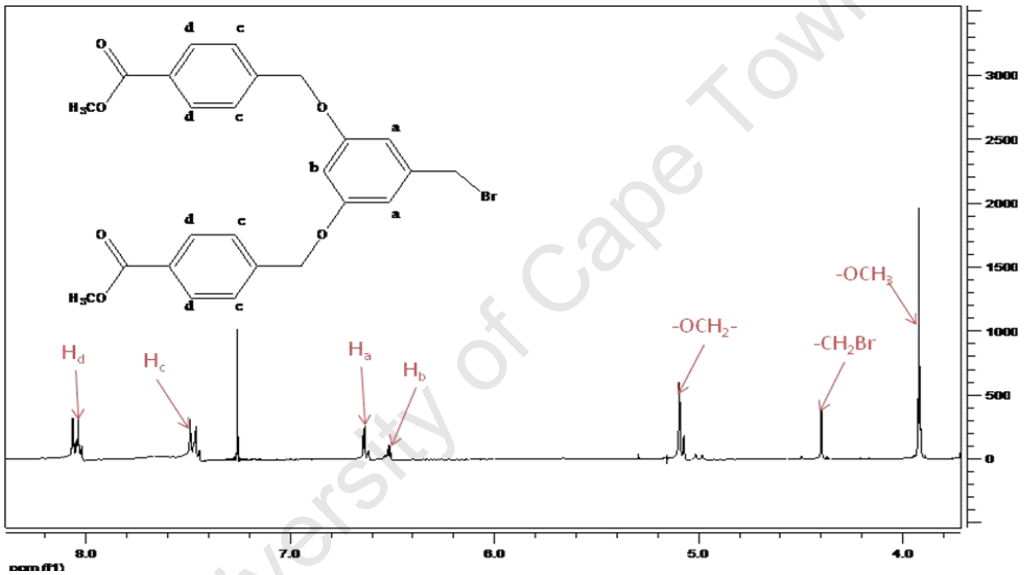

Fig. 4.3: The ^{1}H-NMR spectrum of the *G1* brominated wedge, **38**.

4.2.11. Infrared (IR) spectrum, melting point, elemental analysis and mass spectrometry of dendritic benzyl bromide (*G1* wedge), 38.

The infrared spectrum of **38** also shows similar bands to that reported by Hawker *et al*.[12] The spectrum shows the presence of a medium intensity absorption band at 1720 cm^{-1} attributed to the C=O functionality. The melting point of **38** was recorded to be 137-140 °C, which is similar to the reported melting point of 139-140°C by Hawker *et al*.[12] Elemental analysis of **38** shows all the values are in close agreement with the calculated values. Mass spectrometry (EI+) shows a 100% molecular ion peak accounting for the product molecule (i.e. *m/z* 499.7, [M]$^{+}$).

4.3. Synthesis of dendritic ligands, 39 (*G0*) and 40 (*G1*)

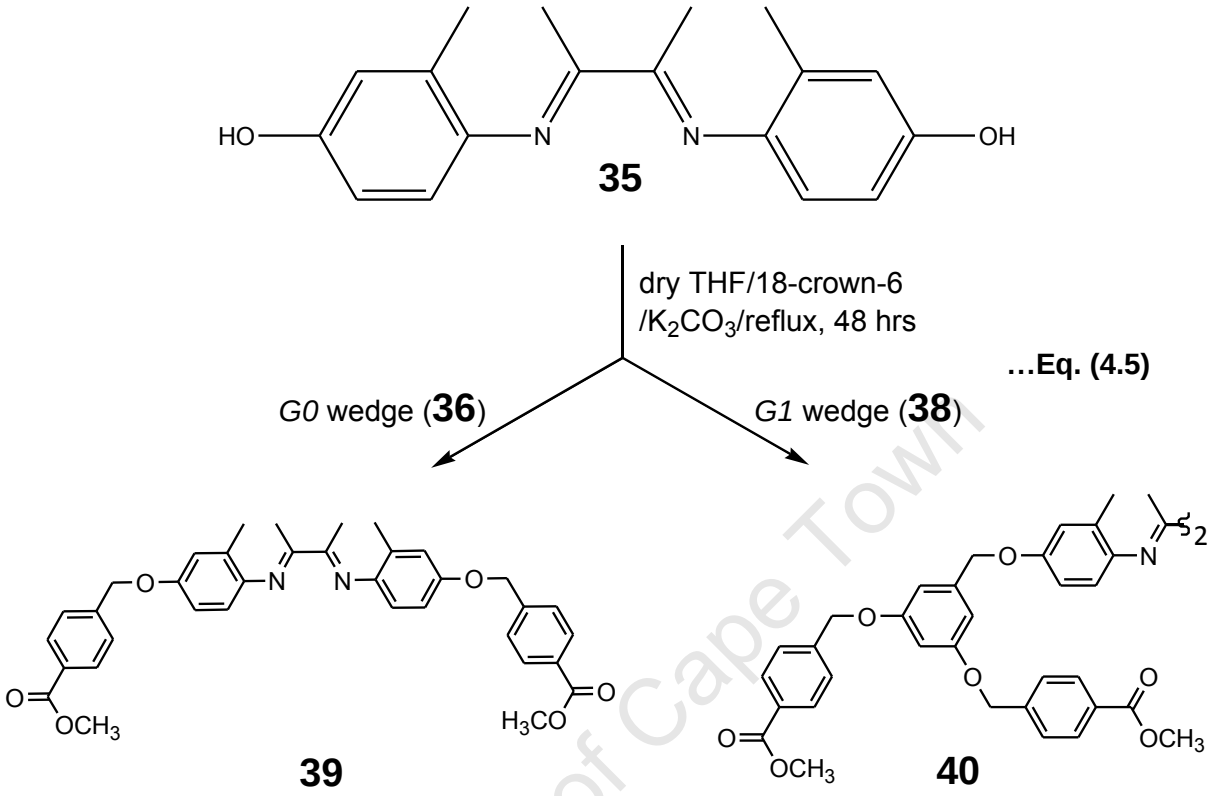

The reactions (**equation (4.5)**) were performed under inert atmosphere. The dendritic ligands (**39** and **40**) were prepared using the standard Williamson ether synthesis, whereby 2,3-bis(2-methyl-4-hydroxylphenylimino)butane (**35**) was reacted with two molar equivalents of the dendritic benzyl bromides (**36** or **38**). Hawker *et al*.[12] previously reported the synthesis of poly(aryl)ether dendrimers and applying the same conditions the dendritic ligands (**39** and **40**) were synthesized in dry tetrahydrofuran heated under reflux, using potassium carbonate as a base and 18-crown-6 as a phase transfer catalyst. The product (**39** or **40**) was separated from the inorganic salts using an aqueous work-up. The dendritic ligands were isolated as an orange-brown solid (**39**) and orange oil (**40**) in moderate to low yields of 57% and 28%, respectively.

4.3.1. ^{1}H-NMR spectra of dendritic ligands, 39 (*G0*) and 40 (*G1*).

The ^{1}H-NMR spectra of the ligands accounted for all expected proton peaks. The methyl protons appear upfield at 2.03 ppm and 2.10 ppm (for both sets of methyl protons) for **39** (**Fig. 4.4**) and **40**, respectively, whereas the methoxy proton peaks appear at 3.81 ppm and 3.92 ppm for **39** and **40**, respectively. The alkyl proton peaks appear slightly more downfield at 5.63 ppm for **39** and 4.98-5.11 ppm for **40**. The methyl and alkyl proton peaks appear as singlets. The aromatic proton peaks of the benzyl groups adjacent to the imine bonds appear in the region between 6.58-6.90 ppm (**39**) and 6.62-6.97 ppm (**40**), as a singlet and two doublets in each spectrum. The protons on the terminal benzene moieties display proton peaks in similar regions for **39** and **40** (i.e. 7.56-7.93 ppm and 7.56-8.05 ppm, respectively). The peaks occurring at 6.50 ppm and 6.58 ppm in the spectrum of **40** are due to the protons on the benzene adjacent to the three alkoxy groups.

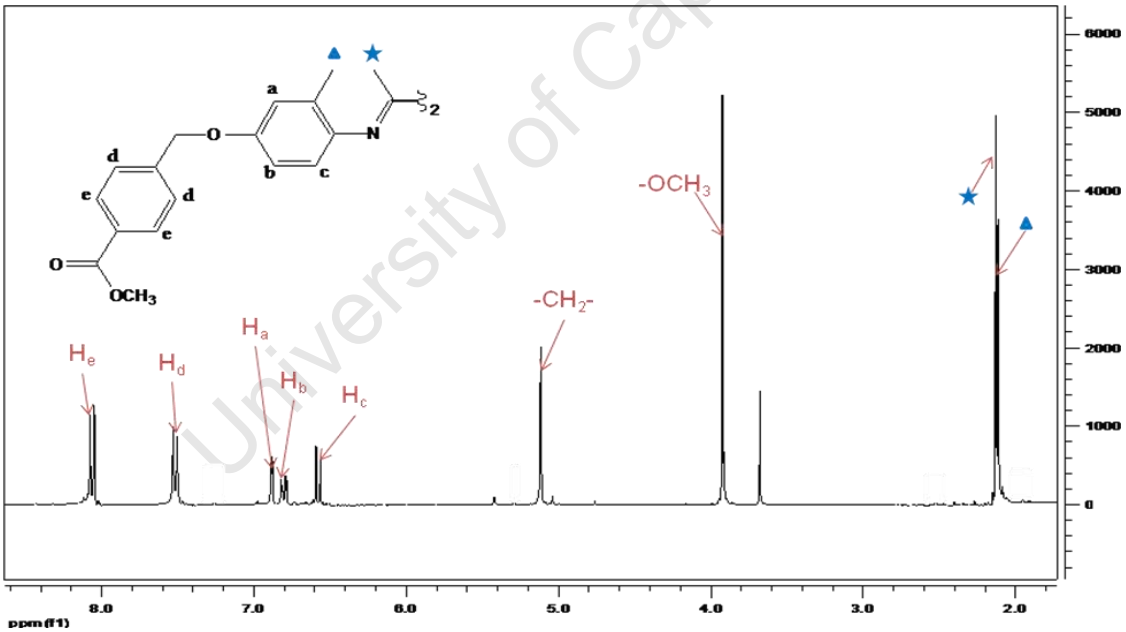

Fig. 4.4: The ^{1}H-NMR spectrum of the *G0* ligand, **39**.

4.3.2. Infrared spectra, melting point, elemental analysis and mass spectrometry of dendritic ligands, 39 (*G0*) and 40 (*G1*).

The characteristic medium intense absorption band occurring at 1638 cm^{-1} and 1636 cm^{-1} in the IR spectra of **39** and **40**, respectively, are attributed to the imine functionality. This band is at a slightly higher frequency when compared to the absorption band at 1629 cm^{-1} attributed to the imine functionality of the core, **35**. This could possibly be due to the added wedge decreasing the electron withdrawing effect of the oxygen on the core component of the ligand. There are also bands above 2900 cm^{-1} which are characteristic of ν(C-H) aliphatic frequencies, as well as an intense absorption band at 1716 cm^{-1} and 1720 cm^{-1} for **39** and **40**, respectively, which could be attributed to the RCOOR functionality.

The melting point of the newly synthesized *G0* ligand (**39**) was recorded at 149-153°C, higher than the melting points recorded for its component parts, the core (**35**) and the *G0* wedge (**36**). The elemental analysis was in close agreement to the calculated values for the *G0* ligand, and mass spectrometry (**Fig. 4.5**) gave a 100% protonated molecular ion peak (i.e. m/z 593.3, $[M+H]^+$) for the ligand, **39**.

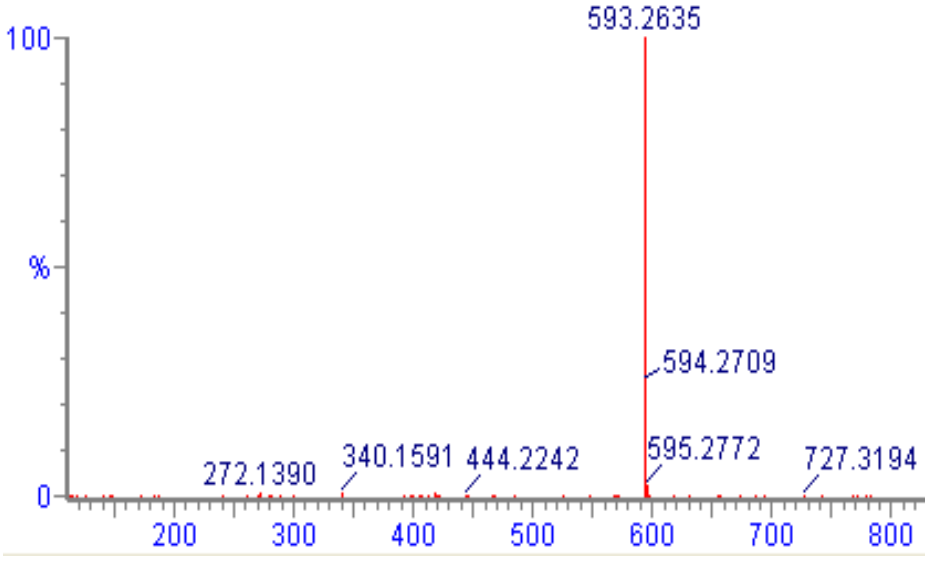

Fig. 4.5: Mass spectrometry (ESI) of *G0* ligand, **39**.

4.4. Synthesis of dendritic complexes, 41 (*G0*) and 42 (*G1*)

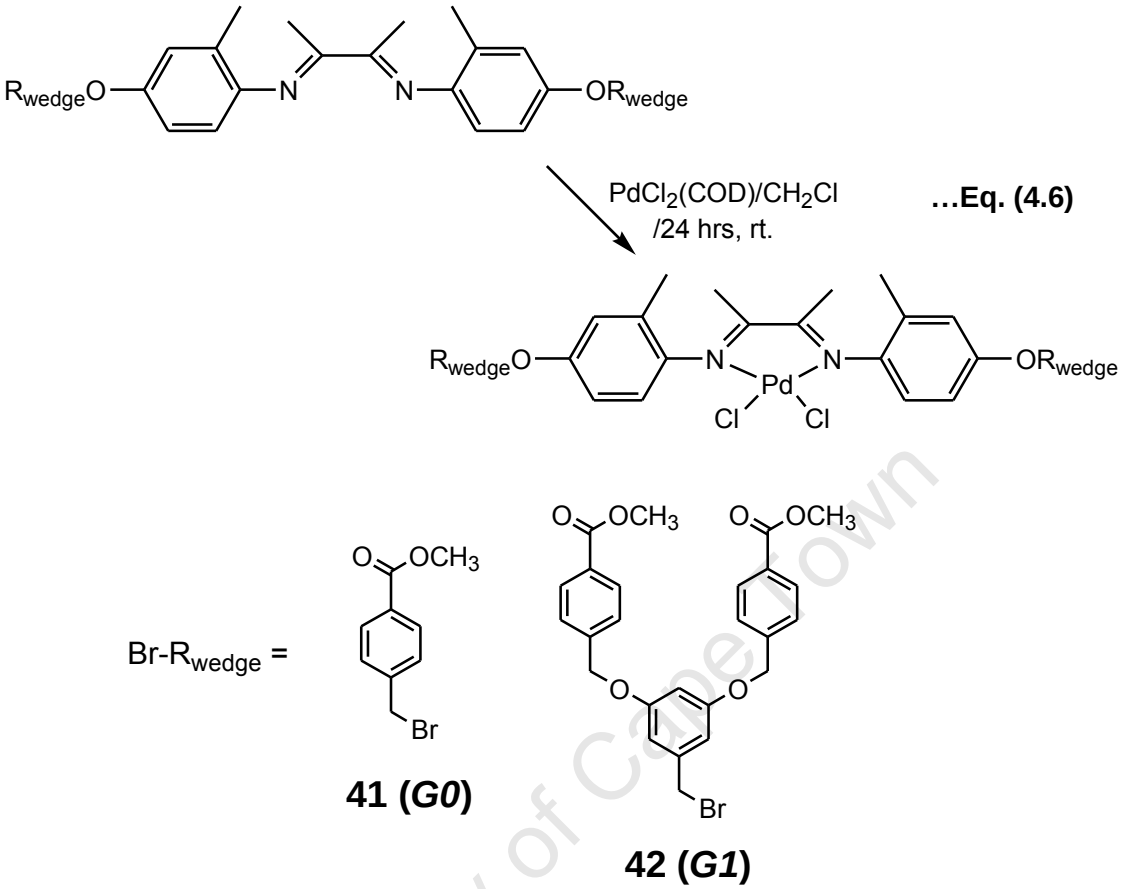

The reactions for the synthesis of **41** and **42** (**equation (4.6)**) were performed under an inert atmosphere using conditions described by Blom *et al*.[22] for similar complexes. The newly synthesized palladium complexes (**41** and **42**) of the α-diimine ligands were prepared by treating a slight excess of the ligand with $PdCl_2(COD)$ in dry dichloromethane. The reactions were allowed to stir for 24 hours at room temperature. The products were isolated as yellow-orange solids in moderate to good yields of 58% and 73% for **41** and **42**, respectively.

4.4.1. ^{1}H-NMR spectra of dendritic complexes, 41 (*G0*) and 42 (*G1*).

The ^{1}H-NMR spectra of the complexes (**41** and **42**) show similar peak shifts as is seen in the spectra of the dendritic ligands (**39** and **40**). This is expected as the coordination of the palladium to the core could possibly only cause a shift in the

protons of the methyls bonded to the imines. However, there are no significant shifts observed for these peaks.

4.4.2. Infrared spectra, melting points and elemental analyses of dendritic complexes, 41 (*G0*) and 42 (*G1*).

The infrared spectra of **41** and **42** show a characteristic medium intensity absorption band occurring at 1578 cm^{-1} and 1571 cm^{-1}, respectively, which can be attributed to the imine functionality. This was lower than the attributed $\nu(C{=}N_{imine})$ frequencies of the respective ligands, **39** and **40**, which occur at 1640 cm^{-1} and 1639 cm^{-1}, respectively. These shifts are also reported by Blom *et al*.[22] for similar compounds (i.e. a shift from 1640-1639 cm^{-1} for the ligands to 1579-1570 cm^{-1} for the complexes). The shifts are most likely due to the palladium withdrawing electron density from the ligands.

Table 4.1: Absorption bands (cm^{-1}) attributed to the imine functionalities observed in the IR spectra (using KBr pellets) of **39**-**42** compared to absorption bands (cm^{-1}) observed by Blom *et al*.[22] (in brackets) for similar compounds.

Generation	**39-42 (Blom *et al*.[22])**	
	Ligands	**Complexes**
G0	1638 (1640)	1578 (1579)
G1	1636 (1639)	1571 (1570)

The melting point determination revealed that the *G0* complex (**41**) decomposed (without melting) above 290°C, proving that the product is not unreacted ligand (melting point = 149-153 °C), which further suggests complexation had occurred.

4.5. Radiolabelling studies

The dendritic ligands, subsequent to their synthesis, were tested for their radiolabelling ability with ^{109}Pd. The dendritic ligand (**39** or **40**) in an organic solution (ethanol, acetonitrile or dichloromethane) was reacted with [^{109}Pd]$PdCl_2$ in HCl/H_2O. The reactions were heated at 41-55°C for 1-1.5 hours, after which the reaction mixtures were analysed using a HPLC coupled to a radiodetector. The HPLC chromatograms of the reactions using both ligands show no significant new peak similar to that of the cold complexes (a peak just below 5 minutes for both **41** and **42**) in the 0 - 700 keV region. However, the chromatogram for the reaction using the *G0* ligand in dichloromethane shows a relatively small peak just above 21 minutes. This suggests that a radiolabelled species had formed. This peak could not be further analyzed as the nuclide had decayed too much overnight (i.e. there were no visible peaks in the chromatograms after radioanalysis was carried out the following day). The chromatograms show a peak at approximately 3 minutes which could be due to free [^{109}Pd]$PdCl_2$. HPLC-MS was also used to analyze the reaction mixture. However, no new information could be extracted. Gamma spectrum analysis shows that the ^{109}Pd nuclide was present in the mixture for the reaction using the *G0* ligand, however, it does not show whether the nuclide was free or part of a complex.

4.6. Conclusion/Summary and Future work

Two new dendritic poly(aryl)ether ligands were synthesized in moderate yields via a series of steps. These ligands were characterized using various spectroscopic and analytical techniques. The ligands were subsequently reacted with $PdCl_2$(COD) to afford dendritic poly(aryl)ether complexes, which were also characterized. The ligands were tested for their radiolabelling ability with ^{109}Pd (in the form of $^{109}PdCl_2$) in different organic solvents. There is a currently unidentified peak in the HPLC chromatogram, found when analyzing the reaction mixture in dichloromethane as reaction solvent. This suggests that a radiolabelled species had formed. However, this peak could not be further analyzed due to the decay of ^{109}Pd. Future works would include the synthesis of radiolabelled palladium(II) dendrimers in dichloromethane using synthesized $^{109}PdCl_2$(COD).

4.7. References

1. I. J. Majoros, C. R. Williams and J. R. Baker, Jr., *Curr. Top. Med. Chem.*, 2008, **8**, 1165.

2. I. J. Majoros, T. P. Thomas, C. B. Mehta and J. R. Baker, Jr., *J. Med. Chem.*, 2005, **48**, 5892.

3. D. J. Bharali, M. Khalil, M. Gurbuz, T. M. Simone and S. A. Mousa, *Int. J. Nanomed.*, 2009, **4**, 1.

4. D. A. Tomalia, L. A. Reyna and S. Svenson, *Biochem. Soc. Trans.*, 2007, **35**, 61.

5. H. –T. Chen, M. F. Neerman, A. R. Parrish and E. E. Simanek, *J. Am. Chem. Soc.*, 2004, **126**, 10044.

6. R. Duncan and L. Izzo, *Adv. Drug Deliv. Rev.*, 2005, **57**, 2215.

7. S. Bai, C. Thomas, A. Rawat and F. Ahsan, *Crit. Rev. Ther. Drug Carrier Syst.*, 2006, **23**, 437.

8. E. R. Gillies and J. M. Frechet, *Drug Discov. Today*, 2005, **10**, 35.

9. C. J. Hawker and J. M. J. Frechet, *J. Am. Chem. Soc.*, 1992, **114**, 8405.

10. C. J. Hawker and J. M. J. Frechet, *Macromolecules*, 1990, **23**, 4726.

11. K. L. Wooley, C. J. Hawker and J. M. J. Frechet, *J. Chem. Soc. Perkin Trans. 1*, 1991, 1059.

12. C. J. Hawker, K. L. Wooley and J. M. J. Frechet, *J. Chem. Soc. Perkin Trans. 1*, 1993, 1287.

13. C. Cordovilla, S. Coco, P. Espinet and B. Donnio, *J. Am. Chem. Soc.*, 2010, **132(4)**, 1424.

14. G. R. Newkome, C. N. Moorefield and F. Vogtle, In *Dendrimers and Dendron: Concepts, Synthesis and Applications*, Wiley & Sons., Weinheim, 2001.

15. E. C. Constable, *Chem. Commun.*, 1997, 1073.

16. M. A. Hearshaw and J. R. Moss, *Chem. Commun.*, 1999, 1.

17. D. Méry and D. Astruc, *Coord. Chem. Rev.*, 2006, **250**, 1965.

18. Y. Qu and N Farrell, *J. Inorg. Biochem.*, 1990, **40**, 255.

19. X. Zhao, S. C. J. Loo, P. P. –F. Lee, T. T. Y. Tan and C. K. Chu, *J. Inorg. Biochem.*, 2010, **104**, 105.

20. P. Govender, A. K. Renfrew, C. M. Clavel, P. J. Dyson, B. Therrien and G. S. Smith, *Dalton Trans.*, 2011, **40(5)**, 1158.

21. P. Govender, N. C. Antonels, J. Mattsson, A. K. Renfrew, P. J. Dyson, J. R. Moss, B. Therrien and G. S. Smith, *J. Organomet. Chem.*, 2009, **694(21)**, 3470.

22. B. Blom, M. J. Overett, R. Meijboom and J. R. Moss, *Inorg. Chim. Acta*, 2005, **358**, 3491.

23. J. M. Aizpurua, B. Lecea and C. Palomo, *Can. J. Chemistry*, 1986, **64(12)**, 2342.

Chapter 5:

Experimental

5.1. General Procedure

5.1.1. Chemicals and radiochemicals

All complexation reactions were carried out under nitrogen, using a glovebox (MBraun Unilab) or standard Schlenk line techniques under argon. The starting materials, thiosemicarbazide and 4,4-dimethyl-3-thiosemicarbazide, were purchased from Sigma-Aldrich Co. and were used as delivered. Acetophenone, 2-furaldehyde, 2-pyrrolecarboxaldehyde, 2-pyridinecarboxaldehyde, 3-pyridinecarboxaldehyde, 2-acetylpyridine, 2-acetylfuran, 2-acetylpyrrole, 3-acetylpyridine and sodium acetate were also purchased from Sigma-Aldrich Co. and were used without any further purification. Benzaldehyde was purchased from Merck and was used without any further purification. All reaction solvents were AR grade, purchased from Kimix Chemicals. The metal salts, gallium(III) chloride and gallium(III) nitrate, were both purchased from Sigma-Aldrich Co. The cation exchange resin was obtained from Bio-Rad. The gallium(III) chloride was stored in a glovebox under inert atmosphere. Reactions performed using gallium(III) chloride required the use of dry ethanol. Radiolabelling reactions were carried out in absolute ethanol stored over 4Å molecular sieves.

Caution was taken when working with radioisotopes. For any work with an open radioactive source, gloves (long-cuffed), a full-length lab coat and close-toed shoes were worn. All radioisotopes were handled inside lead pots, and all radiolabelling experiments were performed behind lead-brick walls. ^{67}Ga was produced at iThemba LABS, making use of the ^{nat}Zn(p,2n)^{66,67}Ga nuclear reaction. After the target bombardment process, the radionuclidic impurity, ^{66}Ga, having a much shorter half-life (9.4 hours) than ^{67}Ga (78.3 hours), was allowed to decay to an acceptable low level before the chemical separation process was started. The irradiated target was dissolved in 10M HCl and the solution was loaded onto an AmberChrom Cg-71 cd

synthetic absorbent resin, pre-equilibrated with 7M HCl. The column was then washed with 200 mL 7M HCl to remove the target material and other radionuclidic impurities. Finally, the ^{67}Ga was eluted with 25 mL 0.5M HNO_3. The solution was evaporated to dryness and the activity re-dissolved in 6 mL 0.01M HCl to render [^{67}Ga]$GaCl_3$. A few labelling reactions were carried out using the acidic aqueous [^{67}Ga]$GaCl_3$ solution. However, a few others were also carried out using an acidic acetonic solution. This was prepared as follows: A 1 mL solution of [^{67}Ga]$GaCl_3$ in 0.01M HCl was loaded on a small cation exchange resin column (70 mg AGMP-50 resin, 200-400 mesh, H^+ form, pre-equilibrated with 1 mL 0.1M HCl). Elution through the resin was facilitated by applying a small negative pressure inside the receiving vial. The resin was subsequently eluted with a mixture of 80% acetone in 0.15M HCl (0.5 mL), followed by 98% acetone in 0.05M HCl (0.5 mL). The latter eluate contained the bulk of the activity and was used in a few labelling reactions. All labelling reactions using [^{67}Ga]$GaCl_3$ were carried out in 2 mL glass vials (approximately 6 mm in diameter). The palladium(II) radioisotope, ^{109}Pd, was produced at the South African Nuclear Energy Corporation (NECSA) at Pelindaba, making use of the ^{108}Pd(n,g)^{109}Pd nuclear reaction. The target bombardment process lasted 84 hours, with a cooling time of 47 hours and 45 minutes.

5.1.2. Physical Measurements

The Nuclear Magnetic Resonance (NMR) spectra were recorded on a Varian Unity XR400 (^{1}H: 399.95 MHz), Varian Mercury XR300 (^{1}H: 300.08 MHz, ^{13}C{^{1}H}: 75.46 MHz) or Bruker Ultrashield 400 Plus (^{1}H: 400.20 MHz) spectrometer at ambient temperature with tetramethylsilane (TMS) as an internal standard. IR spectra were measured on a Perkin-Elmer Spectrum One FT-IR Spectrometer using KBr (4000-400 cm^{-1}) pellets. Elemental analysis was carried out using a Fision EA 110 CHNS elemental analyzer and melting points were determined using a Kofler hot stage microscope (Riechart Thermover). Radioactivity measurements were carried out in a Vinten Isocal II Radionuclide Assay Calibrator, using the millicurie (mCi) as the radioactivity unit. High Performance Liquid Chromatography (HPLC) was carried out on a Perkin Elmer Series 200 lc pump (for binary elution) using a Phenomenex Luna 5µ C18 250x4.6 mm^2 column and 2 mM ethylenediaminetetraacetic acid (EDTA) pH4: acetonitrile (MeCN) as the mobile phase. A gradient elution method was

employed, whereby an 80: 20 (2 mM EDTA pH4: MeCN) mixture was used as the mobile phase for the first 5 minutes, followed by a gradual change to 40: 60 for the next 5 minutes, and thereafter maintaining this ratio for a further 5 minutes. Finally, the ratio was changed to 100% MeCN over 5 minutes. The column outlet was coupled to a NaI (Tl) radioactivity detector, which in turn was connected to an ORTEC ratemeter and a high voltage power supply (1 kV). A Hewlett Packard HP3394 integrator was used to record chromatograms. An alternative HPLC system was also used, consisting of an Agilent 1100 Series pump, equipped with an HP 1100 Series Control Module for binary gradient elution and a Rheodyne Model 7725 injector. The same type of column was used. The column outlet was coupled to a Spectra Series UV100 detector, set at 254 nm, which, in turn, was coupled in series with a Carroll & Ramsey Model 105S-1 CsI(Tl) radioactivity detector. Chromatograms were recorded on a dual channel Chromatopac C-R8A from Shimadzu. An identical gradient elution programme to the one described above was used. Retention times of the cold complexes (detected by the UV detector and recorded on channel 1) were compared with those of the radiolabelled complexes (detected by the radioactivity detector and recorded on channel 2) in order to prove the authenticities of the latter.

5.2. Synthesis and Characterisation

5.2.1. Synthesis of monthiosemicarbazone ligands.

5.2.1.1. Synthesis of benzaldehyde thiosemicarbazone, ***1***.[1]

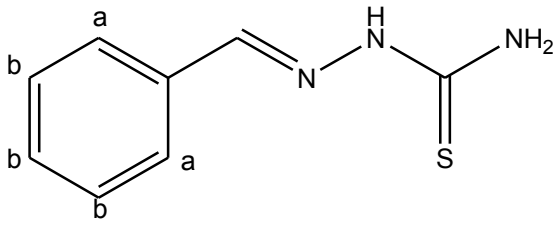

1

Warm ethanol (30 mL) was added to benzaldehyde (0.60 mL; 0.0059 mol.). Thiosemicarbazide (0.55 g; 0.0060 mol.) dissolved in warm water (30 mL) was added to the benzaldehyde/ethanol mixture. The reaction mixture was refluxed at 65°C for 2 hours. The reaction mixture was allowed to cool to room temperature before it was cooled further in ice. A white product precipitated out of solution during cooling in an ice-bath. The white precipitate was collected by suction filtration and was isolated as a white powder. The white powder was recrystallized in aqueous ethanol (50%). A pure white powder of **1** (0.55 g; 51 %) was yielded. **Melting point** = 161-162°C (lit. M.P. = 159°C[1]). **Elemental analysis** calculated for $C_8H_9N_3S$: C, 53.61; H, 5.06; N, 23.44; S, 17.89%. Found: C, 53.60; H, 5.23; N, 23.76; S, 18.14%. **^{1}H-NMR** (400 MHz, DMSO-d_6): δ 7.42 ppm (m, 3H, H_b); 7.81 ppm (m, 2H, H_a); 7.98 ppm (s, 1H, -HN-**H**); 8.09 ppm (s, 1H, -CH=N-); 8.19 ppm (s, 1H, -HN-**H**); 11.42 ppm (s, 1H, -NH-). **FT-IR** (KBr pellet): ν ($C=N_{imine}$) 1591 cm^{-1} (*s*).

5.2.1.2. Synthesis of 2-furaldehyde thiosemicarbazone, **2**.[2]

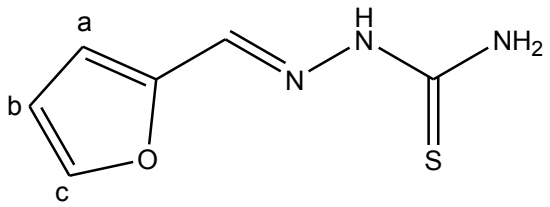

2

Thiosemicarbazide (0.91 g; 0.010 mol) was dissolved in warm distilled water (50 mL). The thiosemicarbazide solution was added to an ethanolic solution (30 mL) of 2-furaldehyde (0.83 mL; 0.010 mol). The reaction mixture was allowed to reflux at 60°C for 24 hours. The reaction mixture was allowed to cool to room temperature before it was put in an ice-bath to further cool. An orange solid precipitated out of solution on cooling in the ice-bath. The orange solid was collected by suction filtration and was washed with cold ethanol. The product, **2**, was isolated as an orange powder (0.69 g; 41%). **Melting point** = 150-151 °C (Lit. M.P. = 159 °C[3]). **Elemental analysis** calculated for $C_6H_7N_3SO$: C, 42.59; H, 4.17; N, 24.83; S, 18.95%. Found: C, 42.45; H, 4.11; N, 26.00; S, 19.12%. **^{1}H-NMR** (400 MHz, DMSO-d_6): δ 6.63 ppm (s, 1H, H_b); 6.99 ppm (s, 1H, H_a); 7.61 ppm (s, 1H, -HN-**H**); 7.81 ppm (s, 1H, H_c); 8.00 ppm (s, 1H, -CH=N-); 8.19 ppm (s, 1H, -HN-**H**); 11.41 ppm (s, 1H, -NH-). **FT-IR** (KBr pellet): ν (C=N_{imine}) 1583 cm^{-1} (*s*).

5.2.1.3. Synthesis of phenyl-4,4-dimethylthiosemicarbazone, ***3***.[4]

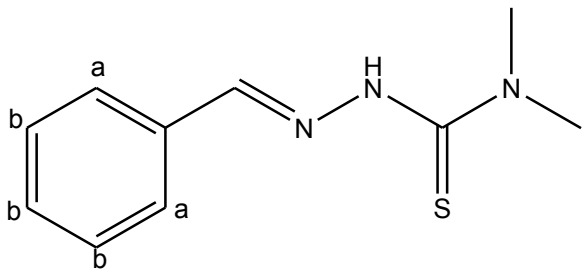

3

Benzaldehyde (0.18 mL; 0.0018 mol) was added to a round-bottom flask. Ethanol (10 mL) was added to the flask and the mixture was stirred at room temperature. Ethanol (16 mL) was added to 4,4-dimethyl-3-thiosemicarbazide (0.20 g; 0.0017 mol) in a beaker. The mixture in the beaker was heated to dissolve the 4,4-dimethyl-3-thiosemicarbazide in the ethanol. The 4,4-dimethyl-3-thiosemicarbazide solution was added dropwise to the flask containing the benzaldehyde in ethanol solution. The mixture turned yellow upon the dropwise addition of the 4,4-dimethyl-3-thiosemicarbazide solution. The reaction mixture was allowed to reflux at 90°C for 5 hours before it was cooled back to room temperature with stirring. The reaction mixture was stirred overnight at room temperature. A yellowish precipitate had formed overnight. The reaction mixture was put in an ice-bath to further cool. A white precipitate was seen to have formed and was collected by suction filtration. The white precipitate was washed with cold distilled water. A white powder of **3** (0.21 g; 60 %) was yielded. **Melting point** = 155-160°C (Lit. M.P. = 167-168°C[5]). **Elemental analysis** calculated for $C_{10}H_{13}N_3S$: C, 57.94; H, 6.32; N, 20.27; S, 15.47%. Found: C, 57.58; H, 6.21; N, 19.90; S, 15.31%. **^{1}H-NMR** (300 MHz, DMSO-d_6): δ 3.29 ppm (s, 6H, -N(CH_3)$_2$); 7.40 ppm (m, 3H, H_b); 7.63 ppm (m, 2H, H_a); 8.17 ppm (s, 1H, -CH=N-); 10.81 ppm (s, 1H, -NH-). **FT-IR** (KBr pellet): ν (C=N_{imine}) 1599 cm^{-1} (*w*).

*5.2.1.4. Synthesis of 3-pyridine thiosemicarbazone, **4**.*

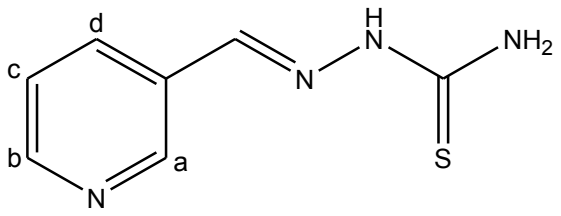

4

Ethanol (10 mL) was added to 3-pyridinecarboxaldehyde (0.84 mL; 0.0089 mol) in a round-bottom flask. The mixture was allowed to stir at room temperature. Thiosemicarbazide (0.81 g; 0.0089 mol) proved to be insoluble in ethanol (30 mL), even upon heating. The thiosemicarbazide in ethanol was added to the 3-pyridinecarboxaldehyde in ethanol mixture as a suspension. The reaction mixture was refluxed at 90-100°C for 6 hours before it was allowed to cool to room temperature with stirring. The reaction mixture was stirred for 3 days. A white precipitate had formed upon stirring at room temperature and the reaction mixture was put in an ice-bath to further cool. The white precipitate was collected by suction filtration and was washed with cold distilled water. The white powder that was collected was dried in an oven at 100°C for 2 hours. A white powder of **4** (1.4 g; 87 %) was yielded. **Melting point** = 212-213°C (Lit. M.P. = 221-222°C[6]). **Elemental analysis** calculated for $C_7H_8N_4S$: C, 46.65; H, 4.47; N, 31.09; S, 17.79%. Found: C, 46.66; H, 4.39; N, 30.07; S, 17.34%. **^{1}H-NMR** (400 MHz, DMSO-d_6): δ 7.43 ppm (m, 1H, H_c); 8.10 ppm (s, 1H, -CH=N-); 8.12 ppm (s, 1H, H_d); 8.26 ppm (m, 2H, -NH_2); 8.59 ppm (m, 1H, H_b); 8.95 ppm (s, 1H, H_a); 11.56 ppm (s, 1H, -NH-). **FT-IR** (KBr pellet): ν (C=N_{imine}) 1591 cm^{-1} (*m*).

5.2.1.5. Synthesis of 2-formylpyridine thiosemicarbazone, ***5***.[7]

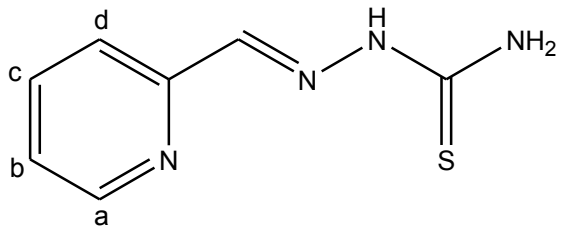

5

Ethanol (10 mL) was added to 2-pyridinecarboxaldehyde (0.95 mL; 0.010 mol) in a round-bottom flask. The mixture was allowed to stir at room temperature. Ethanol (30 mL) was added to thiosemicarbazide (0.91 g; 0.010 mol) in a beaker. The thiosemicarbazide was a suspension in the ethanol. The thiosemicarbazide suspension was added to the stirring 2-pyridinecarboxaldehyde/ethanol mixture in the flask. The reaction mixture was allowed to reflux at 80-90°C for 6 hours. The reaction mixture was a milky-yellow colour. After refluxing, the reaction mixture was cooled to room temperature and was stirred overnight. The round-bottom flask was further cooled in an ice-bath. A milky-yellow precipitate was formed, collected by suction filtration and washed with cold ethanol. The product was dried in an oven at 100°C for 2 hours. The product **5** (1.4 g; 79 %) was isolated as a white powder. **Melting point** = 206-207 °C (Lit. M.P. = 197-198 °C[8]). **Elemental analysis** calculated for $C_7H_8N_4S$: C, 46.65; H, 4.47; N, 31.09; S, 17.79 %. Found: C, 46.76; H, 4.38; N, 30.88; S, 17.84 %. **^{1}H-NMR** (300 MHz, DMSO-d_6): δ 7.35 ppm (t, 1H, ^3J = 7.45 Hz, H_b); 7.80 ppm (t, 1H, ^3J = 7.38 Hz, H_c); 8.07 ppm (s, 1H, HN-**H**); 8.11 ppm (s, 1H, -CH=N-); 8.22 ppm (d, 2H, ^3J = 7.99 Hz, H_d + HN-**H**); 8.56 ppm (d, 1H, ^3J = 4.85 Hz, H_a); 11.55 ppm (s, 1H, -NH-). **FT-IR** (KBr pellet): ν (C=N_{imine}) 1588 cm^{-1} (*m*).

5.2.1.6. Synthesis of 2-acetylpyridinethiosemicarbazone, **6**.[9]

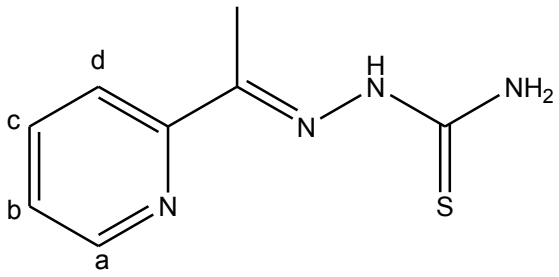

6

Ethanol (5 mL) was added to 2-acetylpyridine (1.12 mL, 0.01 mol) in a round-bottom flask, followed by stirring of the mixture. Thiosemicarbazide (0.9126 g, 0.01 mol.) was added to the round-bottom flask subsequent to the addition of more ethanol (15 mL) to the stirring mixture. Acetic acid (1 mL) was added followed by refluxing (at 80-90 °C) of the reaction mixture for 5 hours. The reaction solution was yellow during and after refluxing. The reaction mixture was allowed to stir overnight at room temperature. After stirring overnight, the reaction mixture was further cooled in an ice-bath. This allowed for a yellow solid to be precipitated out of the solution. The solid was collected using a Büchner funnel and was dried in an oven (at 100 °C). A light-yellow powder of **6** (1.5771 g, 81 %) was isolated. **Melting point** = 163-165 °C (Lit. M.P. = 161-162 °C[9]). **Elemental analysis** calculated for $C_8H_{10}N_4S$: C, 49.46; H, 5.19; N, 28.84; S, 16.51 %. Found: C, 49.15; H, 5.21; N, 29.16; S, 16.53 %. **^{1}H-NMR** (400 MHz, DMSO-d_6): δ 2.41 ppm (s, 3H, -CH_3); 7.40 ppm (t, 1H, ^3J = 6.03 Hz, H_b); 7.80 ppm (t, 1H, ^3J = 7.93 Hz, H_c); 8.13 ppm (s, 1H, -HN-**H**); 8.38 ppm (s, 1H, -HN-**H**); 8.42 ppm (d, 1H, ^3J = 8.10 Hz, H_d); 8.60 ppm (d, 1H, ^3J = 4.38 Hz, H_a); 10.29 ppm (s, 1H, -NH-). **FT-IR** (KBr pellet): ν (C=N_{imine}) 1600 cm^{-1} (*m*).

5.2.1.7. Synthesis of 2-acetylfuranthiosemicarbazone, **7**.[10]

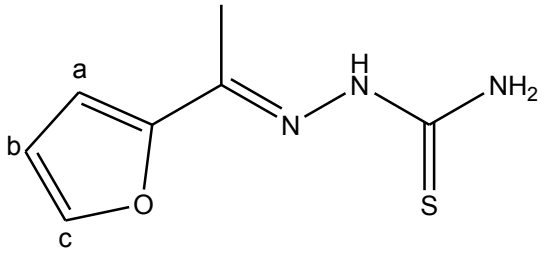

7

Ethanol (20 mL) was added to 2-acetylfuran (1.1012 g, 0.01 mol.) in a round-bottom flask. The mixture was stirred to dissolve the 2-acetylpyridine. Thiosemicarbazide (0.9118 g, 0.01 mol.) was added to the round-bottom flask subsequent to the addition of more ethanol (15 mL) to the stirring mixture. Acetic acid (1 mL) was added followed by refluxing (at 80-90 °C) of the reaction mixture for 5 hours. The reaction solution mixture was clear (with a slight yellow colour). As refluxing continued the reaction solution became more yellow. The reaction mixture was allowed to stir overnight at room temperature. The reaction mixture was further cooled in an ice-bath but no precipitate formed. The volume of the solvent (ethanol) was reduced on the rotary evaporator. Hexane was added to the mixture, which afforded a white powder on addition of the hexane. Hexane was added in excess and the mixture was allowed to stand overnight. Yellow solids had formed overnight. The yellow solid of **7** (1.1953 g, 65 %) was collected. The product **7** was recrystallized from ethanol/water. **Melting point** = 74-77 °C (Lit. M.P. = 108-110 °C[10]). **Elemental analysis** calculated for $C_7H_9N_3SO$: C, 45.88; H, 4.95; N, 22.93; S, 17.50 %. Found: C, 42.54; H, 5.34; N, 23.35; S, 17.03 %. **^{1}H-NMR** (400 MHz, DMSO-d_6): δ 2.26 ppm (s, 3H, -CH_3); 6.60 ppm (s, 1H, H_b); 7.10 ppm (s, 1H, H_a); 7.69 ppm (s, 1H, -HN-**H**); 7.78 ppm (s, 1H, H_c); 8.24 ppm (s, 1H, -HN-**H**); 10.24 ppm (s, 1H, -NH-). **FT-IR** (KBr pellet): ν (C=N_{imine}) 1591 cm^{-1} (*m*).

5.2.1.8. Synthesis of acetophenone thiosemicarbazone, ***8****.*[11]

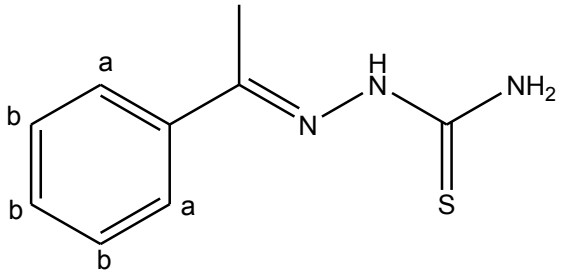

8

Ethanol (5 mL) was added to acetophenone (1.17 mL, 0.01 mol.) in a round-bottom flask, followed by stirring of the mixture. Thiosemicarbazide (0.9134 g, 0.01 mol.) was added to the stirring mixture. More ethanol (15 mL) followed by glacial acetic acid (1 mL) was added to the reaction mixture. The reaction mixture was allowed to reflux (at 80-90 °C) for 5 hours, after which it was cooled to room temperature and stirred overnight. During overnight stirring (at room temperature) a solid had formed. The reaction mixture was further cooled in ice for 1 hour, after which the which the solid was collected via suction filtration. A white solid of **8** (0.8538 g, 44 %) was obtained. The product **8** was recrystallized from ethanol/hexane. **Melting point** = 114-115 °C (Lit. M.P. = 110 °C[11]). **Elemental analysis** calculated for $C_9H_{11}N_3S$: C, 55.93; H, 5.74; N, 21.74; S, 16.59 %. Found: C, 55.58; H, 5.70; N, 23.10; S, 17.01 %. **^{1}H-NMR** (400 MHz, DMSO-d_6): δ 2.33 ppm (s, 3H, -CH_3); 7.41 ppm (t, 3H, ^3J = 2.83 Hz, 3H_b); 7.95 ppm (m, 3H, 2H_a + -HN-**H**); 8.26 ppm (s, 1H, -HN-**H**); 10.21 ppm (s, 1H, -NH-). **FT-IR** (KBr pellet): ν (C=N_{imine}) 1588 cm^{-1} (*s*).

5.2.1.9. Synthesis of 2-acetylpyrrole thiosemicarbazone, ***9.***[12]

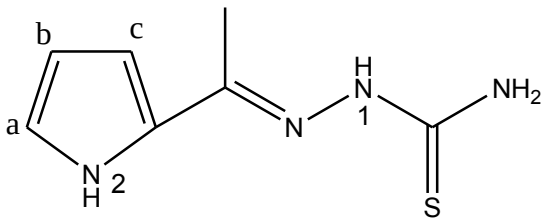

9

Thiosemicarbazide (0.4579 g, 5.0 mmol) was added to a round-bottom flask and was dissolved in methanol (15 mL), with heating. Methanol (15 mL) was added to 2-acetylpyrrole (0.5457 g, 5.0 mmol) in a beaker, and the resultant solution was added to the reaction flask. Acetic acid (0.5 mL) was added followed by refluxing (at 80-90 °C) of the reaction mixture for 4.5 hours. The reaction mixture was allowed to cool to room temperature. Water was added to the reaction mixture and was left overnight at just below 10 °C. This allowed for a white solid to be precipitated out of the solution. The solid was collected using a Büchner funnel and was dried under vacuum. A white solid of **9** (0.3250 g, 36 %) was isolated. **Melting point** = 169-172 °C (Lit. M.P. = 160-171 °C[12]). **Elemental analysis** calculated for $C_7H_{10}N_4S$: C, 46.13; H, 5.53; N, 30.74; S, 17.59 %. Found: C, 46.28; H, 5.57; N, 30.80; S, 18.41 %. **^{1}H-NMR** (400 MHz, DMSO-d_6): δ 2.15 ppm (s, 3H, -CH_3); 6.04 ppm (t, 1H, ^3J = 3.62 Hz, H_b); 6.44 ppm (d, 1H, ^3J = 2.28 Hz, H_c); 6.88 ppm (d, 1H, ^3J = 2.18 Hz, H_a); 8.08 ppm (s, 1H, -HN-**H**); 8.21 ppm (s, 1H, -HN-**H**); 9.97 ppm (s, 1H, -N^{2}H-); 11.35 ppm (s, 1H, -N^{1}H-). **FT-IR** (KBr pellet): ν (C=N_{imine}) 1589 cm^{-1} (*m*).

5.2.1.10. Synthesis of 2-acetylpyridine-4,4-dimethylthiosemicarbazone, ***10.***[3]

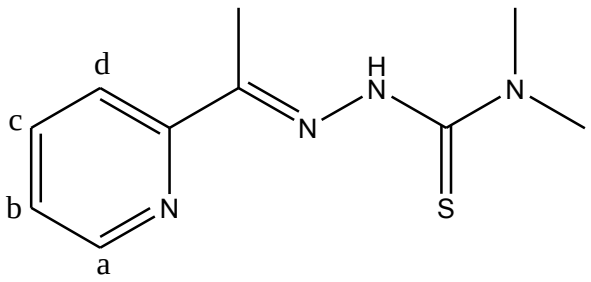

10

A mixture of 4,4-dimethylthiosemicarbazide (0.2083 g, 1.68 mmol) in aqueous (19 mL) 5 % acetic acid (1 mL) was stirred at 50-55 °C until a transparent solution was formed. The mixture was placed under an inert atmosphere and 2-acetylpyridine (0.19 mL, 1.68 mmol) in aqueous 5 % acetic acid (0.6 mL) was added dropwise to the stirring mixture over 5 minutes. Yellow solids were observed to have precipitated out of solution upon addition of the 2-acetylpyridine solution. The resultant mixture was stirred for 4 hours. After cooling to room temperature, the yellow solid was collected by suction filtration and washed with some cold ethanol followed by diethyl ether. A yellow powder of **10** (0.2071 g, 56 %) was isolated. **Melting point** = 147-149 °C (Lit. M.P. = 148-150 °C[13]). **Elemental analysis** calculated for $C_{10}H_{14}N_4S$: C, 54.03; H, 6.35; N, 25.20; S, 14.42 %. Found: C, 54.18; H, 6.39; N, 25.31; S, 15.82 %. NMR data was shown to contain a mixture of three isomers; *E*, *E'* and *Z*. **^{1}H-NMR:** ***E isomer*** (400 MHz, $CDCl_3$): δ 2.65 (3H, s, CH_3), 3.48 (6H, m, $N(CH_3)_2$), 7.31 (1H, m, H_c), 7.54 (1H, m, H_d), 7.78 (1H, m, H_b), 8.46 (1H, br s, NH), 8.73 (1H, m, H_a); ***E' isomer*** (400 MHz, $CDCl_3$): δ 2.41 (3H, s, CH_3), 3.48 (6H, m, $N(CH_3)_2$), 7.25 (1H, m, H_c), 7.67 (1H, m, H_b), 7.96 (1H, m, H_d), 8.57 (1H, m, H_a), 14.82 (1H, br s, NH); ***Z isomer*** (400 MHz, $CDCl_3$): δ 2.55 (3H, s, CH_3), 3.48 (6H, m, $N(CH_3)_2$), 7.38 (1H, m, H_c), 7.61 (1H, m, H_d), 7.92 (1H, m, H_b), 8.63 (1H, m, H_a), 15.51 (1H, br s, NH). **FT-IR** (KBr pellet): ν ($C=N_{imine}$) 1582 cm^{-1} (*w*).

5.2.1.11. Synthesis of 2-formylpyridine-4,4-dimethylthiosemicarbazone, ***11.***[14]

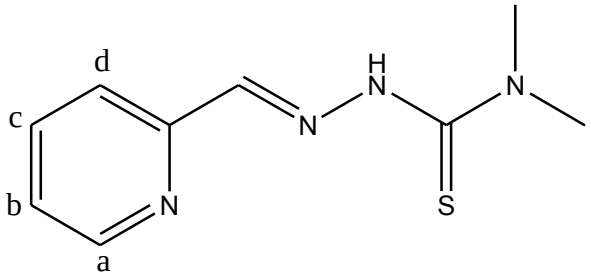

11

A mixture of 4,4-dimethylthiosemicarbazide (0.2074 g, 1.68 mmol) in water (15 mL) was stirred at 50-55 °C until a transparent solution was formed. Pyridine-2-carboxaldehyde (0.19 mL, 1.68 mmol) was added, dropwise, to the stirring solution. The reaction mixture gradually changed from a clear to a yellow/orange solution upon addition of the 2-pyridinecarboxaldehyde. The reaction mixture was allowed to stir overnight at room temperature. Light-yellow solids were observed to have formed after stirring overnight. The solids were collected by suction filtration and were dried *in vacuo*. A light-yellow powder of **11** (0.2078 g, 59 %) was isolated. **Melting point** = 126-128 °C (Lit. M.P. = 126-129 °C[14]). **Elemental analysis** calculated for $C_9H_{12}N_4S$: C, 51.90; H, 5.81; N, 26.90; S, 15.39 %. Found: C, 52.14; H, 5.86; N, 27.19; S, 15.62 %. **^{1}H-NMR** (300 MHz, $CDCl_3$): δ 3.48 ppm (6H, s, $N(CH_3)_2$), 7.37 ppm (1H, t, ^3J = 7.63 Hz, H_c), 7.47 ppm (1H, d, ^3J = 7.95 Hz, H_d), 7.50 ppm (1H, s, -CH=N-), 7.88 ppm (1H, t, ^3J = 7.77 Hz, H_b), 8.63 ppm (1H, d, ^3J = 4.40 Hz, H_a), 15.10 ppm (1H, s, NH). **FT-IR** (KBr pellet): ν ($C=N_{imine}$) 1592 cm^{-1} (*s*).

5.2.1.12. Synthesis of 2-acetylpyrrole-4,4-dimethylthiosemicarbazone, ***12.***

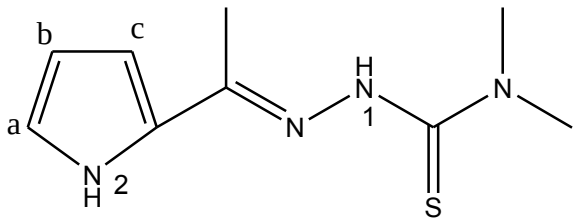

12

A mixture of 4,4-dimethylthiosemicarbazide (0.2035 g, 1.68 mmol) in water (15 mL) was stirred at 50-55 °C until a transparent solution was formed. Glacial acetic acid (6 drops) was added to the mixture, followed by the dropwise addition of a methanolic solution (1 mL) of 2-acetylpyrrole (0.1892 g, 1.68 mmol). The reaction mixture was stirred for 5 hours at room temperature and was stored at -16 °C for 24 hours. White solids were observed to have formed, were collected by suction filtration and were dried *in vacuo*. A white powder of **12** (0.1456 g, 41 %) was isolated. **Melting point** = 101-103 °C. **Elemental analysis** calculated for $C_9H_{14}N_4S$: C, 51.40; H, 6.71; N, 26.64; S, 15.25 %. Found: C, 51.78; H, 6.77; N, 27.70; S, 15.51 %. **Mass Spectrometry (EI+)**: *m/z* 211.3 (100%, $[M+H]^+$). **^{13}C-NMR** (75 MHz, $CDCl_3$): δ 17.8, 40.2, 111.4, 117.3, 124.7, 125.4, 135.5, 182.5. **^{1}H-NMR** (300 MHz, $CDCl_3$): δ 2.53 ppm (3H, s, CH_3), 3.36 ppm (6H, s, $N(CH_3)_2$), 6.40 ppm (1H, t, ^3J = 3.36 Hz, H_b), 6.85 ppm (1H, d, ^3J = 2.25 Hz, H_c), 7.20 ppm (1H, t, ^3J = 2.12 Hz, H_a), 12.08 ppm (1H, br s, -N^{2}H-), 12.97 ppm (1H, br s, -N^{1}H-). **FT-IR** (KBr pellet): ν ($C=N_{imine}$) 1615 cm^{-1} (*m*).

5.2.1.13. Synthesis of 2-formylpyrrole-4,4-dimethylthiosemicarbazone, ***13.***[15]

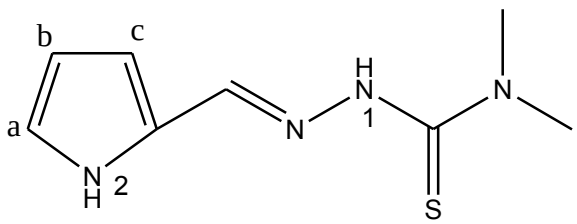

13

A mixture of 4,4-dimethylthiosemicarbazide (0.199 g, 1.68 mmol) in water (15 mL) was stirred at 50-55 °C until a transparent solution was formed. A methanolic

solution (1 mL) of 2-pyrrolecarboxaldehyde (0.166 g, 1.68 mmol) was added dropwise. The reaction mixture was stirred for 3 days at room temperature. Solids were observed to have formed during the stirring process and were collected by suction filtration. A cream solid of **13** (0.26 g, 80 %) was isolated. **Melting point** = 76-79 °C (Lit. M.P. = 102 °C[15]). **Elemental analysis** calculated for $C_8H_{12}N_4S$: C, 48.96; H, 6.16; N, 28.55; S, 16.34 %. Found: C, 48.81; H, 6.21; N, 28.96; S, 17.13 %. **^{1}H-NMR** (400 MHz, $CDCl_3$): δ 3.36 ppm (6H, s, $N(CH_3)_2$), 6.39 ppm (1H, t, ^3J = 3.38 Hz, H_b), 6.84 ppm (1H, d, ^3J = 2.26 Hz, H_c), 7.20 ppm (2H, m, -CH=N- + H_a), 11.36 ppm (1H, br s, -N^{2}H-), 12.90 ppm (1H, br s, -N^{1}H-). **FT-IR** (KBr pellet): ν ($C=N_{imine}$) 1628 cm^{-1} (*m*).

5.2.1.14. Synthesis of 2-acetylpyrrole thiosemicarbazone, ***14.***[16]

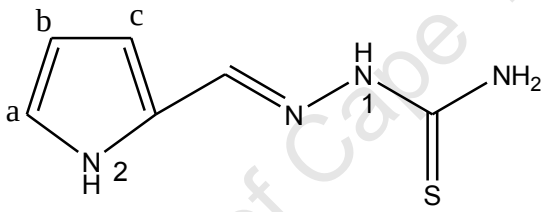

14

Thiosemicarbazide (0.4797 g, 5.0 mmol) was added to a round-bottom flask and was dissolved in methanol (15 mL), with heating. Methanol (15 mL) was added to 2-pyrrolecarboxaldehyde (0.5053 g, 5.0 mmol) in a beaker, and the resultant solution was added, dropwise, to the reaction flask. The reaction mixture was allowed to refux (at 70 °C) for 24 hours. The reaction mixture was allowed to cool to room temperature. Water was added to the reaction mixture and was left overnight at just below 10 °C. This allowed for a purple solid to precipitate out of the solution. The solid was collected using a Büchner funnel and was dried under vacuum. A purple solid of **14** (0.70 g, 83 %) was isolated. **Melting point** = 204-207 °C (Lit. M.P. = 195-197 °C[16]). **Elemental analysis** calculated for $C_6H_8N_4S$: C, 42.84; H, 4.79; N, 33.31; S, 19.06 %. Found: C, 42.58; H, 4.85; N, 33.10; S, 19.17 %. **^{1}H-NMR** (400 MHz, DMSO-d_6): δ 6.06 ppm (t, 1H, ^3J = 3.58 Hz, H_b); 6.34 ppm (d, 1H, ^3J = 2.28 Hz, H_c); 6.90 ppm (d, 1H, ^3J = 2.14 Hz, H_a); 7.80 ppm (s, 1H, -CH=N-), 7.85 ppm (s, 1H, -HN-

H); 7.95 ppm (s, 1H, -HN-**H**); 11.16 ppm (s, 1H, -N^{2}H-); 11.28 ppm (s, 1H, -N^{1}H-). **FT-IR** (KBr pellet): ν (C=N$_{imine}$) 1617 cm^{-1} (*s*).

5.2.1.15. Synthesis of 2-formylfuran-4,4-dimethylthiosemicarbazone, ***15.***[17]

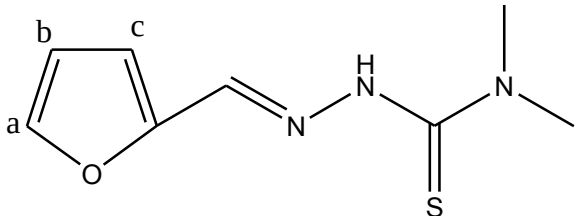

15

A mixture of 4,4-dimethylthiosemicarbazide (0.208 g, 1.70 mmol) in water (15 mL) was stirred until a transparent solution was formed. A solution of 2-furaldehyde (0.141 mL, 1.70 mmol) was added dropwise. The reaction mixture was stirred for 24 hours at room temperature. Solids were observed to have formed during the stirring process and were collected by suction filtration. A white solid of **15** (0.28 g, 84 %) was isolated. **Melting point** = 141-143 °C. **Elemental analysis** calculated for $C_8H_{11}N_3SO$: C, 48.71; H, 5.62; N, 21.30; S, 16.26 %. Found: C, 48.98; H, 5.70; N, 22.14; S, 16.76 %. **^{1}H-NMR** (300 MHz, DMSO-d$_6$): δ 3.23 ppm (6H, s, N(CH$_3$)$_2$), 6.58 ppm (1H, br s, H$_b$), 6.78 ppm (1H, d, ^3J = 3.78 Hz, H$_c$), 7.76 ppm (1H, br s, H$_a$), 8.08 ppm (1H, s, -CH=N-), 10.77 (1H, s, -NH-). **FT-IR** (KBr): ν (C=N$_{imine}$) 1617 cm^{-1} (*m*).

5.2.1.16. Synthesis of 2-acetylfuran-4,4-dimethylthiosemicarbazone, ***16.***

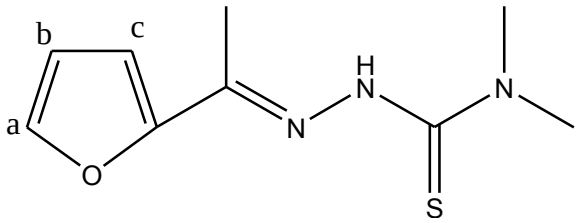

16

A solution of 4,4-dimethylthiosemicarbazide (0.205 g, 1.70 mmol) in water (15 mL) was stirred until a transparent solution was formed. A solution of 2-acetylfuran

(0.189 g, 1.70 mmol) in methanol (1 mL) was added dropwise, along with glacial acetic acid (6 drops). The reaction mixture was stirred for 24 hours at room temperature. Solids were observed to have formed during the stirring process and were collected by suction filtration. A yellow powder of **16** (0.24 g, 66 %) was isolated. **Melting point** = 141-143 °C. **Elemental analysis** calculated for $C_9H_{13}N_3SO$: C, 51.16; H, 6.20; N, 19.89; S, 15.18 %. Found: C, 51.48; H, 6.42; N, 20.15; S, 16.29 %. **Mass Spectrometry (EI+)**: *m/z* 212.3 (100%, $[M+H]^+$). **^{13}C-NMR** (75 MHz, $CDCl_3$): δ 17.1, 43.1, 111.8, 113.0, 113.8, 121.3, 144.0, 146.0. **^{1}H-NMR** (300 MHz, $CDCl_3$): δ 2.46 ppm (1H, s, $-C(CH_3)=N-$), 3.39 ppm (6H, s, $N(CH_3)_2$), 6.56 ppm (1H, t, ^3J = 3.54 Hz, H_b), 6.02 ppm (1H, br s, H_c), 7.62 ppm (1H, d, ^3J = 1.75 Hz, H_a). **FT-IR** (KBr): ν ($C=N_{imine}$) 1638 cm^{-1} (*w*).

5.2.1.17. Synthesis of 3-formylpyridine-4,4-dimethylthiosemicarbazone, ***17.***

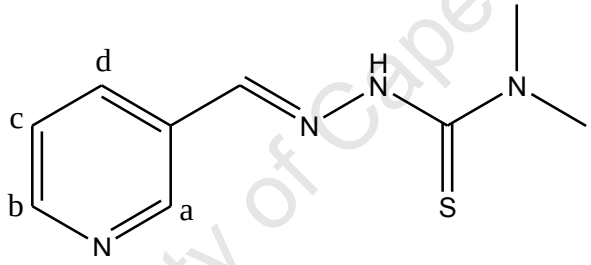

17

A solution of 4,4-dimethylthiosemicarbazide (0.205 g, 1.70 mmol) in water (15 mL) was stirred until a transparent solution was formed. A solution of 3-pyridinecarboxaldehyde (0.16 mL, 1.7 mmol) was added dropwise. The reaction mixture was stirred for 24 hours at room temperature. Solids were observed to have formed during the stirring process and were collected by suction filtration. A light-yellow solid of **17** (0.30 g, 85 %) was isolated. **Melting point** = 148-150 °C. **Elemental analysis** calculated for $C_9H_{12}N_4S$: C, 51.90; H, 5.81; N, 26.90; S, 15.39 %. Found: C, 52.18; H, 5.94; N, 27.13; S, 15.66 %. **Mass Spectrometry (EI+)**: *m/z* 209.3 (100%, $[M+H]^+$). **^{13}C-NMR** (75 MHz, $CDCl_3$): δ 12.5, 44.1, 123.3, 133.1, 144.0, 147.5, 150.1, 152.2, 183.1. **^{1}H-NMR** (300 MHz, $CDCl_3$): δ 3.45 ppm (6H, s, $N(CH_3)_2$), 7.31 ppm (1H, t, ^3J = 7.45 Hz, H_c), 7.70 ppm (1H, s, $-CH=N-$), 7.92 ppm (1H, d, ^3J =

7.89 Hz, H_b), 8.58 ppm (1H, d, ^3J = 7.38 Hz, H_d), 8.79 ppm (1H, s, H_a), 8.94 ppm (1H, s, NH). **FT-IR** (KBr pellet): ν (C=N_{imine}) 1605 cm^{-1} (*m*).

5.2.1.18. Synthesis of 3-acetylpyridine-4,4-dimethylthiosemicarbazone, ***18.***

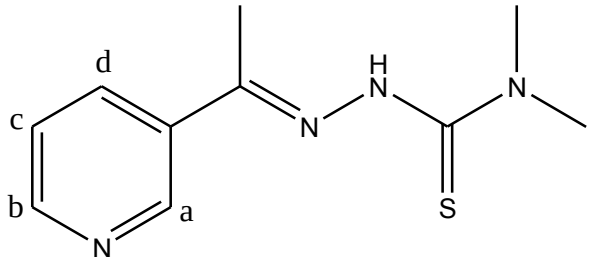

18

A solution of 4,4-dimethylthiosemicarbazide (0.206 g, 1.70 mmol) in water (15 mL) was stirred until a transparent solution was formed. A solution of 3-acetylpyridine (0.18 mL, 1.7 mmol) was added dropwise, along with glacial acetic acid (10 drops). The reaction mixture was stirred for 24 hours at room temperature. Solids were observed to have formed during the stirring process and were collected by suction filtration. A yellow powder of **18** (0.22 g, 59 %) was isolated. **Melting point** = 100-102 °C. **Elemental analysis** calculated for $C_{10}H_{14}N_4S$: C, 54.03; H, 6.35; N, 25.20; S, 14.42 %. Found: C, 54.28; H, 6.42; N, 25.41; S, 15.09 %. **Mass Spectrometry (EI+)**: *m/z* 223.3 (100%, $[M+H]^+$). **^{13}C-NMR** (75 MHz, $CDCl_3$): δ 43.8, 123.7, 130.1, 133.6, 139.2, 149.0, 151.0, 181.6. **^{1}H-NMR** (300 MHz, $CDCl_3$): δ 2.27 ppm (1H, s, -$C(CH_3)$=N-), 3.43 ppm (6H, s, $N(CH_3)_2$), 7.35 ppm (1H, t, ^3J = 7.51 Hz, H_c), 8.00 ppm (1H, d, ^3J = 7.42 Hz, H_b), 8.39 ppm (1H, s, NH), 8.59 ppm (1H, d, ^3J = 7.97 Hz, H_d), 8.94 ppm (1H, d, ^3J = 4.35 Hz, H_a). **FT-IR** (KBr pellet): ν (C=N_{imine}) 1615 cm^{-1} (*m*).

5.2.1.19. Synthesis of N-phenylhydrazinecarbothioamide, **19**.[18]

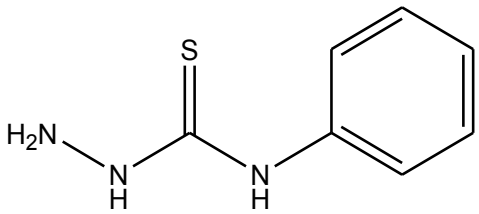

19

Hydrazine hydrate (0.75 mL, 15 mmol) was added to a solution of phenyl isothiocyanate (1.8 mL, 10 mmol) and ethanol (60 mL). The reaction mixture was allowed to stir for 60 minutes as white crystals precipitated out of the reaction mixture. The white crystals were collected on a Büchner funnel and washed with cold ethanol. The product was dried and 1.8 g (72 % yield) of the white crystalline product **19** was collected. **Melting point** = 132-136 °C(Lit. M.P. = 135 °C[18]). **^{1}H-NMR** (300 MHz, DMSO-d_6): δ 4.85 ppm (br s, 2H, -NH_2), 7.07 ppm (t, 1H, ^3J = 7.39 Hz, Ar-H[*p*]), 7.27 ppm (m, 2H, Ar-H[*m*]), 7.63 ppm (d, 2H, ^3J = 7.82 Hz, Ar-H[*o*]), 7.80 ppm (br s, 1H, -NH-CS-), 8.96 ppm (br s, 1H, -NH-Ph).

5.2.1.20. Synthesis of 2-formylpyridine-4-phenylthiosemicarbazone, ***20.***[19]

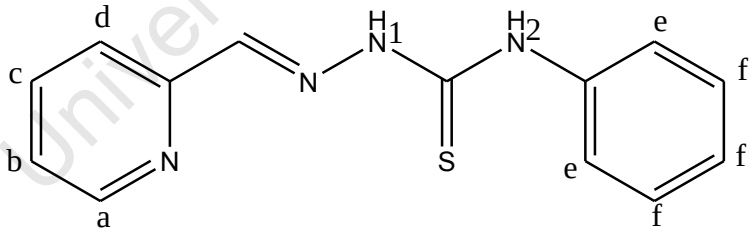

20

A solution of 2-pyridinecarboxaldehyde (0.12 mL, 1.2 mmol) was added, dropwise, to a suspension of *N*-phenylhydrazinecarbothioamide*,* **19,** (0.206 g, 1.20 mmol) in ethanol (20 mL). The reaction mixture was allowed to reflux for 24 hours and was cooled to room temperature. Water (20 mL) was added to the reaction mixture to precipitate out the product. A white powder precipitated out of solution and was collected. A white powder of **20** (0.10 g, 33 %) was isolated. **Melting point** = 204-206 °C (Lit. M.P. = 212-214 °C[19]). **Elemental analysis** calculated for $C_{13}H_{12}N_4S$: C,

60.91; H, 4.72; N, 21.86; S, 12.51 %. Found: C, 61.29; H, 4.75; N, 22.43; S, 12.73 %. **^{1}H-NMR** (300 MHz, DMSO-d_6): δ 7.22 ppm (1H, t, ^3J = 7.36 Hz, H_b), 7.38 ppm (3H, t, ^3J = 8.01 Hz, H_f), 7.59 ppm (2H, d, ^3J = 7.57 Hz, H_e), 7.84 ppm (1H, t, ^3J = 7.75 Hz, H_c), 8.22 ppm (1H, s, -CH=N-), 8.40 ppm (1H, d, ^3J = 8.00 Hz, H_d), 8.59 ppm (1H, d, ^3J = 4.84 Hz, H_a), 10.17 ppm (1H, s, N^2H), 11.91 ppm (1H, s, N^1H). **FT-IR** (KBr pellet): ν (C=N_{imine}) 1597 cm^{-1} (*m*).

5.2.1.21. Synthesis of 2-acetylpyridine-4-phenylthiosemicarbazone, **21.**[19]

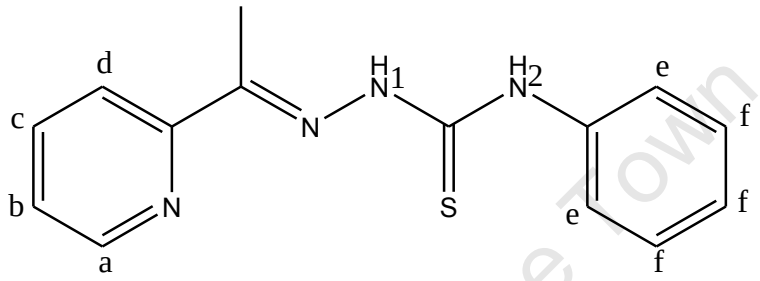

21

A solution of 2-acetylpyridine (0.13 mL, 1.2 mmol) was added, dropwise, to a suspension of *N*-phenylhydrazinecarbothioamide, **19**, (0.200 g, 1.20 mmol) in ethanol (20 mL) in the presence of glacial acetic acid (0.5 mL). The reaction mixture was allowed to reflux for 24 hours and was cooled to room temperature. Water (20 mL) was added to the reaction mixture to precipitate out the product. A light-yellow solid precipitated out of solution and was collected. A light-yellow solid of **21** (0.20 g, 63 %) was isolated. **Melting point** = 173-177 °C (Lit. M.P. = 190-192 °C[19]). **Elemental analysis** calculated for $C_{14}H_{14}N_4S$: C, 62.20; H, 5.22; N, 20.72; S, 11.86 %. Found: C, 62.08; H, 5.30; N, 20.59; S, 11.62 %. **^{1}H-NMR** (300 MHz, DMSO-d_6): δ 3.21 ppm (3H, s, CH_3), 7.23 ppm (1H, t, ^3J = 7.35 Hz, H_b), 7.40 ppm (3H, t, ^3J = 7.99 Hz, H_f), 7.59 ppm (2H, d, ^3J = 7.57 Hz, H_e), 7.82 ppm (1H, t, ^3J = 7.74 Hz, H_c), , 8.50 ppm (1H, d, ^3J = 8.02 Hz, H_d), 8.60 ppm (1H, d, ^3J = 4.84 Hz, H_a), 10.12 ppm (1H, s, N^2H), 10.55 ppm (1H, s, N^1H). **FT-IR** (KBr pellet): ν (C=N_{imine}) 1588 cm^{-1} (*w*).

5.2.2. Synthesis of dithiosemicarbazone ligands.

5.2.2.1. Synthesis of ethane-1,2-dithiosemicarbazide, **22**.[20]

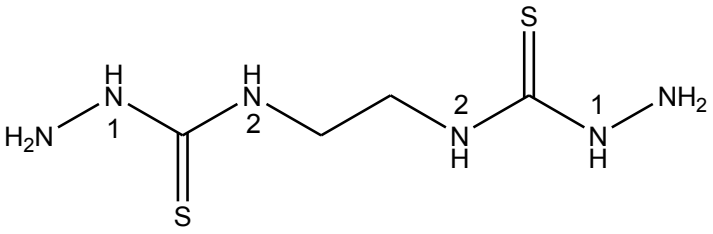

22

Ethane-1,2-diamine (1.67 mL, 0.025 mol) was added to a 250 mL round bottom flask, followed by an aqueous (40 mL) solution of NaOH (2.06 g, ~0.050 mol) and CS_2 (4.50 mL, 0.075 mol). The reaction mixture was stirred for 4 hours, after which sodium chloroacetate (5.83 g, 0.050 mol) was added. The resultant mixture was stirred for a further 19 hours. The reaction mixture was acidified with 2M HCl (5 mL), followed by the addition of H_2NNH_2 (10.8 mL, 0.35 mol). The reaction mixture was refluxed for 2 hours and cooled to room temperature. White solids were seen to have precipitated and the flask was placed in an ice bath to promote further precipitation. The white solids were collected by suction filtration and were washed with water, ethanol and diethyl ether. White solids of **22** (2.1041 g, 40 %) were isolated. **Melting point** = 213-214 °C (Lit. M.P. = 212-214 °C[20]). **^{1}H-NMR** (300 MHz, DMSO-d_6): δ 3.61 ppm (s, 4H, -$(CH_2)_2$-); 4.39 ppm (s, 4H, 2 -NH_2); 7.91 ppm (s, 2H, 2-N^{2}H-); 8.52 ppm (s, 2H, 2-N^{1}H-).

5.2.2.2. Synthesis of 2-formylpyridine ethane-1,2-dithiosemicarbazone, **23.**

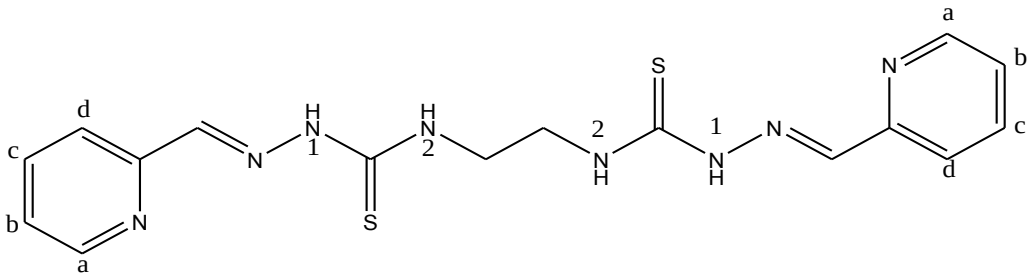

23

Ethane-1,2-dithiosemicarbazide (0.4041 g, 1.93 mmol) was dissolved in dimethylformamide (20 mL) and 2-pyridinecarboxaldehyde (0.365 mL, 3.84 mmol) was added to the flask. A white milky solution was observed before the addition of 2-pyridinecarboxaldehyde, after which the solution became a clear yellow. The reaction mixture was refluxed for 5 hours at 100-110 °C. The reaction mixture was allowed to cool to room temperature, after which water was added to precipitate a light-yellow solid. The yellow solid (0.6026 g, 80 %) of **23** was collected by suction filtration. **Melting point** = 227-229 °C. **Elemental analysis** calculated for $C_{16}H_{18}N_8S_2$: C, 49.72; H, 4.69; N, 28.99; S, 16.59 %. Found: C, 46.62 ; H, 5.14; N, 28.59; S, 15.27 %. **^{1}H-NMR** (400 MHz, DMSO-d_6): δ 3.88 ppm (s, 4H, -$(CH_2)_2$-); 7.38 ppm (t, 2H, ^3J = 6.43 Hz, $2H_b$); 7.79 ppm (t, 2H, ^3J = 7.65 Hz, $2H_c$); 8.12 ppm (s, 2H, 2-CH=N-); 8.28 ppm (d, 2H, ^3J = 7.83 Hz, $2H_d$); 8.56 ppm (d, 2H, ^3J = 3.68 Hz, $2H_a$); 8.80 ppm (s, 2H, 2-N^{2}H-); 11.80 ppm (s, 2H, 2-N^{1}H-). **FT-IR** (KBr pellet): ν (C=N_{imine}) 1587 cm^{-1} (*m*).

Alternate Synthesis*:* Ethane-1,2-dithiosemicarbazide (0.4011 g, 1.93 mmol) was added to ethanol (40 mL) as a suspension followed by 2-formylpyridinecarboxaldehyde (~0.37 mL, 3.85 mmol). The reaction mixture was refluxed (at 90°C) for 24 hours. The reaction was allowed to cool to room temperature and the solids that were present in the reaction flask was collected via suction filtration. Light-yellow solids of **23** (0.6669 g, 89 %) were isolated. **^{1}H-NMR** (300 MHz, DMSO-d_6): δ 3.88 ppm (s, 4H, -$(CH_2)_2$-); 7.34 ppm (t, 2H, ^3J = 6.42 Hz, $2H_b$); 7.74 ppm (t, 2H, ^3J = 7.65 Hz, $2H_c$); 8.10 ppm (s, 2H, 2-CH=N-); 8.22 ppm (d,

2H, ^3J = 7.84 Hz, $2H_d$); 8.54 ppm (d, 2H, ^3J = 3.69 Hz, $2H_a$); 8.73 ppm (s, 2H, 2-N^2H-); 11.69 ppm (s, 2H, 2-N^1H-).

5.2.2.3. Synthesis of 2-acetylpyridine ethane-1,2-dithiosemicarbazone, **24.**[21]

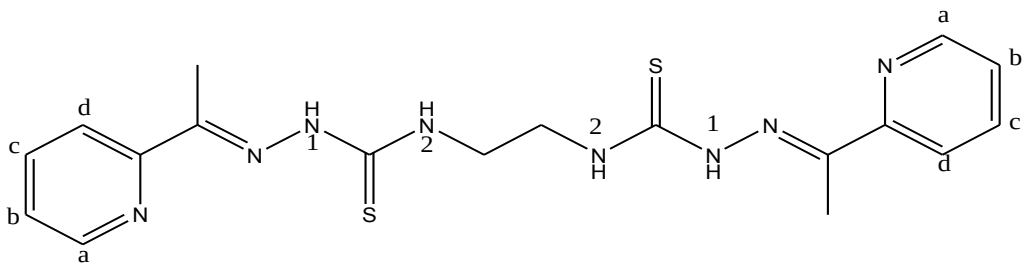

24

Ethylene dithiosemicarbazide (0.2047 g, 0.96 mmol) was dissolved in dimethylformamide (10 mL) and 2-acetylpyridine (0.22 mL, 1.92 mmol) was added to the flask, after which acetic acid (0.5 mL) was added. The reaction mixture was refluxed for 5 hours at 110-120 °C. The reaction mixture was allowed to cool to room temperature, after which water was added. The reaction mixture was left overnight at below 10 °C. A pale yellow solid (0.1695 g, 43 %) of **24** was observed and was collected by suction filtration. **Melting point** = 196-199 °C (Lit. M. P. = 214-216 °C[21]). **Elemental analysis** calculated for $C_{18}H_{22}N_8S_2$: C, 52.15; H, 5.35; N, 27.03; S, 15.47 %. Found: C, 52.36; H, 5.27; N, 27.47; S, 15.65 %. **^{1}H-NMR** (400 MHz, DMSO-d_6): δ 2.42 ppm (s, 6H, 2-CH_3); 3.93 ppm (s, 4H, -$(CH_2)_2$-); 7.39 ppm (t, 2H, ^3J = 5.87 Hz, $2H_b$); 7.73 ppm (t, 2H, ^3J = 8.04 Hz, $2H_c$); 8.40 ppm (d, 2H, ^3J = 8.06 Hz, $2H_d$); 8.60 ppm (d, 2H, ^3J = 4.73 Hz, $2H_a$); 8.80 ppm (s, 2H, 2-N^2H-); 10.43 ppm (s, 2H, 2-N^1H-). **FT-IR** (KBr pellet): ν (C=N_{imine}) 1582 cm^{-1} (*m*).

5.2.3. Synthesis of gallium(III) thiosemicarbazones.

5.2.3.1. Synthesis of gallium(III) 2-acetylpyridinethiosemicarbazone, **25**.[22]

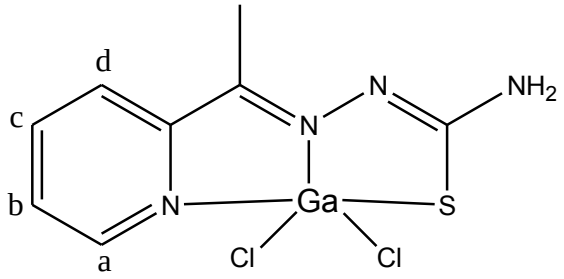

25

The reaction was performed under an inert atmosphere. A solution of $GaCl_3$ (0.48 g, 2.6 mmol) in dry ethanol (4 mL) was added, dropwise over a period of 10 minutes, to a stirring solution of ligand **6** (0.101 g, 0.515 mmol) in dry ethanol (12 mL). The reaction mixture was refluxed for 1 hour and was allowed to cool to room temperature. Yellow solids of **25** (0.092 g, 54 %) were observed to have formed. **Melting point** = 236-239 °C. **Elemental analysis** calculated for $C_8H_9N_4SGaCl_2$: C, 28.76; H, 2.72; N, 16.77; S, 9.60 %. Found: C, 28.75; H, 2.76; N, 16.68; S, 8.54 %. **Mass Spectrometry (EI+)**: *m/z* 333.7 (100%, $[M]^+$). **^{1}H-NMR** (400 MHz, DMSO-d_6): δ 2.72 ppm (3H, s, CH_3), 7.28 ppm (2H, s, NH_2), 7.90 ppm (1H, t, ^3J = 5.35 Hz, H_c), 8.16 ppm (1H, d, ^3J = 8.00 Hz, H_d), 8.37 ppm (1H, t, ^3J = 7.83 Hz, H_b), 9.02 ppm (1H, d, ^3J = 5.34 Hz, H_a). **FT-IR** (KBr pellet): ν (C=N_{imine}) 1603 cm^{-1} (*m*), 1558 cm^{-1} (*s*).

5.2.3.2. Synthesis of gallium(III) 2-acetylpyridine-4,4-dimethylthiosemicarbazone, **26***.*[22]

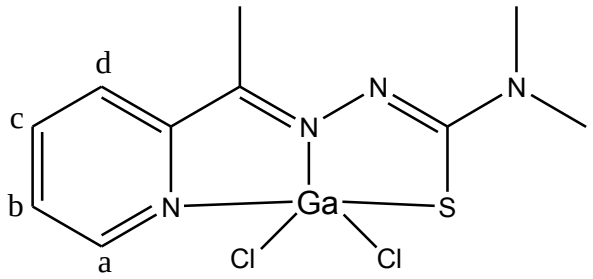

26

The reaction was performed under an inert atmosphere. A solution of $GaCl_3$ (0.771 g, 4.38 mmol) in dry ethanol (5 mL) was added, dropwise over a period of 10 minutes, to a stirring solution of ligand **10** (0.169 g, 0.758 mmol) in dry ethanol (20 mL). During addition of the gallium solution a yellow precipitate appeared. The reaction mixture was stirred for 2 hours. The precipitate was filtered, yielding a yellow solid, **26** (0.16 g, 58 %). **Melting point** = 251-254 °C (Lit. M. P. > 250 °C[23]). **Elemental analysis** calculated for $C_{10}H_{13}N_4SGaCl_2$: C, 33.19; H, 3.62; N, 15.48; S, 8.86 %. Found: C, 32.81; H, 3.68; N, 15.03; S, 6.57 %. **Mass Spectrometry (EI+)**: *m/z* 361.9 (100%, $[M]^+$). **^{1}H-NMR** (400 MHz, DMSO-d_6): δ 2.77 ppm (3H, s, CH_3), 3.31 ppm (6H, s, $N(CH_3)_2$), 7.57 ppm (1H, t, ^3J = 5.32 Hz, H_c), 7.92 ppm (1H, d, ^3J = 5.19 Hz, H_d), 8.20 ppm (1H, m, H_b), 8.25 ppm (1H, m, H_a). **FT-IR** (KBr pellet): ν ($C{=}N_{imine}$) 1601 cm^{-1} (*m*), 1553 cm^{-1} (*s*).

5.2.3.3. Synthesis of gallium(III) 2-formylpyridine-4,4-dimethylthiosemicarbazone, **27***.*

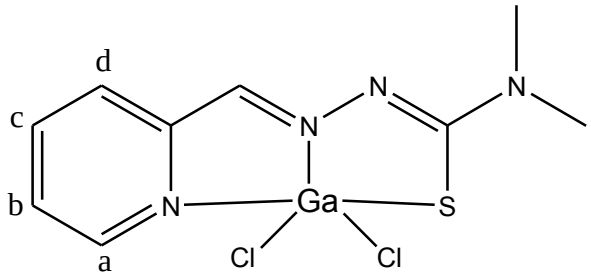

27

The reaction was performed under an inert atmosphere. A solution of $GaCl_3$ (0.649 g, 3.69 mmol) in dry ethanol (5 mL) was added, dropwise over a period of 10 minutes, to a stirring solution of ligand **11** (0.154 g, 0.737 mmol) in dry ethanol (20 mL). During addition of the gallium solution a yellow precipitate appeared, but the reaction became a yellow solution after further stirring. The reaction mixture was refluxed for 1.5 hours and was allowed to cool to room temperature. All the solvent was removed yielding a light-yellow crystalline solid, **27** (0.19 g, 75 %). **Melting point** = 116-120 °C. **Elemental analysis** calculated for $C_9H_{11}N_4SGaCl_2$: C, 31.07; H, 3.19; N, 16.10; S, 9.22 %. Found: C, 30.30; H, 3.25; N, 15.07; S, 7.05 %. **Mass Spectrometry (EI+)**: *m/z* 347.9 (100%, $[M]^+$). **^{1}H-NMR** (400 MHz, DMSO-d_6): δ 3.27 ppm (6H, s, $N(CH_3)_2$), 7.76 ppm (1H, t, ^3J = 5.34 Hz, H_c), 7.86 ppm (1H, d, ^3J = 7.83 Hz, H_d), 8.27 ppm (1H, t, ^3J = 7.74 Hz, H_b), 8.47 ppm (1H, s, -CH=N-), 8.80 ppm (1H, d, ^3J = 5.26 Hz, H_a). **FT-IR** (KBr pellet): ν ($C=N_{imine}$) 1606 cm^{-1} (*m*), 1566 cm^{-1} (*s*).

5.2.4. Synthesis of radiolabelled gallium(III) thiosemicarbazones.

For the general synthesis of the radiolabelled gallium(III) thiosemicarbazones, an acidic solution of $[^{67}Ga]GaCl_3$ in 0.01M HCl (30 µL, 1.17-1.70 mCi) was firstly transferred to a glass vial. Acetonitrile (50 µL) was added to the vial and the mixture was evaporated to dryness using a flow of N_2 gas and heat. Acetonitrile (100 µL) was again added to the residue and the evaporation step was repeated. The activity of $[^{67}Ga]GaCl_3$ was again measured and no significant loss of activity was observed. Alternatively, an acidic acetonic solution of $[^{67}Ga]GaCl_3$ (30 µL, 2.34-2.87 mCi) was placed in a vial and evaporated to dryness without the aid of acetonitrile. Dried

absolute ethanol (150 µL) was added to the vial followed by a 1 mg/mL solution (50 µL) of the ligand (**6**, **10**, **11**, **20**, **21**, **23** or **24**) in dried absolute ethanol. The vial was sealed, vortexed for 20-40 seconds and suspended in a water bath (at 75-85 °C) for 20-60 minutes. The reaction vial was allowed to cool to room temperature, after which quality control was employed on the product (**28**-**34**).

5.2.4.1. Analysis of [^{67}Ga]-2-acetylpyridine thiosemicarbazone, ***28****.*

HPLC: t_r = 5.5 min (87 %).

5.2.4.2. Analysis of [^{67}Ga]-2-acetylpyridine-4,4-dimethylthiosemicarbazone, ***29****.*

HPLC: t_r = 15.6 min. (>99 %).

5.2.4.3. Analysis of [^{67}Ga]-2-formylpyridine-4,4-dimethylthiosemicarbazone, ***30****.*

HPLC: t_r = 13.0 min. (90 %).

5.2.4.4. Analysis of [^{67}Ga]-2-formylpyridine-4-phenylthiosemicarbazone, ***31****.*

HPLC: t_r = 13.0 min. (90 %).

5.2.4.5. Analysis of [^{67}Ga]-2-acetylpyridine-4-phenylthiosemicarbazone, ***32****.*

HPLC: t_r = 13.8 min. (>99 %).

5.2.4.6. Analysis of [^{67}Ga]-2-formylpyridine ethane-1,2-dithiosemicarbazone, ***33****.*

HPLC: t_r = 10.7-11.5 min. (95 %).

5.2.4.7. Analysis of [^{67}Ga]-2-acetylpyridine ethane-1,2-dithiosemicarbazone, ***34****.*

HPLC: t_r = 11.3-12.5 min (>99 %).

5.2.5. Synthesis of poly(aryl)ether dendrimers ligands (and wedges).

5.2.5.1. Synthesis of 2,3-bis(2-methyl-4-hydroxylphenylimino) butane, **35**.[24]

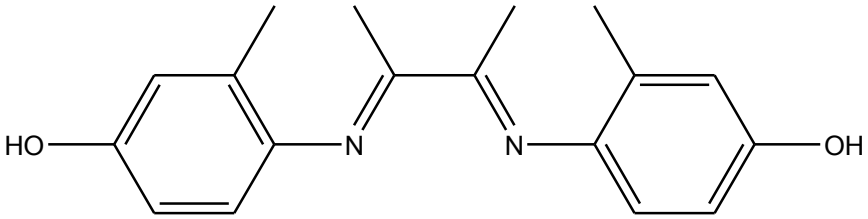

35

Reaction was performed under inert atmosphere. A mixture of 2,3-butadione (912 mg, 10.6 mmol), 2-methyl-4-hydroxyaniline (3.25 g, 26.4 mmol) and formic acid (0.25 mL) was stirred in dry MeOH (35 mL) at room temperature for 24 h. The mixture was concentrated to less than half. The reaction mixture was stored at -16 °C for 24 hours to precipitate out any product. A dark precipitate was observed to have formed after storage, after which the precipitate was recovered by filtration. After recrystallisation from hot methanol, **35** (1.1g, 40%) was obtained as a yellow solid. **Melting point** = 122–125 °C (Lit. M. P. = 122-126 °C[24]). **^{1}H-NMR** (400 MHz, acetone-d_6): δ 2.03 (6H, s, aryl-Me), 2.09 (6H, s, -N=CMe), 6.45–6.75 (6H, m, H_{aryl}), 7.99 (2H, br s, -OH). **FT-IR** (KBr pellet): ν (C=N_{imine}) 1629 cm^{-1} (*s*).

5.2.5.2. Synthesis of methyl p-bromomethylbenzoate (G0 wedge), **36**.[25]

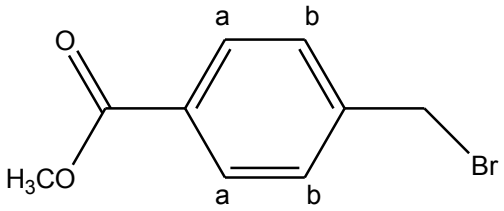

36

A solution of methyl p-hydroxymethylbenzoate (1.0013 g, 6.0 mmol) in dry toluene (30 mL) was stirred under argon at 0 °C. Phosphorus tribromide (0.19 mL, 2.0 mmol) was added dropwise to the solution which was then allowed to warm to room temperature. After 2 hours, the reaction mixture was evaporated to dryness and

partitioned between water (20 mL) and CH_2Cl_2 (20 mL). The aqueous layer was extracted with CH_2Cl_2 (4 x 20 mL) and the combined extracts were dried and evaporated to dryness to give **36** (1.19 g, 87 %) as a white crystalline solid. **Melting point** = 51-53 °C (Lit. M. P. = 53-55 °C[26]). **^{1}H-NMR** (400 MHz, $CDCl_3$): δ 3.90 ppm (3H, s, OCH_3), 4.48 ppm (2H, s, CH_2Br), 7.44 ppm (2H, d, ^3J = 7.84 Hz, H_b), 7.98 ppm (4H, d, ^3J = 7.73 Hz, H_a).

5.2.5.3. Synthesis of dendritic benzyl alcohol (G1), **37**.[25]

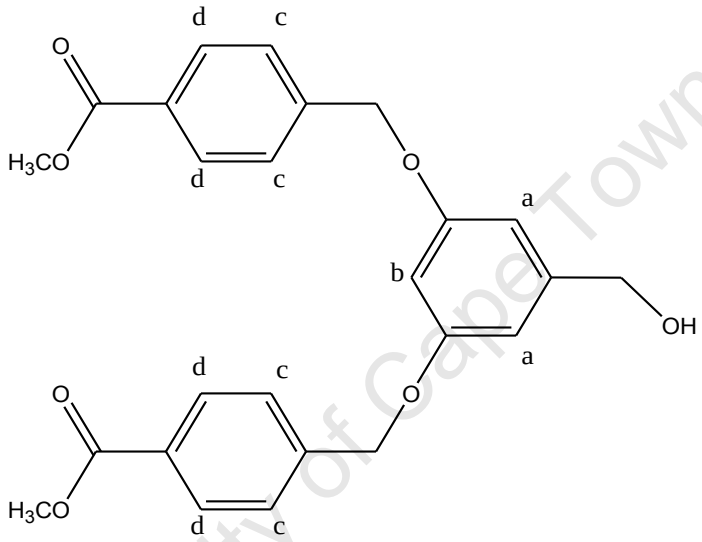

37

A mixture of methyl p-bromomethylbenzoate (0.500 g, 2.18 mmol), 3,5-dihydroxybenzyl alcohol (0.152 g, 1.09 mmol), potassium carbonate (0.377 g, 1.50 mmol) and 18-crown-6 (0.577 g, 2.18 mmol) in dry acetone (15 mL) was heated at reflux (60°C) and stirred vigorously under nitrogen for 24 hours. The mixture was allowed to cool to room temperature and was evaporated to dryness under reduced pressure. The residue was partitioned between water (8 mL) and CH_2Cl_2 (8 mL) and the aqueous layer was extracted with CH_2Cl_2 (3 x 10 mL). The combined extracts were dried ($MgSO_4$) and evaporated and the product (**37**) was isolated as a white solid (63%). **Melting point** = 56-59 °C. **^{1}H-NMR** (300 MHz, $CDCl_3$): δ 3.66 ppm (1H, s, OH), 3.92 ppm (6H, s, OCH_3), 4.62 ppm (2H, s, C**H_2**OH), 5.10 ppm (4H, s, -OCH_2-), 6.51 ppm (1H, t, ^3J = 2.18 Hz, H_b), 6.61 ppm (2H, d, ^3J = 2.23 Hz, H_a), 7.47 ppm

(4H, d, ^3J = 8.61 Hz, H_c), 8.00 ppm (4H, d, ^3J = 8.48 Hz, H_d). **FT-IR** (KBr pellet): ν (C=O) 1715 cm^{-1} (*m*).

5.2.5.4. Synthesis of dendritic benzyl bromide (G1 wedge), **38**.[25]

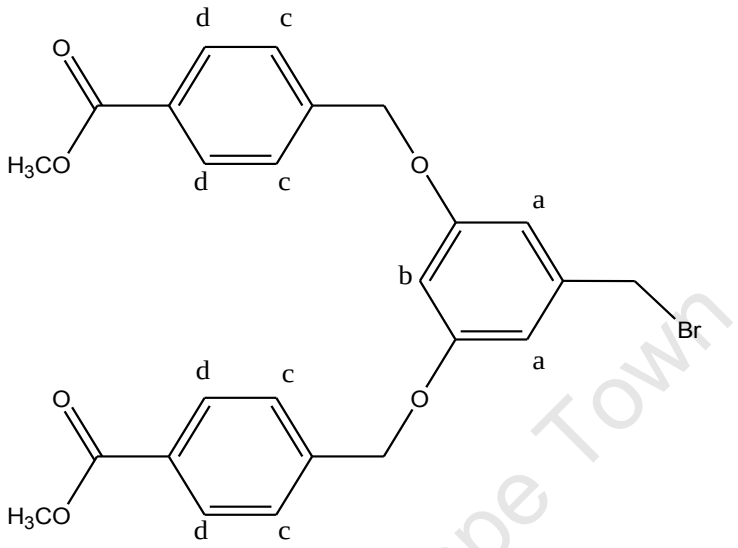

38

A mixture of dendritic benzyl alcohol (*G1*), **37**, (0.151 g, 0.344 mmol), phosphorus tribromide (0.065 mL, 0.688 mmol) and triphenylphosphine (0.183 g, 0.688 mmol) in toluene (15 mL) was stirred vigorously for 24 hours. The reaction mixture was filtered by gravity and was evaporated to dryness under reduced pressure. The residue was partitioned between water (8 mL) and CH_2Cl_2 (8 mL), and the aqueous layer was extracted with CH_2Cl_2 (3 x 10 mL). The combined extracts were dried ($MgSO_4$), evaporated to dryness and the product (**38**) was isolated as a white solid (0.092 g, 54 %). **Mass Spectrometry (EI+)**: *m/z* 499.7 (100%, $[M]^+$). **Melting point** = 137-140 °C (Lit. M. P. = 139-140 °C[25]) **^{1}H-NMR** (300 MHz, $CDCl_3$): δ 3.92 ppm (6H, s, OCH_3), 4.24 ppm (2H, s, C**H_2**Br), 5.10 ppm (4H, s, -OCH_2-), 6.51 ppm (1H, t, ^3J = 2.17 Hz, H_b), 6.61 ppm (2H, d, ^3J = 2.24 Hz, H_a), 7.47 ppm (4H, d, ^3J = 8.66 Hz, H_c), 8.03 ppm (4H, d, ^3J = 8.51 Hz, H_d). **FT-IR** (KBr pellet): ν (C=O) 1720 cm^{-1} (*m*).

5.2.5.5. Synthesis of generation zero (G0) ligand, **39**.

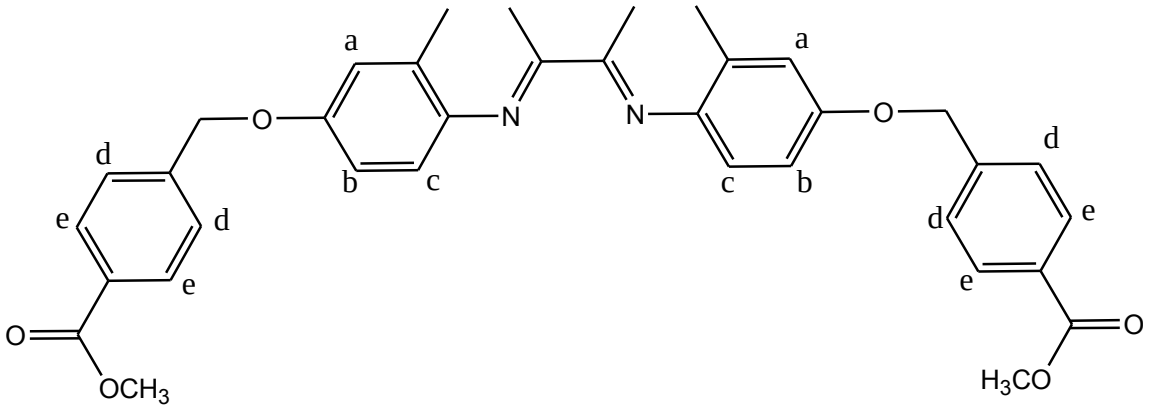

39

The reaction was performed under an inert atmosphere. A solution of methyl p-bromomethylbenzoate (**36**, 0.384 g, 1.679 mmol) in dry THF (15 mL) was added, dropwise, to a stirring solution of 2,3-bis(2-methyl-4-hydroxylphenylimino)butane (**35**, 0.2045 g, 0.8125 mmol) in dry THF (15 mL), in the presence of 18-crown-6 (0.075 g, 0.284 mmol) and potassium carbonate (2.03 g, 14.7 mmol). The reaction mixture was allowed to reflux for 48 hours, after which it was cooled to room temperature. The mixture was evaporated to dryness and partitioned between CH_2Cl_2, (15 mL) and water (15 mL). The aqueous layer was then extracted with CH_2Cl_2 (3 x 15 mL) and the combined extracts were dried ($MgSO_4$) and evaporated to dryness. The product, **39**, was isolated as an orange/brown solid (0.28 g, 57 %). **Melting point** = 149-153 °C. **Mass Spectrometry (ESI)**: *m/z* 593.3 (100%, $[M+H]^+$). **^{1}H-NMR** (400 MHz, DMSO-d_6): δ 2.03 ppm (6H, s, aryl-CH_3), 2.04 ppm (6H, s, -N=C(CH_3)-), 3.81 ppm (6H, s, -OCH_3), 5.63 ppm (4H, s, -CH_2-), 6.58 ppm (2H, d, ^3J = 2.27 Hz, H_c), 6.80 ppm (2H, d, ^3J = 2.24 Hz, H_b), 6.90 ppm (2H, s, H_a), 7.56 ppm (4H, d, ^3J = 8.62 Hz, H_d), 7.93 ppm (4H, d, ^3J = 8.52 Hz, H_e). **FT-IR** (KBr pellet): ν (C=N_{imine}) 1638 cm^{-1} (*m*).

5.2.5.6. Synthesis of generation one (G1) ligand, **40**.

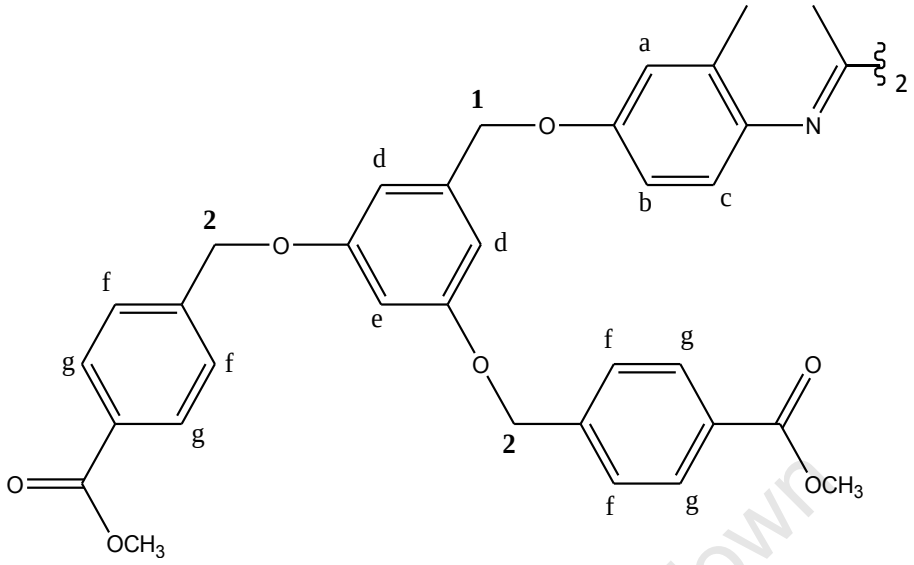

40

The reaction was performed under an inert atmosphere. A solution of dendritic benzyl bromide *(G1 wedge)* (**38**, 0.090 g, 0.18 mmol) in dry THF (10 mL) was added, dropwise, to a stirring solution of 2,3-bis(2-methyl-4-hydroxylphenylimino)butane (**35**, 0.036 g, 0.090 mmol) in dry THF (10 mL), in the presence of 18-crown-6 (0.010 g, 0.030 mmol) and potassium carbonate (0.40 g, 15.8 mmol). The reaction mixture was allowed to reflux for 48 hours, after which it was cooled to room temperature. The mixture was evaporated to dryness and partitioned between CH_2Cl_2 (15 mL) and water (15 mL). The aqueous layer was then extracted with CH_2Cl_2 (3 x 15 mL) and the combined extracts were dried ($MgSO_4$) and evaporated to dryness. The product, **40**, was isolated as an orange oil (28 %). The product could not be isolated as a solid. **^{1}H-NMR** (300 MHz, $CDCl_3$): δ 2.10 ppm (12H, m, aryl-CH_3 + N=C(CH_3)-), 3.92 ppm (12H, s, -OCH_3), 4.98 ppm (4H, s, -CH_2**^{1}**O-), 5.11 ppm (8H, s, -CH_2**^{2}**O-), 6.50 ppm (2H, t, ^3J = 2.34 Hz, H_e), 6.58 ppm (4H, s, H_d), 6.62 ppm (2H, d, ^3J = 2.23 Hz, H_c), 6.86 ppm (2H, d, ^3J = 2.61 Hz, H_b), 6.97 ppm (2H, s, H_a), 7.56 ppm (8H, d, ^3J = 8.52 Hz, H_f), 8.05 ppm (4H, d, ^3J = 8.45 Hz, H_g). **FT-IR** (CH_3Cl, NaCl): ν (C=N_{imine}) 1636 cm^{-1} (*m*).

5.2.6. Synthesis of poly(aryl)ether dendrimer complexes.

5.2.6.1. Synthesis of generation zero (G0) complex, **41**.

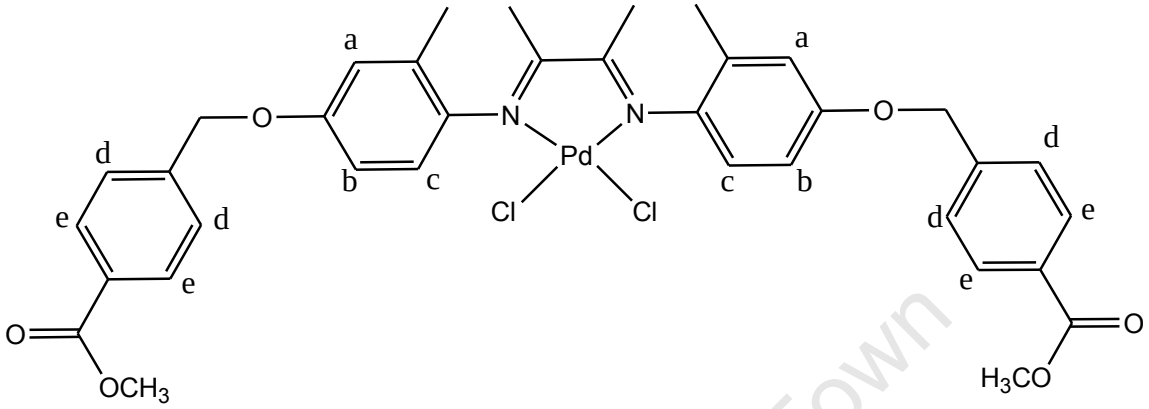

41

A mixture of $PdCl_2$(COD) (0.0458 g, 0.161 mmol) and the G0 ligand **39** (0.112 g, 0.189 mmol) was stirred in dry CH_2Cl_2 (15 mL) for 24 hours. The yellow-orange precipitate that had formed was recovered by suction filtration and washed with CH_2Cl_2 to give **41** (0.084 g, 58 %) as a yellow-orange powder. **Melting point** = decomp. > 290 °C. **^{1}H-NMR** (400 MHz, DMSO-d_6): δ 2.06 ppm (6H, s, aryl-CH_3), 2.07 ppm (6H, s, -N=C(CH_3)-), 3.84 ppm (6H, s, -OCH_3), 5.19 ppm (4H, s, -CH_2-), 6.64 ppm (2H, d, ^3J = 2.28 Hz, H_c), 6.87 ppm (2H, d, ^3J = 2.24 Hz, H_b), 6.98 ppm (2H, s, H_a), 7.60 ppm (4H, d, ^3J = 8.60 Hz, H_d), 7.99 ppm (4H, d, ^3J = 8.52 Hz, H_e). **FT-IR** (KBr pellet): ν (C=N_{imine}) 1578 cm^{-1} (*m*).

5.2.6.2. Synthesis of generation one (G1) complex, **42**.

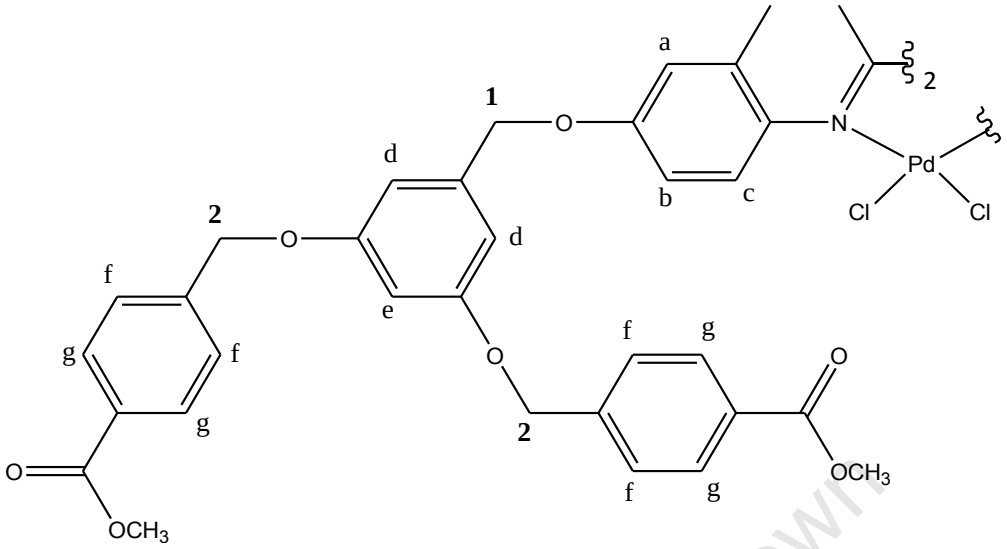

42

A mixture of $PdCl_2$(COD) (0.0255 g, 0.089 mmol) and the G1 ligand **40** (0.0501 g, 0.044 mmol) was stirred in CH_2Cl_2 (10 mL) for 24 hours. No precipitate had formed thus all the solvent was removed to give an orange oil. A minimum volume of CH_2Cl_2 (1 mL) was added and the dissolved product was added to a reservoir of stirring diethyl ether. Upon addition an orange solid precipitated out of solution. The solid was recovered by suction filtration and washed with diethyl ether to give **42** (0.042 g, 73 %) as an orange solid. **^{1}H-NMR** (400 MHz, $CDCl_3$): δ 2.10 ppm (12H, m, aryl-CH_3 + N=C(CH_3)-), 3.92 ppm (12H, s, -OCH_3), 4.98 ppm (4H, s, -$CH_2{}^{\mathbf{1}}$O-), 5.11 ppm (8H, s, -$CH_2{}^{\mathbf{2}}$O-), 6.50 ppm (2H, t, ^3J = 2.34 Hz, H_e), 6.58 ppm (4H, s, H_d), 6.62 ppm (2H, d, ^3J = 2.25 Hz, H_c), 6.86 ppm (2H, d, ^3J = 2.62 Hz, H_b), 6.97 ppm (2H, s, H_a), 7.56 ppm (8H, d, ^3J = 8.52 Hz, H_f), 8.05 ppm (4H, d, ^3J = 8.42 Hz, H_g). **FT-IR** (KBr pellet): ν (C=N_{imine}) 1571 cm^{-1} (*m*).

5.3. Stability studies of radiolabelled gallium(III) thiosemicarbazones

For the stability studies, the radiolabelled complex (**28**-**34**) in an ethanolic solution (200 µL) was evaporated to dryness using a flow of N_2 gas and heat. Subsequently, saline solution (50 µL) or bovine serum (50 µL) was added to the vials containing the evaporated complex. The vials were parafilmed and vortexed (30-60 seconds). Each vial was placed in an oven (at 37°C) for 30, 60 and 120 minutes, respectively (i.e. the stability of each radiolabelled complex was tested in saline and bovine serum after 30, 60 and 120 minutes incubation at 37°C). The vials were removed at the prescribed times, and acetonitrile (100 µL) was added to each vial. The vials were vortexed, followed by quality control being employed on each vial.

5.4. Effect of water on labelling efficiency

The same procedure as for the general synthesis of the radiolabelled gallium(III) thiosemicarbazone was followed, except water (5, 10, 20 and 40 % of the respective reaction mixtures) was added to the ethanolic reaction solution.

5.5. References

1. V. Jatav, P. Mishra, S. Kashaw and J. P. Stables, *Eur. J. Med. Chem.*, 2008, **43**, 135.

2. M. H. Shih, Y. S. Su and C. L. Wu, *Chem. Pharm. Bull.*, 2007, **55(8)**, 1126.

3. M. R. Prathapachandra Kurup and J. Marthakutty, *Synth. React. Inorg. Met. – Org. Chem.*, 2003, **33(7)**, 1275.

4. D. L. Klayman and A. J. Lin, *Org. Prep. Proced. Int.*, 1984, **16(2)**, 79.

5. C. Yamazaki, *Can. J. Chem.*, 1975, **53(4)**, 610.

6. A. Cerny and M. Semonsky, *Cesko-Slovenska Farmacie*, 1960, **9**, 470.

7. S. Chandra, S. Raizada, M. Tyagi and P. K. Sharma, *Spectrochim. Acta A*, 2008, **69A(3)**, 816.

8. A. Balaban, M. Sekerci and B. Erk, *Synth. React. Inorg. Met. –Org. Chem.*, 2003, **33(10)**, 1775.

9. L. Somogyi, *Heterocycles*, 2004, **63(10)**, 2243.

10. S. Chandra and A. Kumar, *Spectrochim. Acta Part A*, 2007, **68**, 1410.

11. A. K. Varshney and S. Varshney, *B. Pol. Acad. Sci. Chem.*, 1989, **37(1-2)**,1.

12. N. Youssef and K. Hegab, *Synth. React. Inorg. Met. –Org. Nano –Met. Chem.*, 2005, **35(5)**, 391.

13. F. Haghighi Moghadam, A. R. Jalilian, A. Nemati and M. Abedini, *J. Radioanal. Nucl. Chem.*, 2007, **272**, 115.

14. A. Wengel, N. Jacobsen, H. Kolind-Andersen, P. Bjerregaard, *Pesticide Science*, 1990, **30(2)**, 223.

15. R. Alonso, E. Bermejo, R. Carballo, A. Castineiras and T. Perez, *J. Mol. Structure*, 2002, **606(1-3)**, 155.

16. F. E. Anderson, C. J. Duca and J. V. Scudi, *J. Am. Chem. Soc.*, 1951, **73**, 4967.

17. M. Schwamborn, L. Heuer, N. Mueller, G. Heywang and G. W. Ludwig, *Ger. Offen.*, 1993, 17.

18. S. K. Chawla, M. Arora, K. Naettinen and K. Rissanen, *Polyhedron*, 2006, **25(3)**, 627.

19. E. M. R. Kiremire, N. Hamata, K. Chibale and H. Kambafwile, *Biosciences, Biotechnology Research Asia*, 2008, **5(1)**, 81.

20. T. Yabuuchi, M. Hisaki and R. Kimura, *Chem. Pharm. Bull.*, 1975, **23**, 663.

21. J. P. Scovill, *Phosphorus, Sulfur Silicon Relat. Elem.*, 1991, **60(1-2)**, 15.

22. F. Kratz, B. Nuber, J. Weiss and B. K. Keppler, *Synth. React. Inorg. Met. – Org. Chem.*, 1991, **21(10)**, 1601.

23. J. Chan, A.L. Thompson, M.W. Jones, J.M. Peach, *Inorg. Chim. Acta*, 2010 , **363(6)**, 1140.

24. B. Blom, M. J. Overett, R. Meijboom and J. R. Moss, *Inorg. Chim. Acta*, 2005, **358**, 3491.

25. C. J. Hawker, K. L. Wooley and J. M. J. Frechet, *J. Chem. Soc. Perkin Trans.*, 1993, 1287.

26. J. M. Aizpurua, B. Lecea and C. Palomo, *Can. J. Chemistry*, 1986, **64(12)**, 2342.